GEOLOGICAL SURVEY OF DENMARK AND GREENLAND BULLETIN 28 • 2013

Review of Survey activities 2012

Edited by
Ole Bennike, Adam A. Garde and W. Stuart Watt

GEOLOGICAL SURVEY OF DENMARK AND GREENLAND
MINISTRY OF CLIMATE, ENERGY AND BUILDING

Geological Survey of Denmark and Greenland Bulletin 28

Keywords
Geological Survey of Denmark and Greenland, survey organisations, current research, Denmark, Greenland.

Cover photographs from left to right

1. The 1097 m high Finnefjeld is located in the central part of the Maniitsoq impact structure, West Greenland. Photograph: Adam A. Garde.
2. Investigation of a coastal cliff section at a potential disposal site for radioactive waste. Photograph: Merete Binderup.
3. Setting up an automatic camera to monitor frontal variations of a glacier in West Greenland. Photograph: Robert Fausto.
4. Collecting samples in Cameroon, using a hand auger. Photograph: Christian Knudsen.

Frontispiece: facing page
In 2012 GEUS published a geological map of the island of Mors in north-west Jylland. The map sheet comprises the coastal cliff section Hanklit on northern Mors, with exposures of light layers of moler and dark layers of volcanic ash, overlain by glaciofluvial deposits from the last ice age. The moler has been folded and up-thrusted by ice advancing from the north. Photograph: Stig A. Schack Pedersen.

Manuscripts received: 22 January 2013 – 14 March 2013
Final versions approved: 15 February 2013 – 21 May 2013
Printed: 10 July 2013

ISSN 1604-8156
ISBN 978-87-7871-357-5

Citation of the name of this series
It is recommended that the name of this series is cited in full, viz. *Geological Survey of Denmark and Greenland Bulletin.*
If abbreviation of this volume is necessary, the following form is suggested: *Geol. Surv. Den. Green. Bull.* 28, 76 pp.

Available from
Geological Survey of Denmark and Greenland (GEUS)
Øster Voldgade 10, DK-1350 Copenhagen K, Denmark
Phone: +45 38 14 20 00, fax: +45 38 14 20 50, e-mail: *geus@geus.dk*

and at *www.geus.dk/publications/bull*

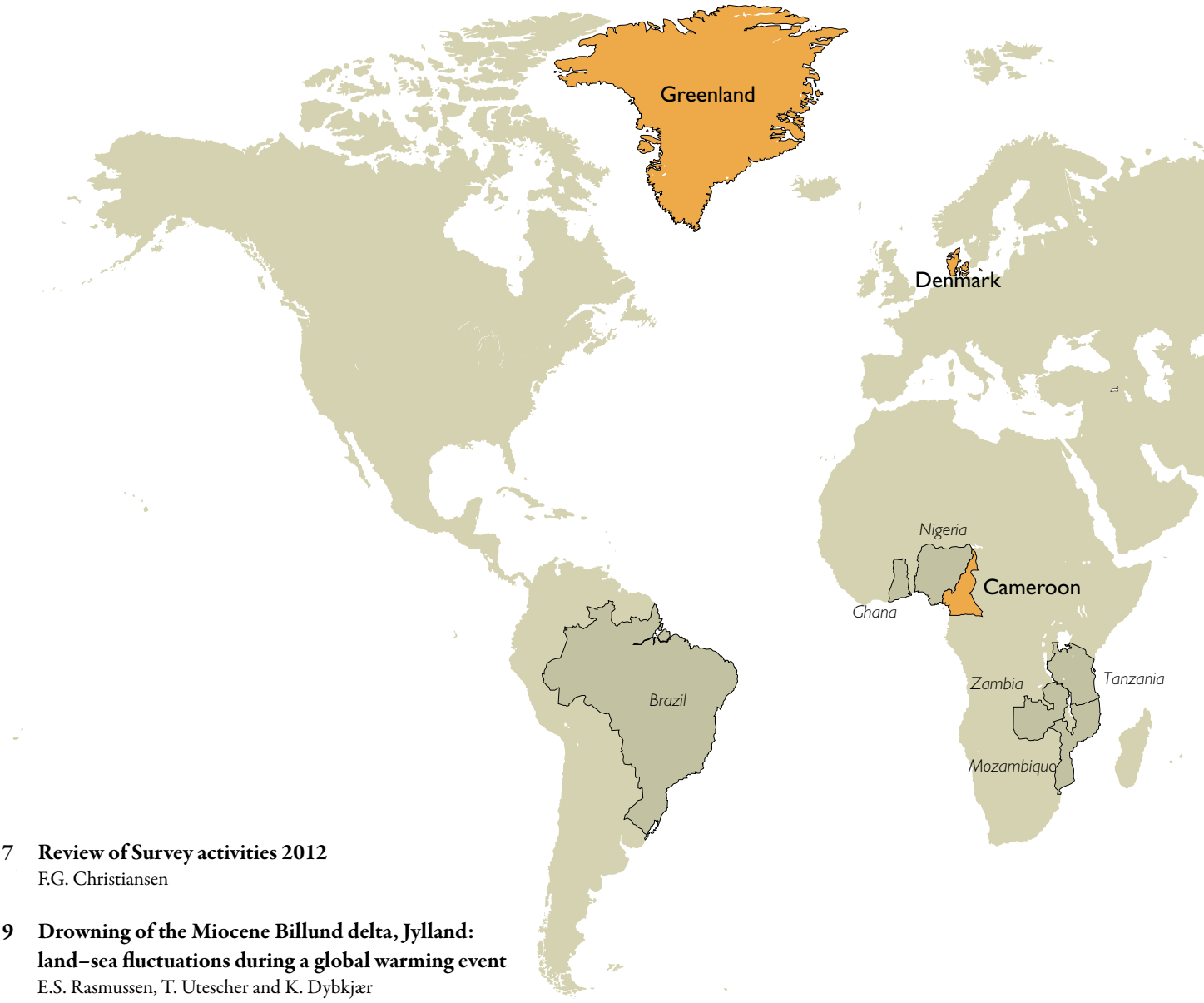

7 **Review of Survey activities 2012**
F.G. Christiansen

9 **Drowning of the Miocene Billund delta, Jylland: land–sea fluctuations during a global warming event**
E.S. Rasmussen, T. Utescher and K. Dybkjær

13 **Geology, seismic activity and groundwater conditions at six potential disposal sites for radioactive waste from Risø, Denmark**
P. Gravesen, B. Nilsson, M. Binderup, T.B. Larsen and S.A.S. Pedersen

17 **A Baltic Ice Lake lowstand of latest Allerød age in the Arkona Basin, southern Baltic Sea**
O. Bennike and J.B. Jensen

21 **Late glacial to early Holocene development of southern Kattegat**
C. Bendixen, J.B. Jensen, O. Bennike and L.O. Boldreel

25 **Terrain subsidence detected by satellite radar scanning of the Copenhagen area, Denmark, and its relation to the tectonic framework**
P. R. Jakobsen, U. Wegmuller, R. Capes and S.A.S. Pedersen

29 **Geological map of Denmark 1:50 000 – map sheet Mors, NW Denmark**
S.A.S. Pedersen, P.R. Jakobsen, L.Tougaard and P. Gravesen

33 **Assessing urban groundwater table response to climate change and increased stormwater infiltration**
M.T. Randall, L. Troldborg, J.C. Refsgaard and J.B. Kidmose

37 **Evaluation of total groundwater abstraction from public waterworks in Denmark using principal component analysis**
B.L. Sørensen and R.R. Møller

41 **Seismic activity in Denmark: detection level and recent felt earthquakes**
T. Dahl-Jensen, P.H. Voss, T.B. Larsen and S. Gregersen

GEUS working areas 2012.
Orange areas are covered in this volume.

45 The norite belt in the Mesoarchaean Maniitsoq structure, southern West Greenland: conduit-type Ni-Cu mineralisation in impact-triggered, mantle-derived intrusions?
A.A. Garde, J. Pattison, T.F. Kokfelt, I. McDonald and K. Secher

49 Geochemistry and petrology of gold-bearing hydrothermal alteration zones on Qilanngaarsuit, southern West Greenland
M. Koppelberg, A. Dziggel, D.M. Schlatter, J. Kolb and F.M. Meyer

53 Fingerprinting of corundum (ruby) from Fiskenæsset, West Greenland
N. Keulen and P. Kalvig

57 Lineament mapping and geological history of the Kangerlussuaq region, southern West Greenland
K.E.S. Klint, J. Engström, A. Parmenter, T. Ruskeeniemi, L.C. Liljedahl and A. Lehtinen

61 Calibration of spectral gamma-ray logs to deltaic sedimentary facies from the Cretaceous Atane Formation, Nuussuaq Basin, West Greenland
G.K. Pedersen, N.H. Schovsbo and H. Nøhr-Hansen

65 A new seamless digital 1:500 000 scale geological map of Greenland
M. Pedersen, W.L. Weng, N. Keulen and T.F. Kokfelt

69 Darkening of the Greenland ice sheet due to the melt-albedo feedback observed at PROMICE weather stations
D. van As, R.S. Fausto, W.T. Colgan, J.E. Box and the PROMICE project team

73 Titanium minerals in Cameroon
C. Knudsen, J. Penaye, M. Mehlsen, R.K. McLimans and F. Kalsbeek

Review of Survey activities 2012

Flemming G. Christiansen
Deputy Director

2012 was a good and stable year for the Geological Survey of Denmark and Greenland (GEUS). In recent years GEUS has been through a long – and very constructive – process of establishing a new strategy that reflects the changes in society and new demands from many different stakeholders. With a new strategy in place there has been greater focus on GEUS' activities and research projects.

2012 was a very active year with many projects, field work and offshore data acquisition, which promises well for maintaining a high level of research in the coming years.

With the establishment of the new series *Geological Survey of Denmark and Greenland Bulletin* in 2003 it was decided to make a yearly *Review of Survey activities*. This issue is the tenth and, together with previous issues, provides a good overview of the Survey's wide range of research and advisory activities. This issue contains a total of 17 four-page papers, nine on Denmark, seven on Greenland and one on a project in Cameroon.

Activities in Denmark

The activities and research in Denmark by GEUS cover many different topics within our main programme areas: data, water, energy, mineral resources as well as nature and climate.

As a follow-up on many previous studies of the Miocene succession and its groundwater resources, one paper gives a detailed discussion of the drowning of the Billund Delta in Jylland during a period of previous global warming.

GEUS has been involved in the technical work that is required before a permanent disposal site can be selected for low- and intermediate-level radioactive waste. One paper describes the geological data and knowledge and key parameters such as lithology, groundwater, seismic activity, effect of climate change and local infrastructure that have been applied to narrow down the initial number of 22 areas to six potential sites.

GEUS is involved in many studies of Quaternary and recent geological processes. One paper describes deposits from the Baltic Ice Lake in the Arkona Basin in the southern Baltic Sea. Another paper presents results on the late glacial to early Holocene development of southern Kattegat. A third paper describes terrain subsidence interpreted from satellite radar scanning with special focus on Copenhagen and its tectonic framework.

Systematic geological mapping on a scale of 1:25 000 and publication of 1:50 000 scale systematic sheets continues. In some places it is appropriate to make regional maps of, for example islands, on a single sheet. An example of this is described in a paper on the map sheet Mors. Geologically, Mors is an interesting island with beautifully exposed glaciotectonic structures in cliff sections, and the characteristic Eocene clayey diatomite with volcanic ash layers, a unit known as 'moler'.

The use of groundwater is very important for Danish society and GEUS carries out many studies on water resources and possible future changes due to climate and use. One paper discusses models for urban groundwater table response to climate change and increased stormwater infiltration using the town of Silkeborg and a proposed course of a new motorway around Silkeborg as a case study. Another paper evaluates groundwater abstraction from public waterworks in Denmark by using advanced statistical methods to correct data.

GEUS records seismological events at six locations in Denmark. One paper describes the developments in detection level and completeness from 2000 to 2012 with examples of recent felt earthquakes (North Sea on 19 February 2010 and Kattegat on 6 August 2012) and explosions.

Activities in Greenland

There was a high level of field activities in Greenland in 2012 with a major mapping and geochemical programme in South-East Greenland, a large field and shallow-core drilling programme in North Greenland, and the LOMROG III cruise in the Arctic Ocean. The latter was the last data acquisition of the Danish Continental Shelf Project. Many other field studies were also carried out. Results from these large and small projects will be presented in the coming years. In this issue results are presented from other completed and ongoing projects.

One paper discusses the possibility that nickel and copper occurrences in the norite belt in the Maniitsoq area could be impact-induced as they are found in a recently described giant and deeply eroded, very old (3 Ga) impact structure

in this area. Gold occurrences have been reported during GEUS expeditions to West Greenland some years ago, and another paper provides more constraints on ore formation and fluid-rock interaction.

Corundum in gem quality (ruby) has been known since the 1960s near Fiskenæsset in southern West Greenland and it is possible that mining will start within a few years. One paper gives a detailed description of the geochemistry that can be used to fingerprint the Greenlandic rubies.

Since 2008, the Greenland Analogue Project (GAP) has carried out a wide range of studies in an area near Kangerlussuaq in West Greenland to understand the many different processes that might take place if a deep geological repository for spent nuclear fuel is affected by glaciation. One paper focuses on structural investigations in this area, especially the mapping of lineaments and other late features. As a follow-up on several decades of studies in the Nuussuaq Basin in West Greenland, a spectral gamma-ray characterisation has been made on the Cretaceous Atane Formation to set up a better model for interpretation of lithology and grain-size variation in wells without cores.

Systematic geological overview mapping of Greenland has been the backbone of the Survey's work in Greenland over the past 65 years ago. In the period 1971–2004, 14 maps were published on a scale of 1:500 000. With the development of the Internet, geological maps worldwide are rapidly changing from traditional paper sheets to digital publications. GEUS has produced a new seamless digital 1:500 000 scale map covering the whole of Greenland. One paper describes the background, the digitisation and the geological harmonization involved. It is expected that such maps will be widely used in the future. The new map is an important GEUS contribution to the global OneGeology portal.

The important monitoring programme of the Greenland Ice Sheet (PROMICE) continuously supplies new crucial data and one paper discusses the darkening of the Greenland ice sheet and the increase in surface melting.

International activities

Internationally GEUS works in many different countries with a variety of projects. The last paper in this issue is about titanium minerals in Cameroon and it focuses on understanding the primary formation, weathering and re-deposition of rutile in the area.

Drowning of the Miocene Billund delta, Jylland: land–sea fluctuations during a global warming event

Erik Skovbjerg Rasmussen, Torsten Utescher and Karen Dybkjær

Lower Miocene strata from boreholes and, in particular, at outcrops in the Lillebælt and Limfjorden areas of Jylland provide a natural laboratory for studying the drowning of a major delta system during a period of global warming. Detailed studies of sedimentary structures, fossil algae, spores and pollen give information about depositional environments, local temperatures and precipitation. By comparing with the global climatic record from the same period, a detailed reconstruction of the flooding of a low-relief delta system can be made, with emphasis on the global warming after the glacial event Mi1a. The local temperature increase following the Mi1a event is estimated to be *c.* 5°C.

The Billund delta

During the Early Miocene, a delta system prograded into the eastern part of the North Sea (Fig. 1), with a sediment source in present-day Norway and central Sweden. For more than 100 million years, the eastern North Sea was a relatively deep basin, but due to tectonism associated with the Alpine Orogeny and the opening of the North Atlantic both the hinterland and the marginal areas of the basin were uplifted during the latest Oligocene – Early Miocene (e.g. Knox *et al.* 2010). Inversion tectonism in the Norwegian–Danish Basin resulted in shallower water depths of *c.* 100 m in the eastern North Sea. Contemporaneous uplift of the Norwegian mountains provided a high sediment supply sourcing a major delta system prograding southwards into the North Sea region. The delta front was shaped by wave action, similar to the present-day Nile and Danube deltas (Bhattacharya & Giosan 2003), with a size comparable to the latter. Spit and barrier systems formed east of the main delta lobes (Fig. 1) due to the prevailing westerly winds in the North Sea area at that time. From the geological record, it is seen that the delta system prograded as far south as present-day southern Jylland (Fig. 1A).

Drowning of the land

The depositional environments of the Billund delta system are reconstructed from sedimentological studies (Figs 1, 2). During the maximum extent of the delta, most of present-day Jyl-

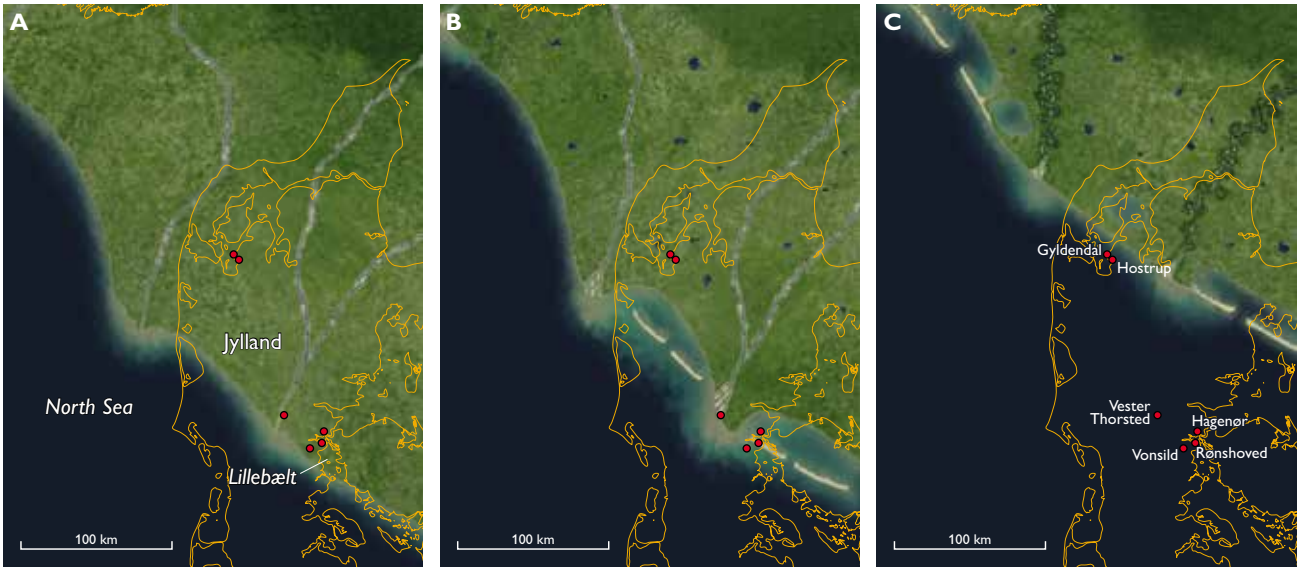

Fig. 1. Palaeogeographic reconstruction of the Early Miocene in the eastern part of the North Sea basin. **A**: Billund Formation during maximum regression. **B**: Klintinghoved Formation during initial transgression (Kolding Fjord Member). C: Klintinghoved Formation during maximum transgression. Modified from Rasmussen *et al*. 2010.

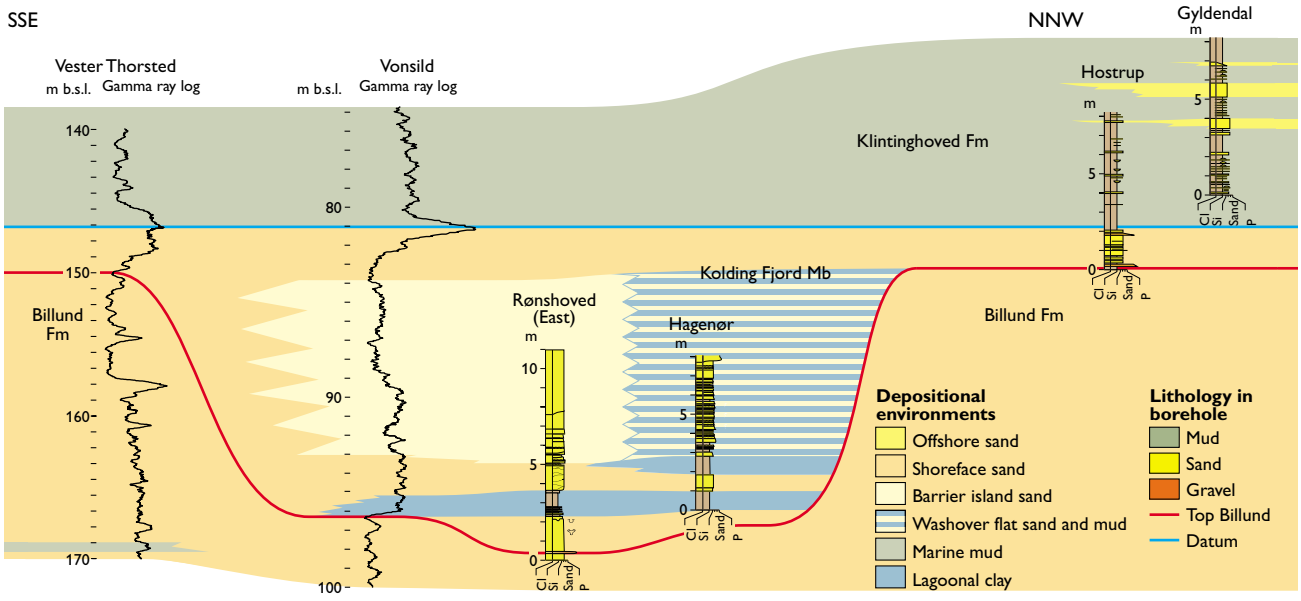

Fig. 2. Correlation panel of the Lillebælt area and Limfjorden.

land was covered by braided fluvial channels and flood-plain environments (Fig. 1A). In the late stage of delta progradation, the delta plain was irregular due to topographic elements formed associated with falling sea level, i.e. down-stepping delta platforms and incisions, and due to minor inversion of the basin (e.g. Rasmussen *et al*. 2010).

During later flooding, most of the deposits were redistributed by the action of waves. Mud and fine-grained sand were winnowed away and transported into the deeper sea, whereas coarse-grained sand and gravel were reworked and redeposited locally. Therefore, a widespread lag of gravel caps the shoreface sand of the underlying Billund Formation (Fig. 3A, C). Intense wave action on the main delta system shed sand towards the east, resulting in the formation of spit and barrier systems in eastern Jylland (Fig. 1B); lagoons and tidal flats developed north of these systems. Both shoreface and lagoonal deposits accumulated in a depositional setting dominated by waves. The shoreface sand is dominated by hummocky and swaley, cross-stratified sand, and the lagoonal mud is commonly intercalated with washover fans (Fig. 3B).

From the sedimentary record, it is seen that the initial drowning of the Billund delta system was characterised by flooding and re-establishment of land in two phases (Fig. 2), which only influenced the distal part (tens of kilometres) of the delta plain. Transgressive deposits up to 15 m thick are found at localities around Lillebælt, Rønshoved and Hagenør (Fig. 2). At Hagenør, two stacked lagoonal mud units separated by shoreface sand show that relatively stable barrier systems were established twice during the transgression (Figs 2, 3B). During the main flooding, the low-relief delta plain (similar present-day delta systems have gradients of *c.* 1/20 000) was flooded relatively quickly, and only up to *c.* 1 m of transgressive sediments were deposited, e.g. at Hostrup (Figs 2, 3C). At this locality, the relatively rapid changes in depositional environment during the main transgression are seen from the coexistence of the marine trace fossil *Ophiomorpha* and rootlets (*Schaubcylendrichnus*; Fig. 3C).

From studies of global sea-level changes in the Early Miocene, it appears that sea-level variations in the order of 25 m occurred during the Mi1a event (Miller *et al.* 2005). This change in sea level resulted in rapid progradation during the sea-level fall. The succeeding flooding can be followed for *c.* 75 km towards the north-east in the Danish area (Fig. 1C). Maximum flooding has not been documented at any outcrop in Denmark, but the sedimentary succession at Hostrup indicates that the shoreline was located not far from this locality at any time because the marine mud of the Klintinghoved Formation is strongly influenced by terrestrial matter throughout the section. Most of the 25 m of sea-level change must be explained by the 15 m transgressive deposits found at Rønshoved and Hagenør (compaction can be ignored in sorted shoreface sand) in the southern part of the delta system where some relief was created during the sea-level fall and lowstand. Additional 5 m of relief of the main delta calculated from 75 km of flooding gives a total of 20 m of transgressive deposits. As the sea-level changes were in the order of 25 m (Miller *et al.* 2005), the remaining 5 m can be ascribed to more or less stable conditions for a period (aggradation of the system) or waning of the inversion tectonism. In the upper part of the Hostrup and Gyldendal sections, the

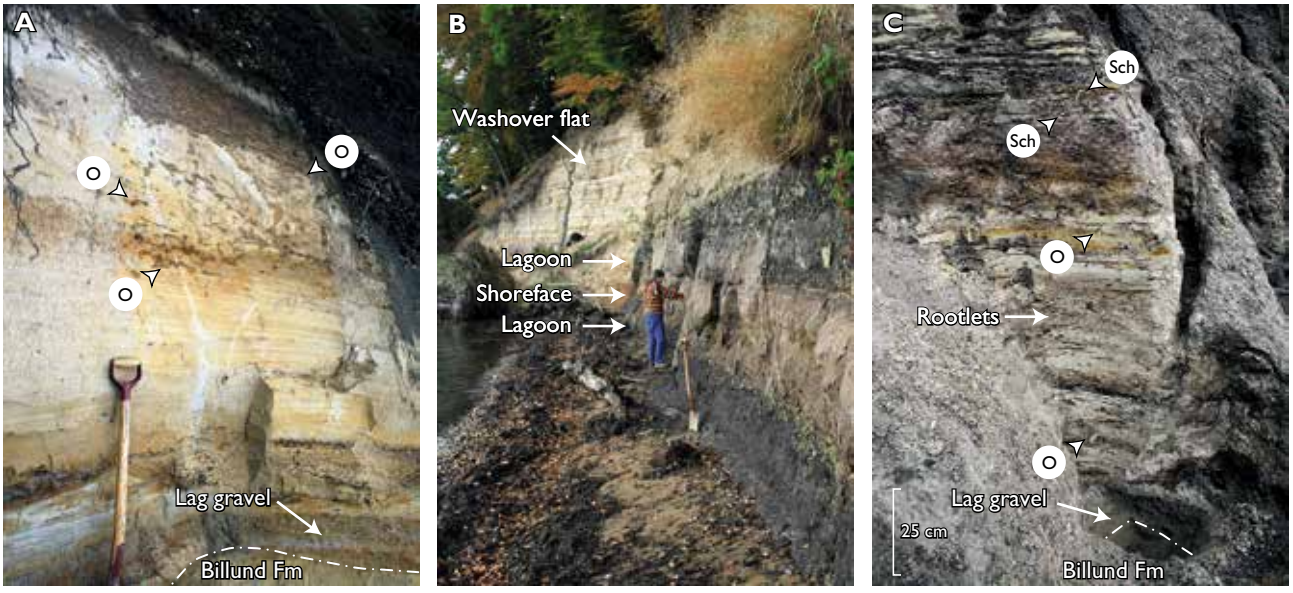

Fig. 3. Photographs of lithologies of the outcrops of the Billund and Klintinghoved Formations. **A**: Shoreface deposits from Rønshoved. Note the gravel layer, the base of which forms the lower part of the Klintinghoved Formation. **B**: Lagoonal deposits from Hagenør. Note that sand-rich washover fans dominate the upper part. **C**: Transgressive sand and marine mud of the Klintinghoved Formation at Hostrup. The lag of gravel at the base of the Klintinghoved Formation is seen in the lower part of the photograph. Both rootlets and marine trace fossils are found in the sand-rich deposits. **O**: *Ophiomorpha*, **Sch**: *Schaubcylindrichnus* (rootlets).

increased intercalation of hummocky, cross-stratified sand layers indicates resumed progradation of the shoreline.

Climate and vegetation change

Changes in continental climate and vegetation in the study area around the Mi1a glacial event and the subsequent drowning of the Billund delta system were reconstructed from pollen and spores (Fig. 4). Although terrestrial signals are commonly diluted in marine strata due to transport and reworking, our data show close correlation with the evolution recorded in the marine part. Climate reconstruction using the 'Coexistence Approach' of Mosbrugger & Utescher (1997) shows distinct cooling during the formation of the Billund delta and the sea-level lowstand that culminated at *c.* 164 m in the Vester Thorsted well (Fig. 4). This is followed by warming that coincides with sea-level rise and drowning of the delta system. The cooling event is characterised by declining winter temperatures, with a fall of *c.* 5°C mean temperature in the coldest month. Summer temperatures were stable to begin with, but later increased during progressive transgression (Hagenør sample). The palynomorph record points to humid conditions with over 1000 mm annual rainfall over the time span analysed. The precipitation was not equally distributed throughout the year but showed distinct seasonality (cf. monthly precipitation records, Fig. 4). The monthly means indicate that cooling was accompanied by declining precipitation during the wettest season and hence to a lesser degree of seasonal rainfall.

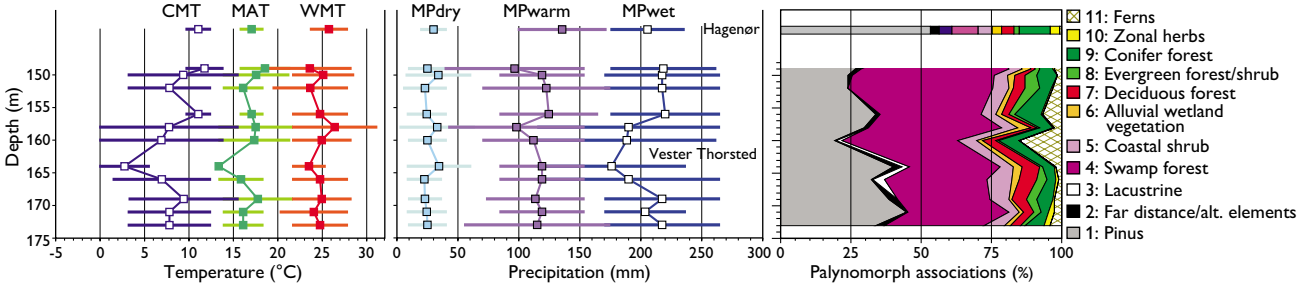

Fig. 4. Climate records and synthesised pollen diagram for depth range 149–173 m of Vester Thorsted borehole. Results obtained from lagoonal silts deposited in the trangressive phase of sequence C are shown on top. The lagoonal silts were sampled in the nearby Hagenør outcrop. **CMT**: Cold month mean, **MAT**: Mean annual temperature, **WMT**: warm month mean, **MPdry**, **MPwarm**, **MPwet**: Mean precipitation of the driest, warmest and wettest month.

In the warmer climate reconstructed higher up in the transgressive systems track (sample Hagenør), the region received more precipitation in the warm season.

The palynomorph record also allows us to follow the evolution of continental ecosystems triggered by climate and sea-level change. The synthesised pollen diagram (Fig. 4) shows frequency variations of groups reflecting regional to local biomes. Pollen groups 1 and 2 comprise the pine family that includes many prolific pollen producers. Association 1 mainly comprises pine, but in the Hagenør sample small percentages of cedar and *Cathaya* are also seen. The latter, monotypic genus occurs today as an endemic relict in central China. Other members of Pinaceae such as *Abies, Picea* and *Larix* (group 2), frequently referred to vegetation of higher altitudes, are not important in the spectra (<3.5%). Pine pollen can be dispersed over long distances and are relatively enriched in open marine palynomorph spectra (e.g. Larsson *et al*. 2011). The overall declining trend of pine pollen recorded in the Vester Thorsted samples (from 45% at the base to 25% at 160 m) traces the falling sea-level and increased terrigenous input during the formation of the delta. The high pine pollen value for Hagenør (>50%) coincides with the rising sea-level of the transgressive phase. Lacustrine group 3, comprising lacustrine plankton, pteridophyte and angiosperm limnophytes, reaches its highest values (*c.* 5%) during the cooling event (at 164 m) and probably marks the most proximal conditions, together with fern group 11 that is frequent at the levels immediately above. These components originate from the local vegetation found on unstable, alluvial deposits on the delta plain. Two groups of palynomorphs (4 + 5) that probably represent the vegetation of coastal swamps attain very high proportions during delta formation and show a distinct increase from *c.* 40 to over 55% which allows us to trace the ongoing regression. Low values at Hagenør (*c.* 10%) indicate that coastal swamps drowned as sea level rose. The arboreal vegetation on the coastal swamps comprises taxodioids (*Taxodium, Sciadopitys* and other Cupressaceae), with Ericaceae and Myricaceae representing the shrub layer. Pollen from alluvial wetland vegetation (6) play a minor role in the spectra and indicate a lack of widespread riverine forests, whereas palynomorphs usually assigned to zonal vegetation (groups 7–10) are present with 10 to 15% as permanent background. The zonal vegetation was a diverse, mixed conifer / broadleaved forest with evergreen and deciduous oak, magnolia, chestnut, sweetgum, members of Juglandaceae, hemlock, coast redwood and palms. It is noteworthy that climate changes recorded in the section affected its generic composition. During the cool phase, between 156 and 164 m, the forest almost completely lost its broadleaved evergreen species, and thus had a more temperate aspect.

Concluding remarks

During a global warming in the Early Miocene when the local temperature increased by 5°C, the Billund delta system was flooded. The displacement of the shoreline was in the order of 75 km and affected the coastal vegetation. Up to 15 m of alternating lagoonal and shoreface deposits were formed in the distal portion of the delta evidencing some stability in the early phase due to antecedent relief and high sediment supply. The main low-relief delta plain was, however, flooded quickly and only left *c.* 1 m of transgressive deposits. Yearly precipitation rates were in the order of 1000 mm; the warming was accompanied by changes in seasonal patterns of rainfall so that during warmer periods there is a tendency to more summer rain.

Acknowledgements

The Nature Agency centres in Ribe, Ringkøbing and Aarhus are thanked for financial support. T.U. thanks the German Science Foundation (DFG) for finacial support.

References

Bhattacharya, J.P. & Giosan, L. 2003: Wave-influenced deltas: geomorphological implications for facies reconstruction. Sedimentology **50**, 187–210.

Knox, R. *et al*. 2010: Cenozoic. In: Doornenbal, J.C. & Stevenson, A.G. (eds): Petroleum geological atlas of the southern Permian Basin area, 210–223. Houten, the Netherlands: European Association of Geoscientists & Engineers (EAGE) Publications.

Larsson, L.M., Dybkjær, K., Rasmussen, E.S., Piasecki, S., Utescher, T. & Vajda, V. 2011: Miocene climate evolution of northern Europe: a palynological investigation from Denmark. Palaeogeography, Palaeoclimatology, Palaeoecology **309**, 161–175.

Miller, KG., Kominz, M.A., Browing, J.V., Wright, J.D., Mountain, G.S., Katz, M.E., Sugarman, P.J., Cramer, B.S., Christie-Blick, N. & Pekar, S.F. 2005: The Phanerozoic record of global sea-level changes. Science **310**, 1293–1298.

Mosbrugger, V. & Utescher, T. 1997: The coexistence approach: a method for quantitative reconstructions of Tertiary terrestrial palaeoclimate data using plant fossils. Palaeogeography, Palaeoclimatology, Palaeoecology **134**, 61–86.

Rasmussen, E.S., Dybkjær, K. & Piasecki, S. 2010: Lithostratigraphy of the upper Oligocene – Miocene succession in Denmark. Geological Survey of Denmark and Greenland Bulletin **22**, 93 pp.

Authors' addresses

E.S.R. & K.D., *Geological Survey of Denmark and Greenland, Øster Voldgade 10, DK-1350 Copenhagen K, Denmark*. E-mail: *esr@geus.dk*

T.U., *Steinmann Institute, University of Bonn, Nußallee 8, 53115 Bonn; Senckenberg Research Institute / BiK F, Senckenberganlage 25, 60325 Frankfurt/Main, Germany.*

Geology, seismic activity and groundwater conditions at six potential disposal sites for radioactive waste from Risø, Denmark

Peter Gravesen, Bertel Nilsson, Merete Binderup, Tine B. Larsen and Stig A. Schack Pedersen

In 2003 it was decided by the Danish Parliament that low- and intermediate-level radioactive waste from the Danish nuclear research facility, Risø, is to be stored at a permanent disposal site (Ministeriet for Sundhed og Forebyggelse 2008; Gravesen *et al*. 2012a). Both the issue of storage and the selection of potential sites have caused considerable public debate. In this paper we report on the most recent geological investigations intended to further improve the data base for the selection and decision process, although no conclusions have been drawn at this stage.

The waste might be deposited on the land surface, partly below surface or totally below surface, and pre-Quaternary rocks and deposits are the main general targets. In 2011 six potential areas were selected for further studyd and evaluation of their suitability for disposal of radioactive waste. The study evaluated local groundwater conditions and earthquake hazards, infrastructure, wildlife, environment, water supply (especially drinking water) and heritage monuments (Gravesen *et al*. 2011, 2012b). The new studies of the six potential sites and their surroundings were performed by the Geological Survey of Denmark and Greenland aided by the Danish Nature Agency (Naturstyrelsen), and included drilling of several new boreholes.

Geological setting

The areas that were chosen for further study were selected from 22 initial targets (Gravesen *et al*. 2011) based on compliance with specific criteria (see below) that had previously been established from geological models (Gravesen *et al*. 2012a). The six selected areas (Fig. 1) are located in different geological settings. The Østermarie-Paradisbakkerne area on Bornholm consists of Precambrian Paradisbakke migmatite and Bornholm gneiss. In the Rødbyhavn area on Lolland, Palaeocene clay rests on Maastrichtian chalk, while the Kertinge Mark area on Fyn comprises thick Palaeocene clay deposits overlying Danian Limestone. In the Hvidbjerg area of north-west Jylland, Palaeocene and Eocene clay for-

Fig. 1. Map of Denmark showing the locations of the six areas selected for detailed studies of their suitability as disposal sites for radioactive waste from Risø.

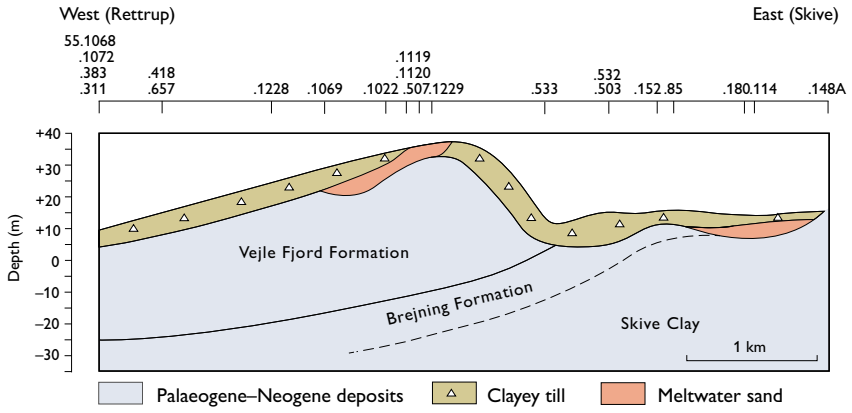

Fig. 2. Geological cross section through Palaeogene–Neogene deposits of the Skive vest area, extending from Rettrup in the west to Skive in the east. The positions of the boreholes with DGU numbers are indicated along the top of the figure.

mations rest on Danian Limestone and are covered by Oligocene and Miocene clay formations. Farther to the east and south-east, at Thise and Skive vest (west), Oligocene and Miocene clay, respectively, are present. Quaternary clayey till overlies the pre-Quaternary rocks and sediments at all sites.

Collection of seismic, borehole and groundwater data

Part of the new study consisted of an evaluation of earthquake potential. The seismic activity in Denmark has been recorded instrumentally since 1929, and in later years by an interconnected network of seismic stations in Denmark and surrounding countries. Older earthquakes were examined from descriptions in the literature. For the three potential sites on Bornholm, Lolland and Fyn available seismic data within a radius of 50 km were evaluated. For the three areas in north-west Jylland a radius of 75 km was used.

In the new study additional boreholes were drilled in each of the six selected areas. Sediment samples were collected from each metre and analysed, and several types of continuous geophysical logs were performed in most boreholes. Such logs are particularly useful for extrapolations between the samples. On Bornholm, eight existing water abstraction wells for domestic use were logged for idenfication of fractures in the bedrock.

Evaluation of groundwater, drinking water and water supplies was based on new information and existing literature, as well as local knowledge of potential groundwater problems. The latter was obtained by interviewing local specialists and acquisition of written accounts and other information collected by the local authorities.

Survey results

Data from the borehole samples and from the geophysical logs have provided important new information on the geological models of the investigated areas, which comprise data on lithology and stratigraphy as well as tectonic and sedimentological structures. All the relevant information has been compiled into six technical reports by the Geological Survey of Denmark and Greenland, which are available at GEUS' website, *http://www.geus.dk/program-areas/nature-environment/denmark/radioaktivt_affald/index-dk.htm*. The main topics are: boreholes and logging, seismic activity and earthquakes, groundwater and drinking water, climate and climate changes and local planning (infrastucture, wildlife, environment, cultural heritage, raw materials, agriculture and water supply structure). All this information will be used in the ongoing evaluation of the areas and identification of the two most suitable areas. In this paper only selected results are presented, including geological traverses through the six areas.

Geological data

The Precambrian crystalline rocks on *Bornholm* are thick and extensive and contain a network of fractures. Knowledge of the fracture systems in the Østermarie-Paradisbakkerne area is important for evaluation of groundwater flow and storage, and for evaluation of the stability of the host rocks. Horizontal and vertical fractures to a depth of 12 m can be observed in quarries. The number of horizontal fractures appears to decrease downwards, while their spacing increases. This is a normal observation in the uppermost crust. The geophysical borehole logs comprise natural gamma-ray, resistivity, sound velocity, fluid temperature, fluid conductivity and flow logs, which can be used to document fractures at various levels from 20 m below the surface down to a depth

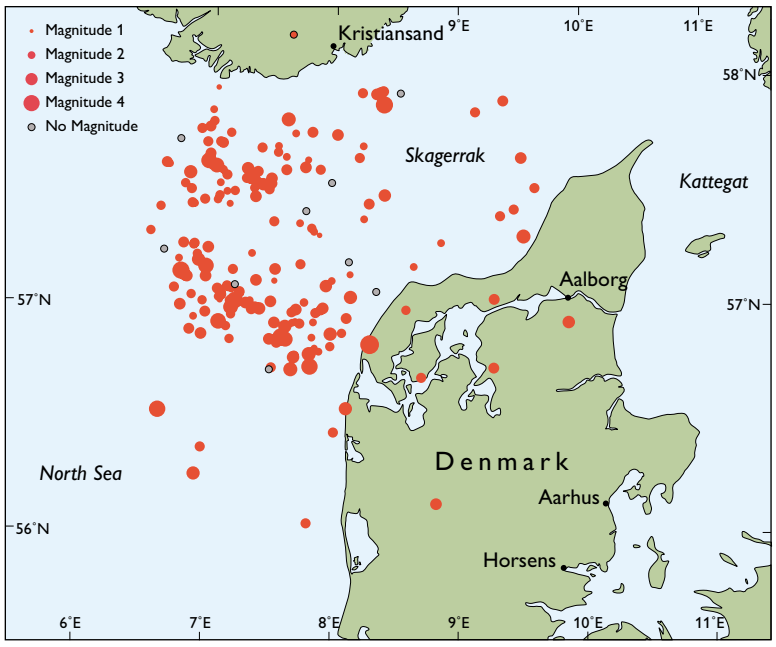

Fig. 3. Earthquake epicentres in the north-west Jylland region. The magnitude on the Richter scale is shown by the size of the dots (from Gravesen *et al.* 2012b). Other earthquake epicentres in the Danish region are not shown on this map.

of 90 m. Extrapolations of the borehole data suggest that some fractures are horizontal or subhorizontal and connected over larger distances. Quaternary clayey and sandy tills on Bornholm are mostly only a few metres thick.

The pre-Quaternary rocks and deposits throughout *the remaining parts of Denmark* are fine-grained, have low permeability, and are covered by Quaternary clayey tills. The clay deposits are generally relatively thick and appear to be of wide horizontal distribution within the selected areas, reflecting the fact that the deposits represent marine depositional environments. Furthermore, the deposits are characterised by low degrees of glaciotectonic disturbance and pre-Quaternary tectonic movements. These characteristics meet the criteria described by Gravesen *et al.* (2011, 2012a) based on the guidelines of the International Atomic Energy Agency (IAEA 1994).

At *Rødbyhavn*, Palaeocene fine-grained deposits and plastic clay from the Ælbelø and Holmehus Formations resting on Maastrichtian chalk have been documented from geophysical surveys and boreholes drilled for bentonite exploration and geotechnical purposes related to the Femern Bælt Fixed Link. The characteristics of the *c.* 80 m thick clay sequence and the overlying up to 40 m thick hard Quaternary clayey till demonstrate that the deposits are *in situ*, although tectonic disturbances are known to exist outside the area.

Within and just outside the *Kertinge Mark* area, up to 75 m thick Palaeocene Kerteminde Marl and Ælbelø Formation overlying Danian limestone have been documented. The new boreholes demonstrate that non-calcareous black clay of the Ælbelø Formation occurs above calcareous grey clay of the Kerteminde marl in the northern part of the Kertinge Mark peninsula, forming the natural stratigraphical sequence. Quaternary clayey till up to 40 m thick is found above these formations. Some layers are very sandy and gravelly as shown by samples from the boreholes and from geophysical logs.

In the *Hvidbjerg* area, Palaeocene and Eocene grey clay of the Kerteminde Marl and diatomite from the Fur Formation rest on Danian Limestone on the northern flank of the Uglev salt diapir. The formations are covered by Oligocene and Miocene black-brown mica clay deposits from the Brejning and Vejle Fjord Formations, with a total of up to 100 m thickness. Thick Quaternary clayey till comprises the top 20 m. The new borehole demonstrates a more complex build-up of the succession with unconformities caused by tectonic episodes and erosion.

In the *Thise* area, more than 100 m thick layers of Oligocene mica clay from the Brejning Formation and green-grey, fine-grained clay from the Branden clay unit are covered by up to 18 m thick Quaternary clayey till. The new borehole penetrated 22 m of Brejning Formation below 19 m of Quaternary clayey till. The Oligocene deposits form an erosional inlier bordered by buried valleys filled with Quaternary till and meltwater deposits.

In the *Skive vest* area, up to 100 m of Oligocene and Miocene deposits of fine-grained grey Skive Clay unit (to the east) and black-brown mica clay from the Brejning and Vejle Fjord Formations (to the west) are present; the layers dip slightly to the west (Fig. 2). Two new boreholes penetrated the two youngest formations down to 50 m below the sur-

face, possibly indicating that the two formations are found *in situ* as also indicated by other borehole data in the area. A thin cover of Quaternary clayey till is present.

Seismic activity and earthquakes

The seismic activity in most of Denmark is low, but a little higher in north-west Jylland than in other parts of the country. The most seismically active region relevant for the current investigation is located in Skagerrak and the North Sea, while epicentres on land are rare (Fig. 3). The earthquake magnitudes are low, with values mainly below 3 on the Richter scale.

No epicentres are found on Bornholm, although some occur in the nearshore areas of the Baltic Sea. Bornholm has not been seismically active in recent historical time, although an earthquake in 1875 possibly had its epicentre on west Bornholm. Small earthquakes in the Baltic Sea and southern Sweden can sometimes be registered on Bornholm. According to instrumental and historical sources, Lolland does not seem to be seismically active, and the seismicity on Fyn is very low. Some minor earthquakes have been measured on Fyn, but the historical literature does not suggest any earthquake activity.

A slightly higher seismicity is found in north-west Jylland around Hvidbjerg, Thise and Skive vest, since many small earthquakes located in the North Sea and Skagerrak are registered on land. Historical literature also suggests many small earthquakes around these three areas, and some damage to buildings has occurred. An earthquake in 1841 is probably the largest earthquake registered in Denmark.

Groundwater conditions and drinking water

All six areas are situated outside areas of Special Drinking Water Interests (OSD), which are the most important Danish supply areas for drinking water. Major regional groundwater reservoirs are also absent, although some small reservoirs are important for local supplies.

On Bornholm the basement rocks form a fractured groundwater reservoir with restricted groundwater flow at various levels. The reservoir has a limited yield but is used locally in an area where connection to public water utilities is difficult and costly.

The Rødbyhavn area is almost totally devoid of groundwater reservoirs, although some surface water is extracted for drinking purposes. The Kertinge Mark area also lacks groundwater reservoirs, but local aquifers close to the surface are used for water supply. Just south-east of this area, groundwater reservoirs in an OSD area supply the town of Kerteminde with drinking water. The reservoir is small and vulnerable because of its restricted size and thickness, and no alternative sources exist in the neighbourhood.

In the Hvidbjerg area, almost no goundwater is pumped because groundwater reservoirs are lacking. The Thise area has some local abstraction from thin meltwater sand reservoirs. An area which is particularly vulnerable to nitrate contamination (NFI) occurs east of Thise waterworks. Just east and north of the area, OSD areas with sand reservoirs are found in buried valleys. Throughout the Skive vest area, local water supplies use sand and gravel reservoirs; no public or private water utilities are found.

Final remarks

The present investigations of the geology, earthquake risks, groundwater and drinking water conditions are crucial for the selection of two areas for further examination before a final disposal site can be chosen. Before the selection of the two areas an Environmental Impact Assessment (EIA) has to be performed. Also the possibilities of export of the waste to a foreign country have to be investigated. Finally the design and establishment of a temporary disposal for the waste have to be described and evaluated.

Acknowledgement

Financial support was provided by the Parliament of Denmark.

References

Gravesen, P., Nilsson, B., Pedersen, S.A.S. & Binderup, M. 2011: Low- and intermediate level radioactive waste from Risø, Denmark. Location studies for potential disposal areas. Report no. 11. Områdebeskrivelser – Description of areas. Geological Survey of Denmark and Greenland Report **2011/51**, 64 pp.

Gravesen, P., Binderup, M., Nilsson, B. & Pedersen, S.A.S. 2012a: Geological characterisation of potential disposal areas for radioactive waste from Risø, Denmark. Geological Survey of Denmark and Greenland Bulletin **23**, 21–24.

Gravesen, P., Nilsson, B., Binderup, M. Larsen, T. & Pedersen, S.A.S. 2012b: Lav- og mellem radioaktivt affald fra Risø, Danmark. Omegnsstudier. Rapport nr. 5. Område Thise, Skive Kommune. Geological Survey of Denmark and Greenland Report **2012/127**, 81 pp.

IAEA 1994: Siting of near surface disposal facilities. Safety guides. Safety Series **111-G-3.1**, 37 pp.

Ministeriet for Sundhed og Forebyggelse 2008: Beslutningsgrundlag for et dansk slutdepot for lav- og mellemaktivt affald, 47 pp. København: Ministeriet for Sundhed og Forebyggelse.

Authors' address

Geological Survey of Denmark and Greenland, Øster Voldgade 10, DK-1350 Copenhagen K, Denmark. E-mail: *pg@geus.dk*

A Baltic Ice Lake lowstand of latest Allerød age in the Arkona Basin, southern Baltic Sea

Ole Bennike and Jørn Bo Jensen

After the last deglaciation, the Baltic Sea underwent a complex salinity history and dynamic shore-level development with several lacustrine and marine stages: the Baltic Ice Lake, the Yoldia Sea, the Ancylus Lake and the Littorina Sea (Björck 1995). In connection with shallow seismic profiling in the south-western Baltic Sea, two marked and widespread erosional unconformities have been identified (Jensen *et al.* 1997, 1999; Lemke *et al.* 1998; Larsen 2004). The older unconformity occurs within sediments deposited in the Baltic Ice Lake, whereas the younger one separates Baltic Ice Lake sediments from Holocene lake and mire deposits. The latter unconformity is dated to the transition between the Younger Dryas and the Holocene, corresponding to *c.* 11.7 cal. ka BP and formed due to a sudden drop in the level of the ice-dammed Baltic Ice Lake of around 25 m, caused by ice recession from Mt. Billingen in south central Sweden.

The age of the older erosional unconformity is poorly constrained. However, it has been suggested that the level of the Baltic Ice Lake also experienced a sudden drop during the Allerød chronozone. The temperature increased during the Allerød, and it is possible that the margin of the Fennoscandian Ice Sheet also receded from the Mt. Billingen area at this time. If so, the older erosional unconformity may have formed in connection with an early drainage of the Baltic Ice Lake.

The question about such an early lake-level fall was discussed by Björck (1995), who listed a number of arguments for and against it. One of the arguments for drainage is that evidence of a rapid lake-level fall is seen in both south-eastern Sweden and in other Baltic countries. A study in south-western Sweden indicates a high discharge of freshwater, and data from south central Sweden indicate a significant glacial recession west of Mt. Billingen during the Allerød, which could have led to drainage of the Baltic Ice Lake. It has been suggested that drainage happened around 13 cal. ka ago (Uścinowicz 2006; Andrén *et al.* 2011).

In connection with sediment coring in the Arkona Basin, firm evidence of an early lowstand was for the first time identified in a sediment core. An organic-rich sediment which can be referred to this lowstand was found, and material was submitted for ^{14}C dating. The aim of this paper is to report on the age and its implications. The location of the coring site in the Arkona Basin is shown in Fig. 1. The basin is up to 49 m deep and the surface of the till is found at a depth of 30 to 70 m (Moros *et al.* 2002).

Material and methods

Sediment coring was carried out using a 10 cm diameter vibrocorer with a 6 m long steel tube. Normally, coring positions are selected from high-resolution, shallow seismic profiles, but in the deeper parts of the Arkona Basin, gas-bearing, organic-rich, Holocene marine sediments are widespread and hamper the use of seismic data. Hence the core described here was collected at a site with poor seismic data. The core was sampled at a water depth of 39.5 m, at 54°45.005′N, 13°45.876′E. The core was collected *c.* 5 km ENE of the northern end of a seismic profile published by Lemke *et al.* (1998), where the unconformity is clearly seen. The lower unconformity is also seen on seismic data collected in the region during the Baltic Pipe survey (Larsen 2004). We collected two cores at the site, designated 258000-1 and 258000-2. The first core was collected in plastic foil, split lengthwise in the ship laboratory and described and subsampled for palaeoecological analysis. The second core was collected in a PVC tube and cut into 1 m sections for storage. However, the second core penetrated somewhat deeper than the first core, and in the core catcher, clay was found with abundant plant remains underlain by clay-rich, medium-grained sand. Ten 1 kg samples from core 258000-1 and from

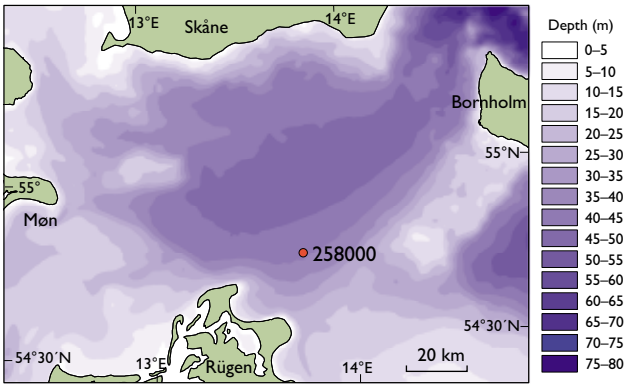

Fig. 1. Bathymetrical map of the Arkona Basin. The red dot shows the location of the studied sediment core. The core site is also shown on Fig. 5.

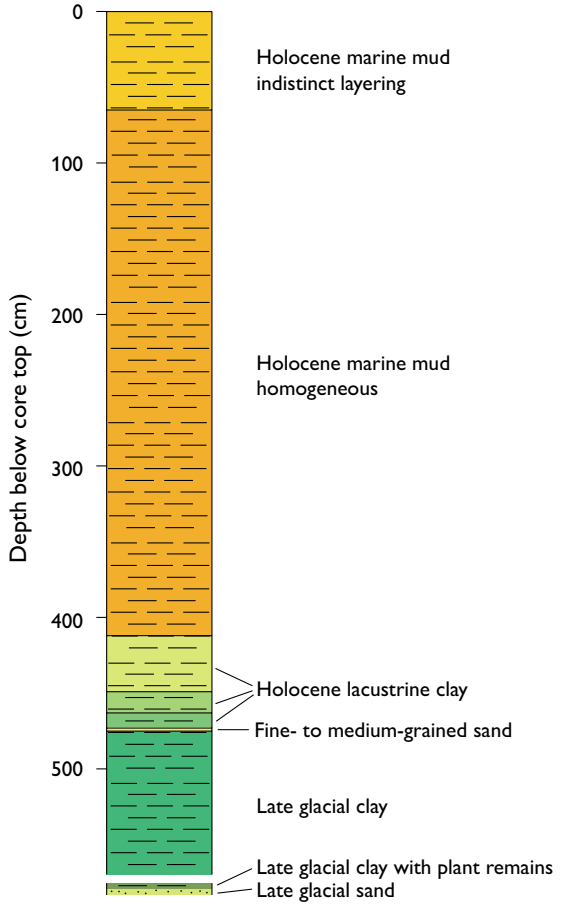

Fig. 2. Composite lithological log of core 258000 from the Arkona Basin. The two lower units were only found in core 258000-2. The core numbers refer to the system used at the Department of Marine Geology at the Institute for Baltic Sea Research in Warnemünde.

the core catcher of 258000-2 were brought to the Geological Survey of Denmark and Greenland, where the samples were wet sieved shortly after the cruise. Fruits of *Cladium mariscus* (a reed plant) were dried and shortly after submitted for accelerator mass spectrometry (AMS) radiocarbon age determination at the Leibniz Laboratory for Radiometric Dating and Isotope Research in Kiel, Germany.

Results and discussion

Core 258000-1 consists of olive-grey mud from the core top down to a depth of 412 cm (Fig. 2). Some shells of *Macoma balthica* and *Mytilus edulis* were noted, which shows that the mud is marine and of Holocene age. From 412 to 473 cm, clay without carbonate is found; this succession was divided into three units according to variations in colour and texture. Shells and head shields of Chydoridae (cladocerans, water fleas) are common, head capsules of larvae of Chironomidae (non-biting midges) are present but rare, egg cocoons of the fish leach *Piscicola geometra* were found in two samples, and statoblasts of the bryozoan *Cristatella mucedo* in four samples (Fig. 3; Table 1). These invertebrate remains show that the clay was deposited in a lake. The presence of rare remains of *Betula* sect. *Albae* (tree birch) and *Pinus sylvetris* (pine) indicates an early Holocene age. The lower part was rich in radicells (tiny roots) of reed plants, which show that the shoreline was not far away from the coring site. The clay was probably deposited in the Ancylus Lake and perhaps in the Yoldia Sea.

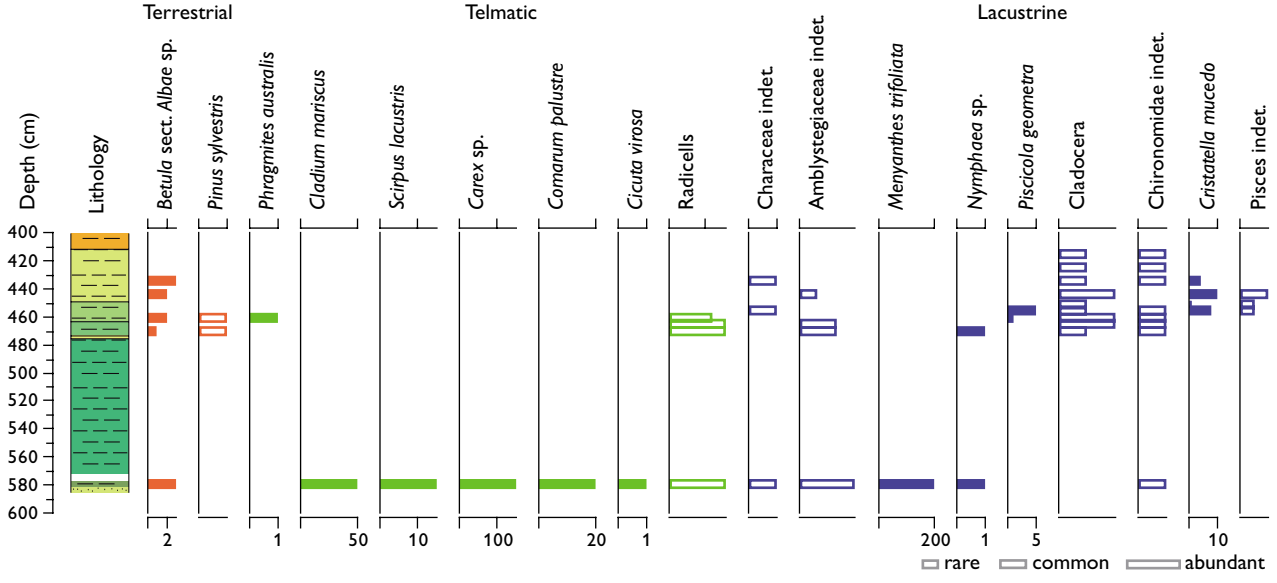

Fig. 3. Macrofossil diagram of the lower parts of cores 258000-1 and 258000-2 from the Arkona Basin. The hollow bars show remains not counted.

Table 1. Macrofossils in core 258000

Depth (cm)	*Betula* sect. *Albae* sp.	*Pinus sylvestris*	*Cladium mariscus*	*Scirpus lacustris*	*Carex* spp.	*Comarum palustre*	*Cicuta virosa*	Radicells	*Menyanthes trifoliata*	*Nymphaea* sp.	*Piscicola geometra*	Chydoridae indet.	Chironomidae indet.	*Cristatella mucedo*
412–420	–	–	–	–	–	–	–	–	–	–	–	c	r	–
420–430	–	–	–	–	–	–	–	–	–	–	–	c	r	–
430–440	3	–	–	–	–	–	–	–	–	–	–	c	r	4
440–449	2	–	–	–	–	–	–	–	–	–	–	c	–	10
449–454	–	–	–	–	–	–	–	–	–	–	–	c	–	1
454–459	–	–	–	–	–	–	–	–	–	–	5	c	r	8
459–463	2	r	–	–	–	–	–	c	–	–	1	c	r	–
463–468	–	–	–	–	–	–	–	c	–	–	–	c	r	–
468–473	1	r	–	–	–	–	–	c	–	1	–	c	r	–
c. 580	3	–	50	15	150	20	1	c	200	1	–	r	r	–

r: rare, c: common.

The clay is underlain by 2 cm of fine- to medium-grained grey sand. This thin sand layer may have been deposited at or after the final drainage of the Baltic Ice Lake. Below the sand layer and down to the bottom of the core at 570 cm, grey clay is found. This unit is rich in carbonate and barren of fossils and it is interpreted as late-glacial clay deposited in the Baltic Ice Lake during the Younger Dryas.

From the deeper core 258000-2, a sample rich in plant remains was analysed for macrofossils. The plant remains were dominated by fruits and seeds of the telmatic plants *Menyanthes trifoliata* and fruits of *Carex*, mainly *Carex vesicaria*, *Cladium mariscus*, *Scirpus lacustris*, *Comarum palustris* and *Cicuta virosa* (Fig. 3). Limnic plants and animals were represented by a seed of *Nymphaea* sp., common stems of Amblystegiaceae (mosses, not shown), rare shells and head shields of Chydoridae and rare head capsules of larvae of Chironomidae. The fossil assemblage and in particular the occurrence of abundant remains of telmatic plants show that the sediment was deposited in shallow water near the shore of a lake, probably just outside the reed belt. The presence of fruits of *Betula* sect. *Albae* indicates that the land was covered by birch forests.

The sample of *Cladium mariscus* fruits yielded an age of 10 980 ± 55 ^{14}C years BP (KIA-21680). This is calibrated to 12.674–13.069 cal. ka BP, according to the INTCAL09 dataset, which corresponds to the youngest part of the Allerød chronozone or the oldest part of the Younger Dryas. An age corresponding to the warm Allerød Chronozone was expected from the fossil assemblage, because *Cladium mariscus* and *Scirpus lacustris* are thermophilous plants. *Cladium mariscus* was recorded from late-glacial deposits in south-eastern Denmark by Bennike & Jensen (1995), but its presence was probably due to down-core contamination, and there are no secure records of it from late-glacial deposits in

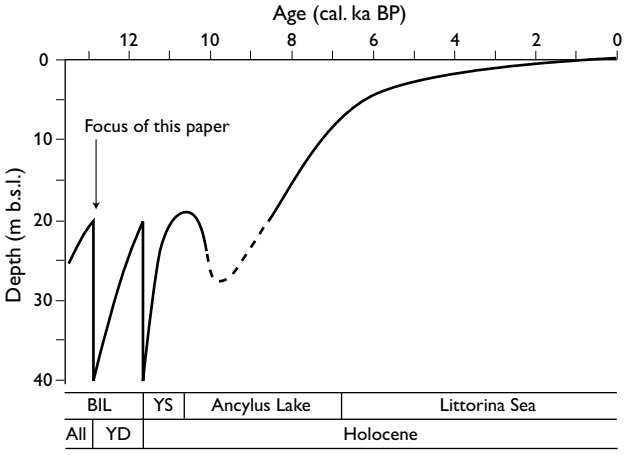

Fig. 4. Tentative curve showing relative shore-level changes in the Arkona Basin during the late-glacial and the Holocene. **ka**: kilo-annum (1000 years), **BIL**: Baltic Ice Lake, **YS**: Yoldia Sea, **All**: Allerød, **YD:** Younger Dryas. Modified from Bennike & Jensen (1998).

Denmark (Iversen 1954; Jensen *et al.* 1997; Bennike *et al.* 2004). Its northern geographical limit during the Allerød may thus have been located near the coring site.

As the core was collected at a water depth of 39.5 m and the sample comes from a core depth of *c.* 5.8 m, the dated sample comes from a depth of *c.* 45.3 m below present sea level. The sediment is fine-grained and was probably deposited at a water depth of several metres, and we suggest that the shore level during deposition was around 40 m lower than at present. Both before and after this lowstand episode, the relative shore level was around 20 m below the present sea level according to Jensen *et al.* (1997). This implies that the shore-level fall towards the end of the Allerød chronozone was of the same magnitude as the fall at the Younger Dryas – Holocene transition, i.e. considerably more than 5–10 m as suggested by Björck (1995). The new data allow us to modify the shore-level model proposed by Bennike & Jensen (1998) and extend it back in time. Figure 4 shows a new model for relative shore-level changes in the Arkona Basin from the last deglaciation to the present. It is seen that transgressions were interrupted by sudden regressions.

South of the Arkona Basin, late-glacial sediments reach elevations lower than 20 m (Lampe 2005). However, the relationship between these sediments and the regional shore level of the southern Baltic Basin is uncertain. Some of the sediments are glaciofluvial and were deposited above shore level, other late-glacial sediments may have been deposited in local basins, perhaps in part dammed by bodies of stagnant ice.

At present, the most enigmatic stage in the history of the Baltic Basin is that of the early Holocene Ancylus Lake; the shore-level curve for this stage has been drawn as a dashed line on Fig. 4. It has been suggested that the Ancylus regres-

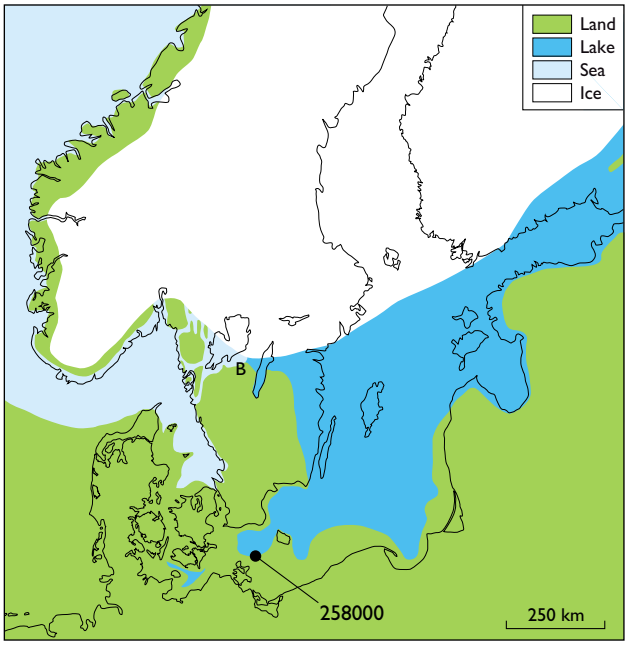

Fig. 5. Generalised palaeogeographical map of the Baltic region after the drainage at the end of the Allerød. Modified from Björck (1995) and Wohlfahrt *et al.* (2008). **B**: Billingen.

sion was around 20 m (Björck 1995), but more recently figures of 5 m and 10 m were also proposed (Björck *et al.* 2008; Rosentau *et al.* 2013). No erosional unconformity has been reported from the south-western Baltic Basin that formed during this regression (Jensen *et al.* 1999).

Figure 5 shows a model of the palaeogeography of the Baltic Basin after the late Allerød drainage. Although the Baltic Basin was now at the same level as the sea, it probably remained a freshwater lake. The connection to the sea was narrow, and we suggest that the outflow of huge amounts of fresh water coming from rivers and from the melting ice sheet hindered seawater from entering the Baltic Basin.

Concluding remarks

The rich occurrence of remains of reed plants at a depth of 45 m below sea level in the Arkona Basin provides firm evidence of a lowstand. A radiocarbon age shows that it occurred at the end of the Allerød Chronozone. We suggest that the shore level fell about 20 m, similar to the shore-level fall at the Younger Dryas – Holocene boundary.

Acknowledgements

The captain and crew of the former R/V *Alexander von Humboldt* from the Institute for Baltic Sea Research in Warnemünde are thanked for their help during the marine cruise. This paper is dedicated to the memory of Wolfram Lemke, who invited us to take part in the cruise during which cores 258000-1 and 258000-2 were collected.

References

Andrén, T., Björck, S., Andrén, E., Conley, D., Zillén, L. & Anjar, J. 2011: The development of the Baltic Sea during the last 130 ka. In: Harff, J. *et al.* (eds): The Baltic Sea Basin, 75–97. Berlin: Springer Verlag.

Bennike, O. & Jensen, J.B. 1995: Near shore Baltic Ice Lake deposits in Fakse Bugt, southeast Denmark. Boreas **24**, 185–195.

Bennike, O. & Jensen, J.B. 1998: Late- and postglacial shore level changes in the southwestern Baltic Sea. Bulletin of the Geological Society of Denmark **45**, 27–38.

Bennike, O., Jensen, J.B., Lemke, W., Kuijpers, A. & Lomholt, S. 2004: Late- and postglacial history of the Great Belt, Denmark. Boreas **33**, 18–33.

Björck, S. 1995: A review of the history of the Baltic Sea, 13.0–8.0 ka BP. Quaternary International **27**, 19–40.

Björck, S., Andrén, T. & Jensen, J.B. 2008: An attempt to resolve the partly conflicting data and ideas on the Ancylus–Littorina transition. Polish Geological Institute Special Papers **23**, 21–26.

Iversen, J. 1954: The Late-Glacial flora of Denmark and its relation to climate and soil. Danmarks Geologiske Undersøgelse II. Række **80**, 87–119.

Jensen, J.B., Bennike, O., Witkowski, A., Lemke, W. & Kuijpers, A. 1997: The Baltic Ice Lake in the southwestern Baltic: sequence-, chrono- and biostratigraphy. Boreas **26**, 217–236.

Jensen, J.B., Bennike, O., Witkowski, A., Lemke, W. & Kuijpers, A. 1999: Early Holocene history of the southwestern Baltic Sea: the Ancylus Lake stage. Boreas **29**, 437–453.

Lampe, R. 2005: Lateglacial and Holocene water-level variations along the NE German Baltic Sea coast: review and new results. Quaternary International **133–134**, 121–136.

Larsen, C.S. 2004: Sequence stratigraphy based on vibrocore description and shallow seismic data from the south-western Baltic Sea. Danmarks og Grønlands Geologiske Undersøgelse Rapport **2004/53**, 28 pp.

Lemke, W., Endler, R., Tauber, F., Jensen, J.B. & Bennike, O. 1998: Late- and postglacial sedimentation in the Tromper Wiek (western Baltic). Meyniana **50**, 155–173.

Moros, M., Lemke, W., Kuijpers, A., Endler, R., Jensen, J.B., Bennike, O. & Gingele, F. 2002: Regression and transgressions of the Baltic basin reflected by a new high-resolution deglacial and postglacial lithostratigraphy for Arkona Basin sediments (western Baltic Sea). Boreas **31**, 151–162.

Rosentau, A. *et al.* 2013: Stone Age settlement and Holocene shore displacement in the Narva-Luga Klint Bay area, eastern Gulf of Finland. Boreas. *http://dx.doi.org/10.1111/bor.12004*

Uścinowicz, S. 2006: A relative sea-level curve for the Polish southern Baltic Sea. Quaternary International **145–146**, 86–105.

Wohlfarth, B., Björck, S., Funder, S., Houmark-Nielsen, M., Ingólfsson, Ó., Lunkka, J.-P., Mangerud, J., Saarnisto, M. & Vorren, T. 2008: Quaternary of Norden. Episodes **31**, 73–81.

Authors' address

Geological Survey of Denmark and Greenland, Øster Voldgade 10, DK-1350 Copenhagen K, Denmark. E-mail: *obe@geus.dk*

Late glacial to early Holocene development of southern Kattegat

Carina Bendixen, Jørn Bo Jensen, Ole Bennike and Lars Ole Boldreel

The Kattegat region is located in the wrench zone between the Fennoscandian shield and the Danish Basin that has repeatedly been tectonically active. The latest ice advances during the Quaternary in the southern part of Kattegat were from the north-east, east and south-east (Larsen *et al*. 2009). The last deglaciation took place at *c*. 18 to 17 ka BP (Lagerlund & Houmark-Nielsen 1993; Houmark-Nielsen *et al*. 2012) and was followed by inundation of the sea that formed a palaeo-Kattegat (Conradsen 1995) with a sea level that was relatively high because of glacio-isostatic depression. Around 17 ka BP, the ice margin retreated to the Øresund region and meltwater from the retreating ice drained into Kattegat. Over the next millennia, the region was characterised by regression because the isostatic rebound of the crust surpassed the ongoing eustatic sea-level rise, and a regional lowstand followed at the late glacial to Holocene transition (Mörner 1969; Thiede 1987; Lagerlund & Houmark-Nielsen 1993; Jensen *et al*. 2002a, b).

Major parts of Kattegat are characterised by thick successions of Late Weichselian and Holocene sediments (Mörner 1969; Bergsten & Nordberg 1992; Gyldenholm *et al*. 1993). At around 9.6 ka BP, a large lagoon–estuary environment in southern Kattegat was partly blocked by transgressive, coastal barrier islands and spits (Bennike *et al*. 2000; Jensen *et al*. 2002a).

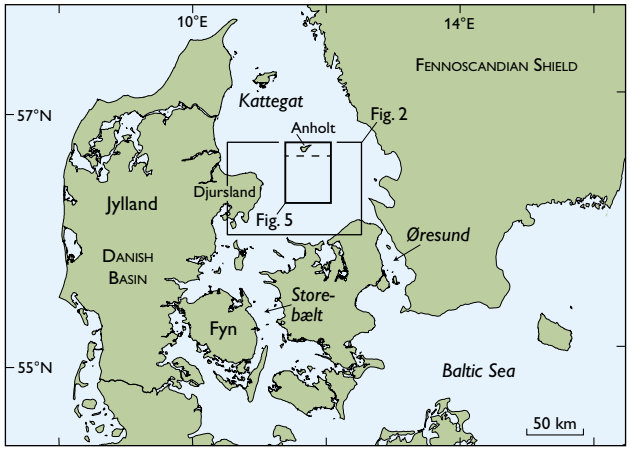

Fig. 1. Map of Denmark showing the location of the study area of Fig. 5 in southern Kattegat.

The aim of this paper is to describe the late glacial and early Holocene development of southern Kattegat, based on a recent study (Bendixen 2012). The study area covers 1696.5 km² and is located south of the island of Anholt in the southern part of Kattegat (Figs 1, 2). The south-western part of the area is shallow but water depths increase to the north-east where depths over 40 m are found (Fig. 2). Two distinct submarine channels running nearly N–S and NE–SW were probably formed by subglacial meltwater erosion; these channels are partly filled by late glacial and Holocene sediments. The area can be seen as a transitional shallow-water area at the entrance to the Baltic Sea (Bennike *et al*. 2000). Detailed 2D seismic work will be conducted in the region over the next years, which will improve the basis for interpretations in the coming years.

Methods

The data used in this study consist of shallow single-channel seismic profiles and sediment cores. The seismic data comprise boomer data acquired by R/V *Alexander von Humboldt* from 1997 to 1999 and sparker data acquired in 2011 using M/V *Laura*. Navigation was based on differential GPS. The sediment cores were collected with a 6 m long vibrocorer

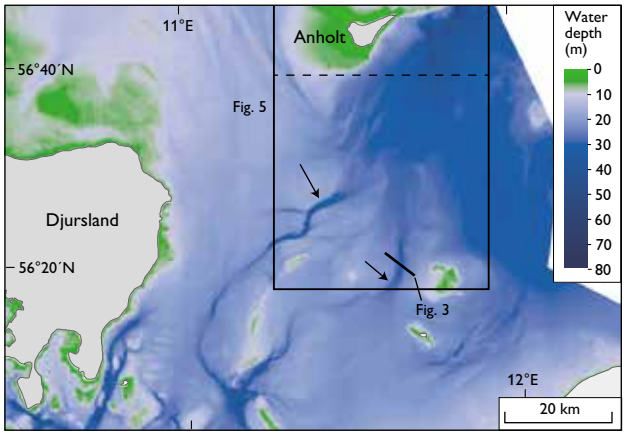

Fig. 2. Bathymetric map of the study area in southern Kattegat showing the two incised palaeo-channels from Storebælt (arrows) that drained into the Kattegat and the location of the shallow seismic profile shown in Fig. 3. The white areas to the east are Swedish territorial waters.

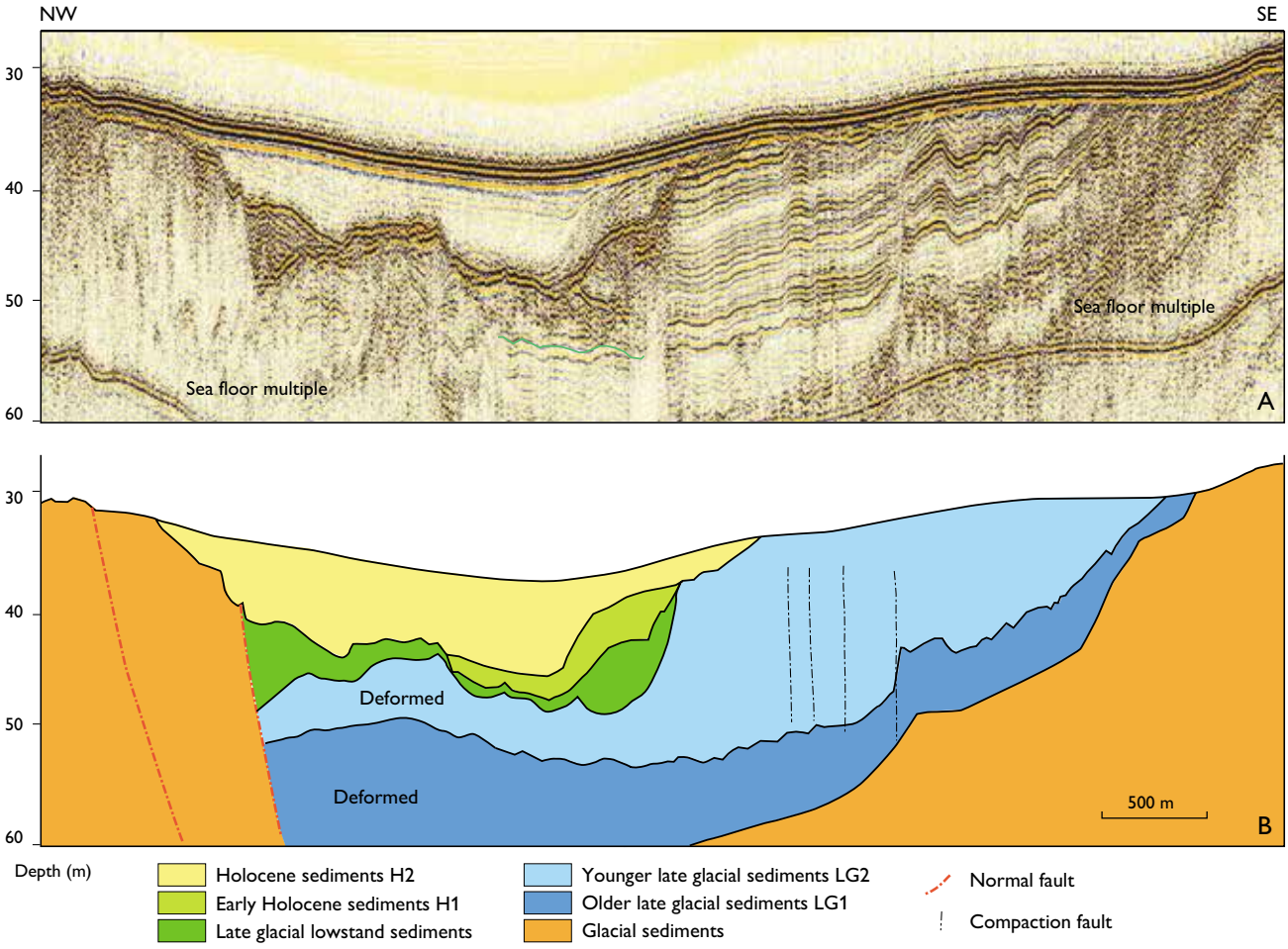

Fig. 3. **A**: Selected part of shallow seismic profile R3_021a obtained by a boomer. **B**. Preliminary interpretation. For location see Fig. 2.

from *Laura* in 2011. The cores were cut into 1 m long sections that were shipped to the Geological Survey of Denmark and Greenland where they were split, photographed, described and subsampled in the laboratory.

Prior to interpreting the seismic profiles, ProMAX seismic data processing software was used to optimise the data quality. The boomer data were subjected to frequency filtering and the sparker data were subjected to the Kirchhoff time-migration method. Interpretation of the seismic data was carried out using the program SeisVision.

Results and discussion

Two late glacial units (LG1 and LG2) have been identified (Fig. 3); they show high variability in thickness in the area studied. The sediments were deposited during a sea-level highstand period, which can be seen from the internal seismic pattern. The older LG1 unit shows draping parallel reflections of low amplitude whereas the LG2 unit shows parallel reflections of high amplitude (Fig. 3). The units are divided by an erosional unconformity in the north-eastern parts of the study area, whereas continued deposition occurred in the west where no unconformity is found. A single radiocarbon dating of a shell of *Hiatella arctica* from LG1 gave an age of 16.1–16.6 cal. ka BP, and dating of shells from LG2 gave ages of 13.3–15.5 cal. ka BP (Jensen *et al.* 2002a).

Distinct normal faults cut the late glacial deposits. Detailed interpretations of the seismic profiles show that faulting occurred during the last stage of the deposition of the LG2 unit. This is evident because the uppermost part was not affected by the faulting whereas the lower-lying sediments are cut by the faults. This finding is consistent with the conclusions of Jensen *et al.* (2002b).

The NW–SE-orientated sparker profile R3_021a (Fig. 3) shows major bounding faults that cut the late glacial sediments to the north-west and south-east and hence limit the distribution of the younger sediments. Within the late glacial units, two major faults are interpreted as strike-slip faults. The faulting postdates the uppermost part of the LG2 unit and was possibly a result of the deglaciation of the Kat-

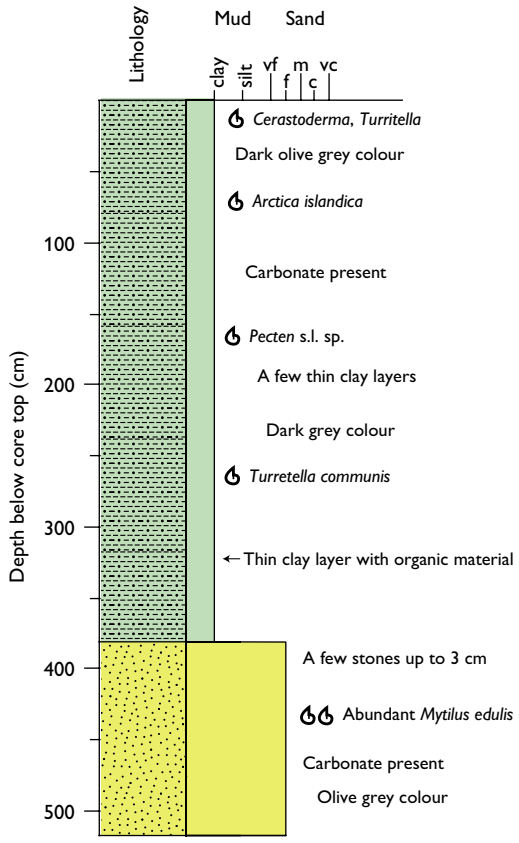

Fig. 4. Sedimentological log of vibrocore DGU 561118.10. For location see Fig. 5.

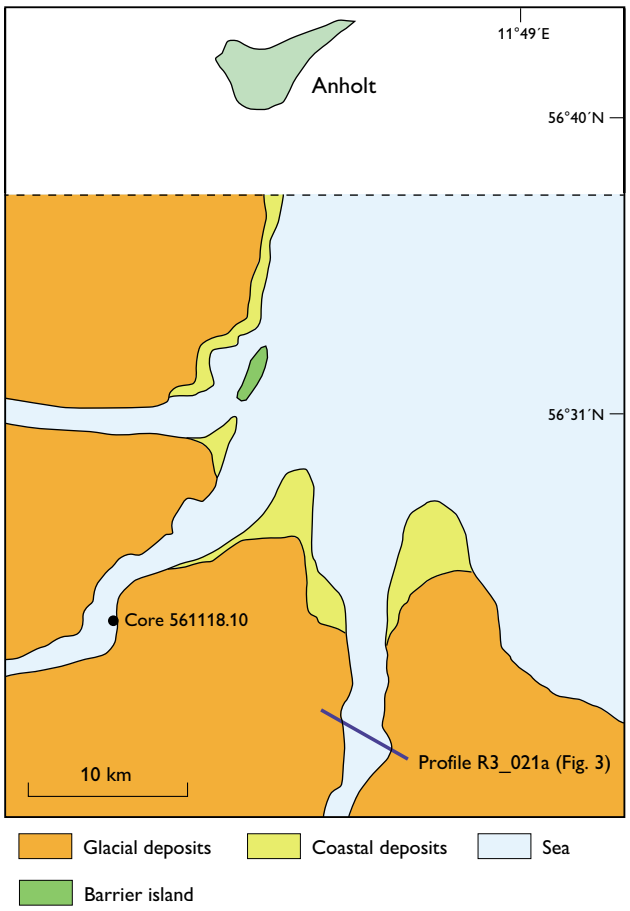

Fig. 5. Palaeogeographic map of the area south of Anholt in Kattegat in early Holocene showing glacial deposits to the south and west, coastal sandy deposits formed by prograding shorelines and a barrier island. The present-day form of Anholt is included to show the location of the map.

tegat region that led to isostatic uplift and reactivation of older faults. This tectonic event may have contributed to the opening of Storebælt.

The late glacial units between the faults show an internal pattern with contorted reflectors. The late glacial deposits have been reworked by faulting and a significant erosional unconformity is found between the late glacial and the Holocene sediments. This unconformity formed during the late glacial – early Holocene lowstand period.

Above the erosion surface, two Holocene units can be separated on the basis of their difference in reflection pattern and infill direction, with H1 showing infill from the south-east and H2 from the north-east. Two lithological units presumably of Holocene age were also found in sediment core no. DGU 561118.10 collected at 56°23.165´N, 11°22.0´E from a water depth of 38.0 m (Fig. 4). The core was 518 cm long and consisted of 136 cm sand with abundant shells of the common blue mussel *Mytilus edulis* that is characteristic of shallow water, overlain by 328 cm of mud with shells of *Turritella communis*, *Arctica islandica*, *Pecten* s.l. sp. and other marine molluscs that are characteristic of deeper water. The marked lithological change 382 cm below the core top probably corresponds to the boundary between units H1 and H2 (Bendixen 2012). We suggest that the sand was deposited during the early Holocene when sea level was low, whereas the mud was deposited after the relative sea level had increased. Radiocarbon dating of Holocene sub-littoral sand deposits in the region has yielded ages of *c.* 11–10 cal. ka BP (Bennike *et al.* 2000; Jensen *et al.* 2002a).

A palaeogeographic map of the region illustrates northward coastal progradation with spits and barriers with back-barrier-enclosed environments in which finer-grained sediments were deposited (Fig. 5).

Conclusions

The late glacial sediments in southern Kattegat consist of a lower and an upper sequence deposited during relatively high sea level; the boundary between the sequences shows an erosional surface towards the north-east. The distribution of the sediments is limited by major faults which were initiated during deposition of the uppermost part of the youngest late glacial unit.

Major faults bounding the late glacial sediments were active during the deposition of the uppermost part of the youngest late glacial unit. We suggest that strike-slip movements occurred due to isostatic reactivation of the Fennoscandian Border Zone and upward movement of the late glacial sediments. An early Holocene lowstand level is identified as an erosional surface, underlying units H1 and H2. Initial transgression resulted in coastal progradation and back-barrier-enclosed environments with deposition of finer-grained sediments (H2) in the former incised valleys.

Acknowledgement

The Danish Nature Agency (Naturstyrelsen) funded the work.

References

Bendixen, C. 2012: Interpretation of shallow seismic and sediment cores from the area stretching from the southern part of Kattegat to the Great Belt in the period Late-Weichselian to early Holocene **1, 2**, 74 pp + 102 pp. Unpublished M.Sc. thesis, University of Copenhagen, Denmark.

Bennike, O., Jensen, J.B., Konradi, P.B., Lemke, W. & Heinemeier, J. 2000: Early Holocene drowned lagoon deposits from the Kattegat, southern Scandinavia. Boreas **29**, 272–286.

Bergsten, H. & Nordberg, K. 1992: Late Weichselian marine stratigraphy of the southern Kattegat, Scandinavia: evidence for drainage of the Baltic Ice Lake between 12,700 and 10, 300 years BP. Boreas **21**, 223–252.

Conradsen, K. 1995: Late Younger Dryas to Holocene palaeoenvironments of the southern Kattegat, Scandinavia. The Holocene **5**, 447–456.

Gyldenholm, K.G., Lykke-Andersen, H. & Lind, G. 1993: Seismic stratigraphy of the Quaternary and its substratum in southeastern Kattegat, Scandinavia. Boreas **22**, 319–327.

Houmark-Nielsen, M., Linge, H., Fabel, D., Schnabel, C., Xu, S., Wilcken, K.M. & Binnie, S. 2012: Cosmogenic surface exposure dating the last deglaciation in Denmark: discrepancies with independent age constraints suggest delayed periglacial landform stabilisation. Quaternary Geochronology **13**, 1–17.

Jensen, J.B., Kuijpers, A., Bennike, O. & Lemke, W. 2002a: BALKAT – The Baltic Sea without frontiers (English version). Geologi, Nyt fra GEUS **2002**(4), 20 pp.

Jensen, J.B., Petersen, K.S., Konradi, P., Kuijpers, A., Bennike, O., Lemke, W. & Endler, R. 2002b: Neotectonics, sea-level changes and biological evolution in the Fennoscandian border zone of the southern Kattegat Sea. Boreas **31**, 133–150.

Lagerlund, E. & Houmark-Nielsen, M. 1993: Timing and pattern of the last deglaciation in the Kattegat region, southwest Scandinavia. Boreas **22**, 337–347.

Larsen, N.K., Knudsen, K.L., Krohn, C.F., Kronborg, C., Murray, A.S. & Nielsen, O.B. 2009: Late Quaternary ice sheet, lake and sea history of southwest Scandinavia: a synthesis. Boreas **38**, 732–761.

Mörner, N.-A. 1969: The Late Quaternary history of the Kattegatt sea and the Swedish west coast. Déglaciation, shorelevel displacement chronology, isostasy and eustasy. Sveriges Geologiska Undersökning Ser. C, **63**(3), 487 pp.

Thiede, J. 1987: The Late Quaternary Skagerrak and its depositional environment. Boreas **16**, 425–432.

Authors' addresses

C.B., J.B.J., O.B. & L.O.B.*, *Geological Survey of Denmark and Greenland, Øster Voldgade 10, DK-1350 Copenhagen K, Denmark*. E-mail: *cb1@geus.dk*

* Also: *Department of Geosciences and Natural Resource Management, University of Copenhagen, Øster Voldgade 10, DK-1350 Copenhagen K, Denmark*.

Terrain subsidence detected by satellite radar scanning of the Copenhagen area, Denmark, and its relation to the tectonic framework

Peter Roll Jakobsen, Urs Wegmuller, Ren Capes and Stig A. Schack Pedersen

In the European Union (EU) project Terrafirma, which is supported by the European Space Agency to stimulate the Global Monitoring Environment System, we are using the latest technology to measure terrain motion on the basis of satellite radar data. The technique we employ is known as persistent scatterer interferometry (PSI); in Denmark, it was previously used to map areas of subsidence susceptible to flooding in the Danish part of the Wadden Sea (Vadehavet) area (Pedersen *et al.* 2011). That study was part of the flooding risk theme under the TerraFirma Extension project. Another coastal protection monitoring activity in the EU seventh framework project SubCoast followed, in which the low-lying south coast of Lolland, prone to flooding, was studied. The Geological Survey of Denmark and Greenland (GEUS) is also involved in the three-year EU collaborative project PanGeo in which GEUS is one of 27 EU national geological surveys. The objective of PanGeo is to provide free and open access to geohazard information in support of the Global Monitoring Environment System. This will be achieved by providing a free, online geohazard information service for the two largest cities in each EU country, i.e. 52 towns throughout Europe with *c.* 13% of EU's population.

The Danish cities selected for investigation under Terrafirma are Copenhagen and Aalborg. Capitals have first priority, and Aalborg was chosen because of good satellite data. In this paper, PSI data for Copenhagen are presented together with interpretations of terrain displacement (Fig. 1).

PSI processing of satellite radar data for Copenhagen

The satellite data covering Copenhagen were obtained from the descending track D480 ERS satellite in the period 1992–2000. The PSI processing was carried out by Gamma Remote Sensing AG, using a method that was carefully qualified and validated in the Terrafirma project (Crosetto *et al.* 2008). GEUS carried out the analysis using the program ArcGIS, in which geological and topographical data provide the basis for interpretation. Based on the PSI data, nine areas were outlined in which subsidence had occurred over the period 1992–2000. The areas are between 0.1 and 2.2 km^2 and here we present two of them. Apart from those mentioned above, minor subsidence differences of regional extent have been recognised; these are interpreted as tectonic.

The Copenhagen area that was processed has a size of 960 km^2 with a reference point at 55.685668°N, 12.493937°E. A total of 419 660 PSI points were identified, corresponding to 437 points per km^2. The majority of the points (94.5%) show small rates of vertical motion, i.e. between –1.5 and +1.5 mm/year. A small number of points (1.6%) show subsidence rates of 3.5 to 1.5 mm/year, and a few (0.2%) show subsidence rates of more than 3.5 mm/year. A few points (0.4%) show uplift rates between 1.5 and 3.5 mm/year; these are regarded as scattered uncertainties in relation to the average annual motion rate of 0.35 mm/

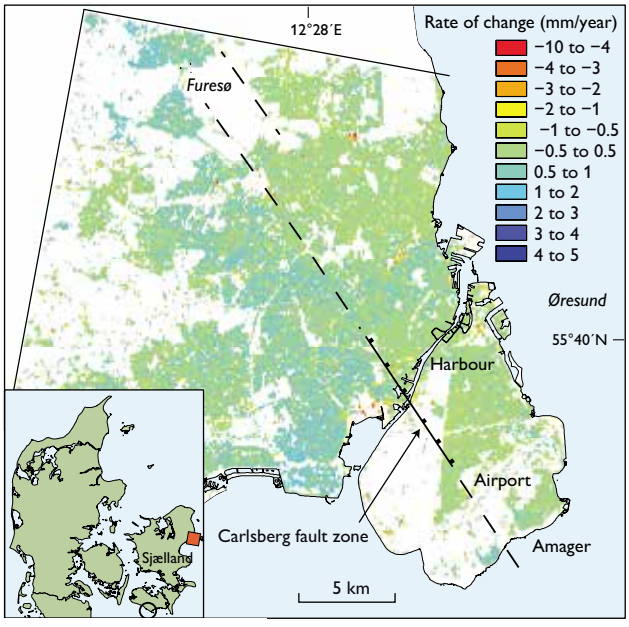

Fig. 1. Map of Greater Copenhagen showing the area covered by PSI data. Vertical movements are represented in a raster grid showing the average movement in 100 × 100 m squares. The concentrations of yellow-red colours show areas with maximum rates of subsidence. Note the regional difference in light and dark green colours which might be caused by tectonic subsidence east of the Carlsberg fault zone.

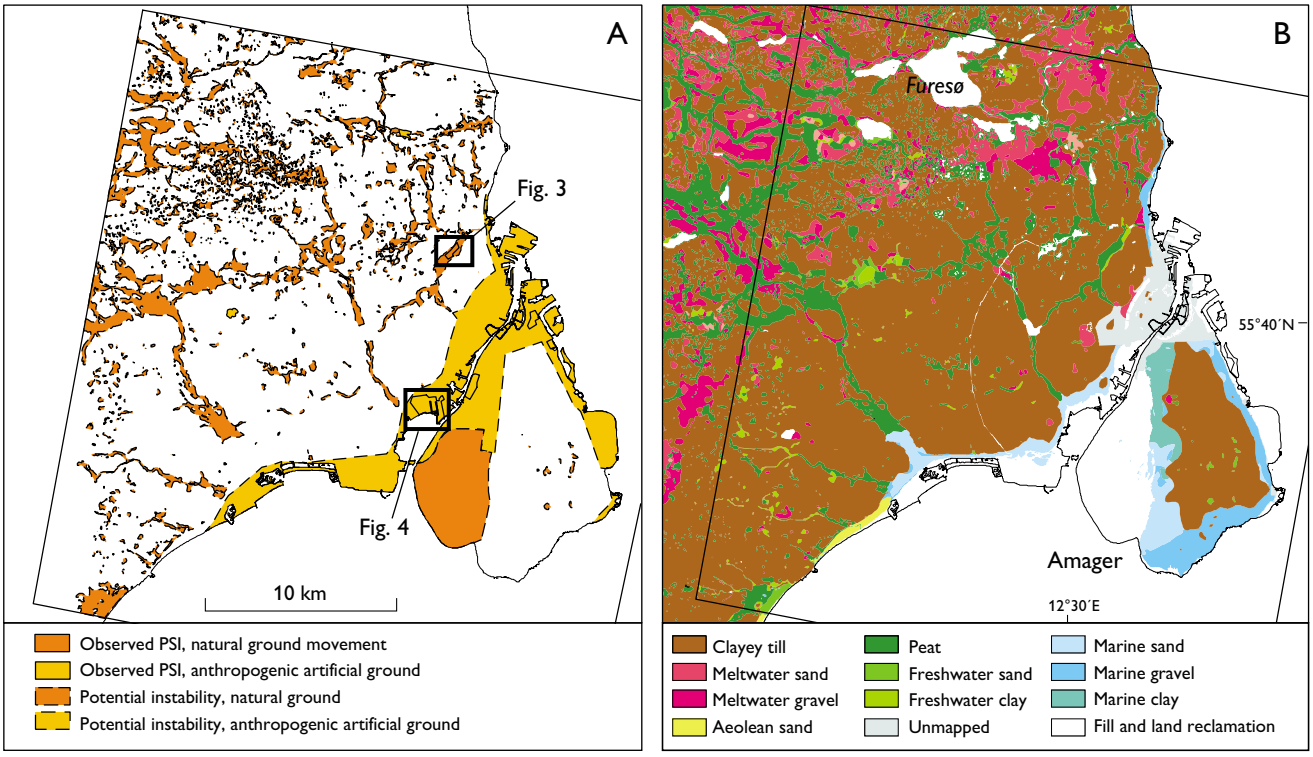

Fig. 2. Correlation between ground stability and surficial deposits in Greater Copenhagen. **A**: Map of classified soft ground areas in Greater Copenhagen. The rectangles show the location of two examples of subsiding areas described in the text. **B**: Geological map of surficial deposits. The fill and reclamation areas did not exist when the region was mapped in 1899 (Rørdam 1899).

year for the entire area, with a standard deviation of annual motion rate amounting to 0.74 mm/year.

The geology of Copenhagen and its relation to subsidence areas

Copenhagen is located on the east coast of the island of Sjælland, which is separated from Sweden by the strait of Øresund (Fig. 1). Part of the city extends onto the smaller, neighbouring island of Amager, and the strait between the two islands is the site of Copenhagen harbour. The airport of Copenhagen, Kastrup, is situated on the southern part of Amager. Most parts of Copenhagen are lowland, i.e. a few metres above sea level, but the terrain rises northwards and westwards where it reaches heights of 50 m a.s.l.

The bedrock of Copenhagen is dominated by Danian limestone. Two units are found: the Stevns Klint Formation that comprises bryozoan limestone rich in chert beds (Surlyk *et al.* 2006) and the København Kalk Formation which is dominated by calcarenitic, calcilutitic limestone with chert beds (Stenestad 1976). An important tectonic feature is the Carlsberg fault zone (Stenestad 1976; Jakobsen *et al.* 2002) that can be followed from the south coast of Amager northwestwards to Furesø (Figs 1, 2).

The Quaternary deposits of Copenhagen comprise ice age and postglacial deposits. The latter consist of terrestrial sediments that accumulated in streams and bogs, and marine sand and gravel which accumulated along the coasts (Fig. 2B). The ice-age deposits are dominated by a widespread young till unit overlying meltwater sand and gravel, and more local, older till units and meltwater clay. Tunnel valleys, depressions in hummocky moraine and stream valleys form wetlands around Copenhagen, where freshwater deposits, mainly peat, accumulated in the Holocene. The western part of Amager is reclaimed sea floor with marine and coastal deposits. Areas with dump and fill deposits occur along the coasts or in peat-dominated depressions and may be characterised by high rates of subsidence.

Examples of areas with subsidence

Based on the geology and records of man-made ground, there are three types of areas with potential risk of subsidence, namely areas underlain by postglacial peat deposits (amounting to 70 km^2), large areas of man-made ground (53 km^2) and small areas of reclaimed land (19.4 km^2).

One of the areas with subsidence identified from the PSI data in the period 1992–2000 is Lersøparken (Figs 2, 3) with

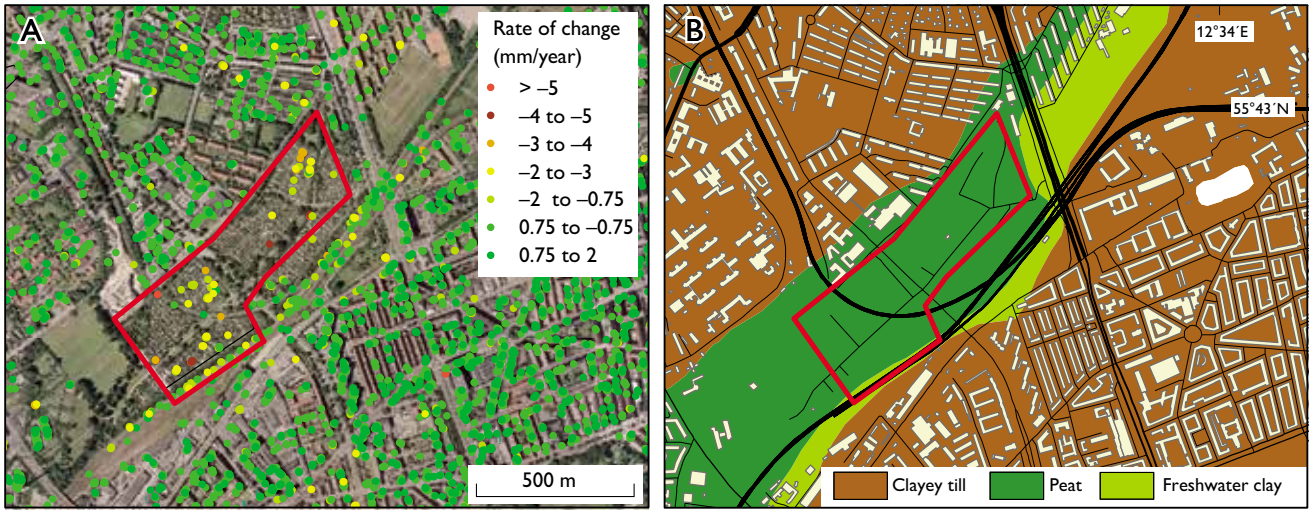

Fig. 3. Detailed map of Lersøparken (red frame). **A**: Orthophotograph of the area with PSI points representing areas of subsidence. **B**: Geological map of the area showingt clay and peat in the NE–SW-striking valley. For location see Fig. 2.

a subsidence rate between 2 and 5 mm/year. The 0.22 km^2 subsiding area is situated in a NE–SW-trending valley where postglacial peat has accumulated above clay in an elongated depression (Fig. 3). The depression was used as a dump site in the period from 1880 to 1920. Peat is easily compressed, and compaction of the waste is an additional factor accounting for the high subsidence rate.

Kalveboderne with Valbyparken and Tippen along the coast of southern Copenhagen is another example of an area with subsidence (Figs 2, 4). A considerable number of PSI points show subsidence of more than 4 mm/year. This area of 1.4 km^2 was used as a dump from 1913 to 1960 when waste was dumped on the beach and in the adjacent shallow sea. In 1961, the area was extended with fill to the present artificial shoreline. Compaction of the soft, natural sediments and waste followed by fill deposits lead to subsidence.

Subsidence related to tectonic features

The most important tectonic feature in the subsurface of Copenhagen is the SE–NW-striking Carlsberg fault zone (Fig. 1). The fault is part of a number of relay faults related

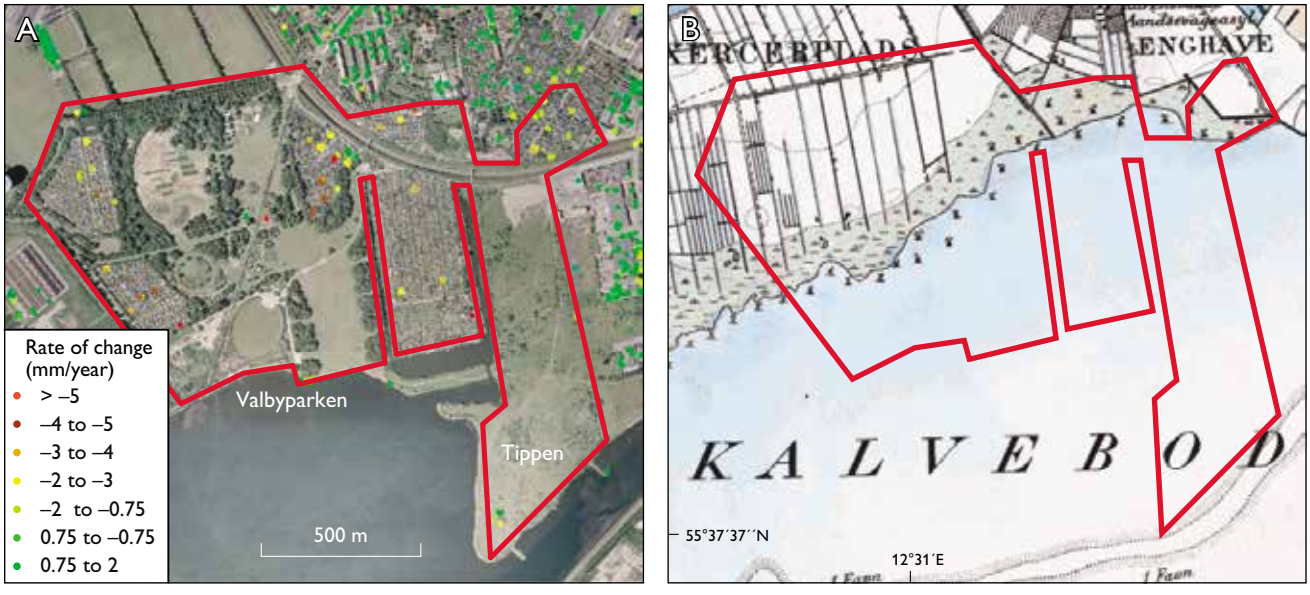

Fig. 4. Detailed map of the Kalveboderne area where waste and fill have been deposited on Holocene marine and coastal deposits. **A**: Orthophotograph with PSI data points. **B**: An old topographical map showing the same area prior to deposition of waste and fill. For location see Fig. 2.

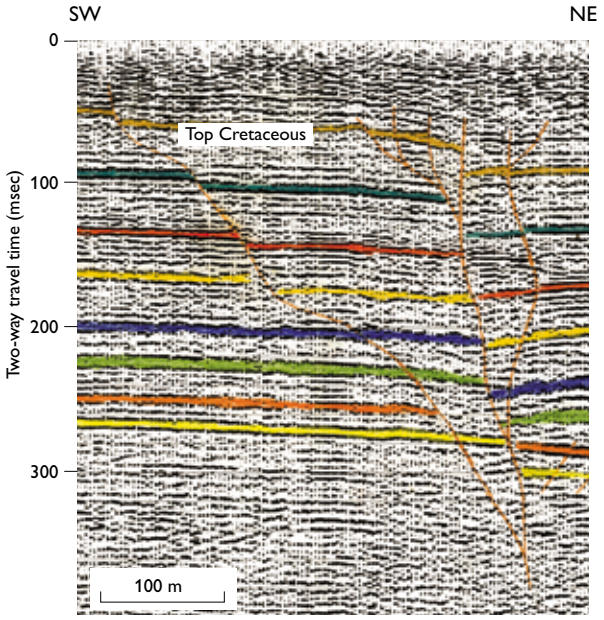

Fig. 5. Seismic cross-section of the Carlsberg fault zone (from Jakobsen *et al.* 2002). Maastrichtian chalk is found at the top of the western block, whereas Danian limestone is present at the top of the eastern block.

to the Tornquist–Sorgenfrei wrench fault zone. A seismic cross-section of the Carlsberg fault zone shows that it can be classified as a negative flower structure with a mean vertical offset of 50–100 m of the limestone deposits. The hanging block is found north-east of the fault zone (Fig. 5; Fallesen 1995; Jakobsen *et al.* 2002). The limestone in the fault zone itself is strongly fractured as documented by low seismic velocity in the fault-affected zone (Nielsen *et al.* 2005). There is clear evidence of weak, regional subsidence east of the fault zone, i.e. the area of the down-thrown fault block (Fig. 1). The Carlsberg fault zone can be followed north-westwards to Furesø, which is the deepest lake in Denmark, and we suggest that the shape of the lake is governed by displacement along the fault zone. This would be an alternative explanation of the origin of the lake, which has hitherto been regarded as formed from a combination of tunnel valleys and kettle holes. The subsidence recorded by the PSI points may correspond to subsidence rates in the Copenhagen area recorded from traditional levelling (Mark & Jensen 1982). Groundwater extraction may also influence subsidence, which could have been the case for Amager. However, the groundwater level on Amager was stable during the period of the satellite data acquisition.

References

Crosetto, M., Monserrat, O., Adam, N., Parizzi, A., Bremmer, C., Dortland, S., Hanssen, R.F. & van Leijen, F.J. 2008: Validation of existing processing chains in Terrafirma stage 2, final report, 15 pp., *http://www.terrafirma.eu.com/validation/ValProj/Final%20Reports/ValProj_Final_report.pdf*.

Fallesen, J. 1995: Stratigraphy and structure of the Danian Limestone on Amager, examined with geophysical investigations – especially with regard to the Carlsberg Fault. Unpublished MSc thesis, University of Copenhagen, Denmark

Jakobsen, P.R., Fallesen, J. & Knudsen, C. 2002: Strukturer i den københavnske undergrund – folder, forkastninger og sprækker. Dansk Geoteknisk Forening Bulletin **19**, 19–29.

Mark, A. & Jensen, J.E. 1982: Niveauændringer i København bestemt ud fra gentagne præcisionsnivellementer. Landinspektøren **32**, 10–21.

Nielsen, L., Thybo, H. & Jørgensen, M.I. 2005: Integrated seismic interpretation of the Carlsberg Fault zone, Copenhagen, Denmark. Geophysical Journal International **162**, 461–478.

Pedersen, S.A.S., Cooksley, G., Gaset, M. & Jakobsen, P.R. 2011: Detection of terrain changes in southern Denmark using persistent scatterer interferometry. Geological Survey of Denmark and Greenland Bulletin **23**, 41–44.

Rørdam, K. 1899: Beskrivelse til geologisk Kort over Danmark, (i Maalestok 1:100,000). Kortbladene Kjøbenhavn og Roskilde. Danmarks Geologiske Undersøgelse I. Række **6**, 88 pp.

Stenestad, E. 1976: Københavnsområdets geologi især baseret på citybaneundersøgelserne. Danmarks Geologiske Undersøgelse III. Række **45**, 149 pp. (with summary in English).

Surlyk, F., Damholt, T. & Bjerager, M. 2006: Stevns Klint: uppermost Maastrichtian chalk, Cretaceous–Tertiary boundary, and lower Danian bryozoan mound complex. Bulletin of the Geological Society of Denmark **54**, 1–48.

Authors' addresses

P.R.J. & S.A.S.P, *Geological Survey of Denmark and Greenland, Øster Voldgade 10, DK-1350 Copenhagen K, Denmark*. E-mail: *prj@geus.dk*

U.W., *Gamma Remote Sensing, Worbstrasse 225, CH-3073 Gümligen, Switzerland*.

R.C., *NPA Satellite Mapping, Crockham Park, Edenbridge, Kent TN8 6SR, UK*.

Geological map of Denmark 1:50 000 – map sheet Mors, NW Denmark

Stig A. Schack Pedersen, Peter Roll Jakobsen, Lisbeth Tougaard and Peter Gravesen

Danish geological maps of deposits occurring at the terrain surface are published under the name of Geological map of Denmark 1:50 000 and are based on geological field mapping at 1:25 000. Most of the published maps follow the map sheet division shown in Fig. 1. However, in some instances it is appropriate to publish geological maps covering a regional unit, such as an island. Hence, the geological map of Mors appears as the 1:50 000 map sheet Mors, which covers parts of map sheets 1116 I, 1116 II and 1116 III (Figs 1, 2; Pedersen & Jakobsen 2012).

Mors shows spectacular examples of glaciotectonic structures that are beautifully exposed in coastal cliff sections. It also has a unique geological history, which is briefly described in this paper.

Geological features of map sheet Mors

The geological map of Mors shows deposits that are present at the terrain surface; they are mainly non-lithified Quaternary deposits. The mapping was carried out using 1 m long hand augers. The soil and its underlying unit were tested at *c.* 100 m intervals with the auger, which collects a sample in a groove at its tip. The auger samples are classified in the field and allotted a symbol on a 1:25 000 field map. During more than 100 years of systematic mapping, about 50 symbols have been established which are used by the mapping geologist. The aim of the work is to map the boundaries between various units shown as polygons on the maps. The testing distance of 100 m provides a semi-statistical documentation of the recognised polygons.

Occasional outcrops of pre-Quaternary deposits are classified with letter symbols. On the geological map of Mors, the pre-Quaternary geology is presented as an inset with structural contour lines showing the elevation of the pre-Quaternary surface and the geological units that occur below the Quaternary deposits (Figs 2, 3). The map is mainly based on information from the Jupiter well data base, but detailed geophysical mapping of Mors (Jørgensen *et al.* 2005) supported the interpretation of the structural contours.

The pre-Quaternary geology

The pre-Quaternary geological features on Mors are influenced by the Erslev structure, a salt diapir in the central part of the island (Larsen & Baumann 1982), and by glaciotectonic deformation (Gry 1940; Pedersen 2000). This is illustrated by three cross-sections documenting the relationship between the pre-Quaternary and the Quaternary geology (Fig. 2). The diameter of the circular salt diapir is 5–6 km,

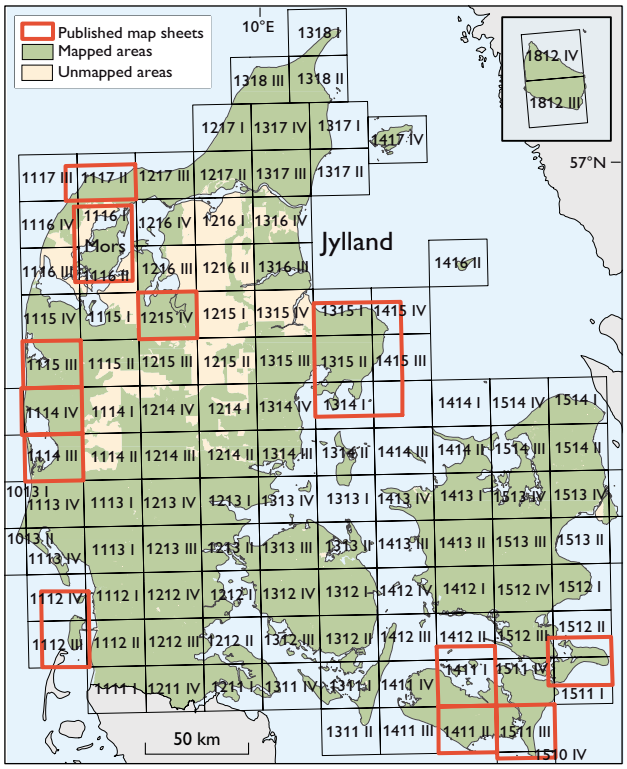

Fig. 1. Map of Denmark showing the sheet divisions of the 1:50 000 geological map series. The red frames show map sheets published under the name of Geological map of Denmark 1:50 000. The map sheets are numbered according to the 1:50 000 topographic maps implemented by the former Danish Geodetic Institute (now the Danish Geodata Agency) in 1953. The map sheet division is based on the UTM system and uses the European Datum 1950. The Survey decided to retain this map sheet division for the geological mapping, although the National Survey and Cadastre (now the Danish Geodata Agency) in 2003 started to use the European Terrestrial Reference System 1989.

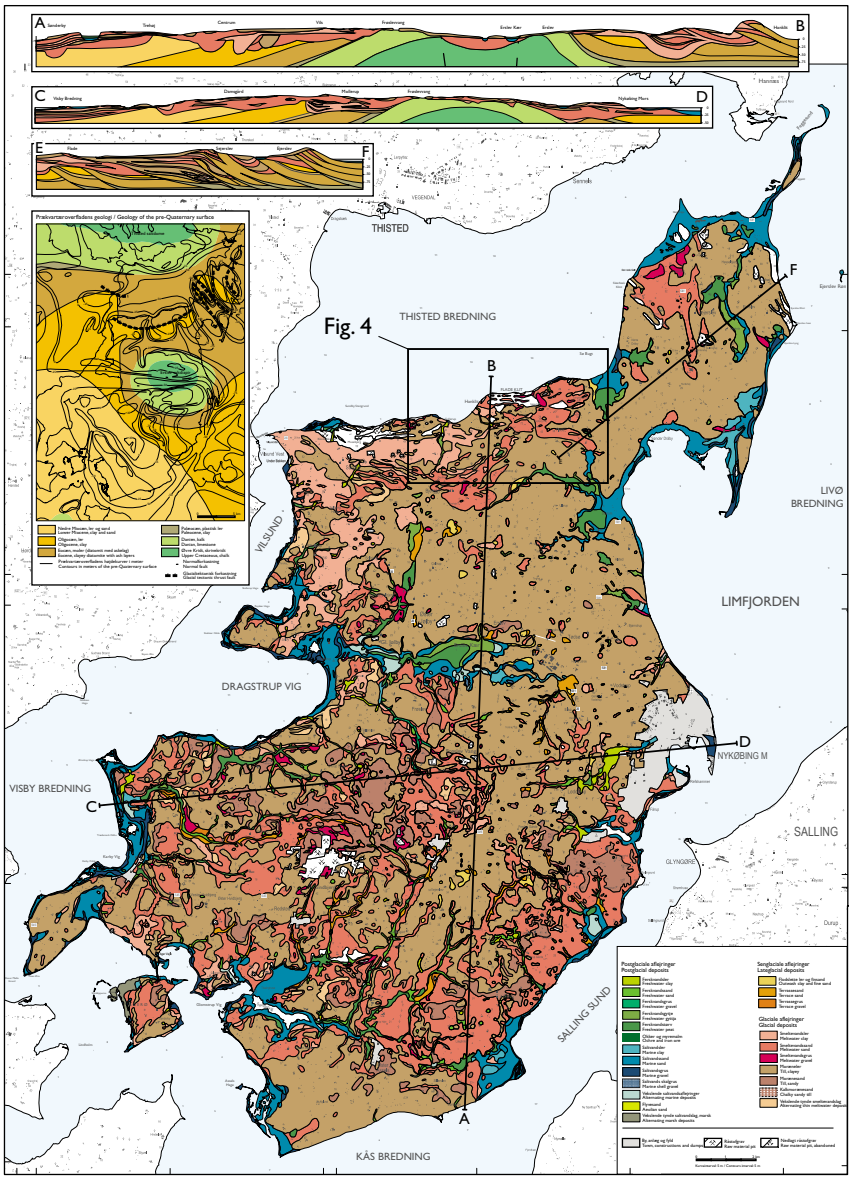

Fig. 2. Strongly reduced and modified version of map sheet Mors with three cross-sections: a N–S section (upper), an E–W section (middle) and a NE–SW section of the northern part of Mors (lower). The inset shows the depression on central Mors which coincides with the depression in the top of the chalk covering the salt diapir (Fig. 3).

and the diapir rises vertically from the base of the Permian salt at a depth of 5–6 km. The top of the salt in the diapir is now found at depths of 600–700 m. A circular dome of chalk caps the salt diapir. Maastrichtian chalk in its centre was formerly quarried in chalk pits, exposing the Cretaceous–Tertiary boundary. The chalk is overlain by bryozoan cherty limestone that forms an aureole around the top of the diapir, and Paleocene clay occurs along the steeply dipping flanks. The uplift of the salt diapir continued in the Paleocene and resulted in an increased thickness of plastic clay away from the diapir centre. In the surrounding marginal depression, Eocene clayey diatomite occurs interbedded with volcanic ash layers. This unit, locally called 'moler', crops out in an old clay pit on the northern flank of the diapir (Pedersen 2000).

The moler is the most characteristic pre-Quaternary unit in the glaciotectonic complexes that occur on northern Mors. The diatomite is exploited and used for light-weight granulates. On northern Mors, glaciotectonic folds are well exposed in the two largest clay pits. These folds and the surrounding hilly terrain were formed by superimposed glaciotectonic deformation (Pedersen 2000). The most impressive glaciotectonic complex with up-thrust sheets of moler is the Hanklit complex (Figs 4, 5), where a thrust sheet is exposed that was displaced *c.* 300 m towards the foreland in the south. Parallel ridges trend from Hanklit towards the west, and also here the moler is the target of diatomite exploitation in pits following the crests of the anticlines.

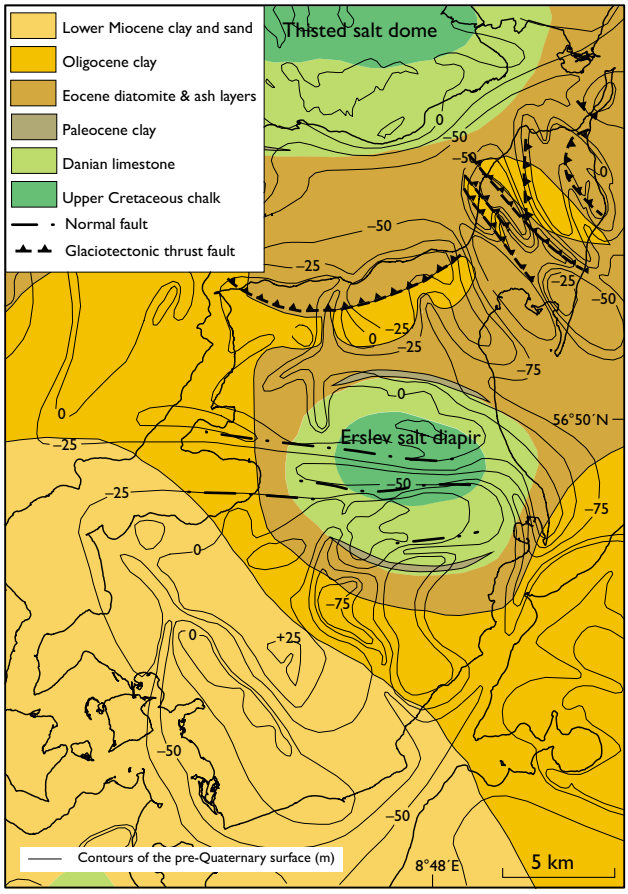

Fig. 3. Bedrock map of Mors (enlarged version of inset in Fig. 2). The structural contour lines at 25 m intervals show the elevation of the pre-Quaternary surface. The dome-like structure on central Mors is made of chalk that covers the top of the Erslev salt diapir. The boundaries between glaciotectonic complexes and their foreland on northern Mors are also shown.

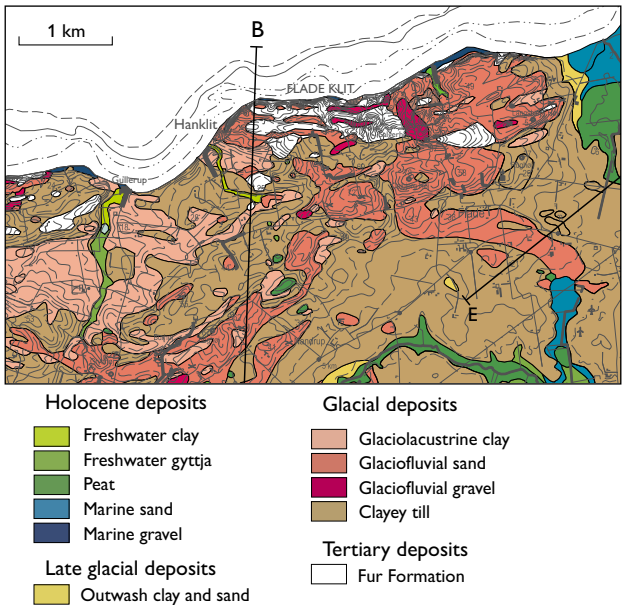

Fig. 4. Part of the map sheet showing the hilly terrain at Flade Klit. The Hanklit glaciotectonic complex is marked by a landscape dominated by elongated hills. The Fur Formation has been thrust-faulted up into parallel ridges in the complex. Farther to the south, the thrust sheets mainly consist of glaciolacustrine clay and glaciofluvial sand. Contour interval 5 m. For location see Fig. 2.

Between the glaciotectonic complexes on northern Mors and the northern flank of the salt diapir, red and green plastic clay of the Røsnæs Ler Formation occurs together with dark brown, micaceous, Oligocene to Early Miocene clay. Local outcrops of the Oligocene–Miocene clay (the Brejning and Viborg Formations) are known in the hills along the strait west of Mors. South of the Erslev structure, Miocene heterolithic deposits with mica-rich clay and sand are known from wells and were recognised during the systematic mapping of southern Mors.

The glaciodynamic geology

The oldest Quaternary deposits on Mors comprise glaciolacustrine clay that is referred to the Elsterian Glaciation exposed in coastal cliffs on south-western Mors. On northern Mors, alternating beds of till and glaciofluvial sand are exposed along the west coast, and similar Elsterian deposits are known from wells penetrating the buried tunnel valleys. A coastal cliff along the west side of northern Mors exposes 8 m thick sandy till, rich in chalk, which was deposited by a Norwegian ice advance during the Saalian Glaciation (about 300 000 years BP). Characteristic erratic blocks of chalk and flint, originating from erosion of the till, are abundant along the shore (Pedersen *et al.* 2012). This till and the underlying glaciofluvial sand and gravel are well known from diatomaceous clay pits on north-eastern Mors. Glaciolacustrine clay is widespread over large parts of northern and north-western Mors. The clay was deposited during the Middle Weichselian prior to the Norwegian Ice advance. The depocentre was located in the depression between the Thisted salt dome north of Mors and the Erslev salt diapir. Both these areas formed elevated terrains, whereas the remaining part of Mors constituted lowlands characterised by lake-filled depressions with glaciofluvial sand and gravel. In the area around Hanklit, glaciolacustrine clay forms an important element in the glaciotectonic complex (Figs 4, 5). The clay is thrust up into sheets, forming a terrain with E–W-trending parallel ridges. The arc-formed complex was created by the Norwegian Ice advance about 27 000 years BP. A lodgement till rich in indicator boulders such as larvikite and rhombohedral porphyries from the Oslo region was deposited during this advance.

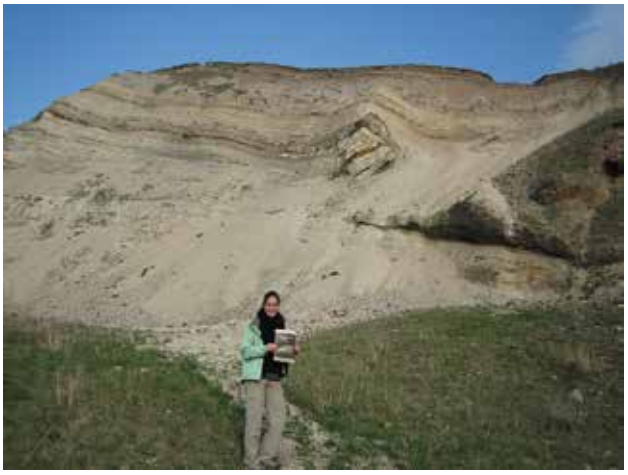

Fig. 5. The impressive glaciotectonic thrust sheet exposed in the Hanklit coastal cliff. The thrust sheet is 60 m thick and was displaced for a distance of 300 m towards the foreland to the south.

After the Norwegian Ice melted back, Mors was characterised by parallel hills intersected by lake-filled valleys with glaciolacustrine clay deposits as patches scattered over the landscape. A few thousand years later the advancing Swedish Ice remodelled the landscape. On northern Mors, thrusting and folding from the north-east superimposed the architecture of the glaciomorphological landscape. When the ice reached south-western Mors it stopped briefly and formed a stationary line, and its meltwater created a cone-shaped outwash plain. At its apex, boulders, stones and gravel were deposited, which are now quarried in gravel pits.

The postglacial geology

During the late glacial and Holocene periods, Mors was affected by three significant events: (1) meltwater erosion during the deglaciation and formation of a kettle-hole landscape caused by melting of dead ice, (2) marine transgression accompanied by sedimentation in straits and fjords after the Ice Age, and (3) glacio-isostatic rebound. During the Atlantic sea-level highstand, coastal plains formed in front of the fossil coastal cliffs.

A number of fossil straits and fjords with marine gyttja and marine sand occur on Mors. The most significant fossil fjord is an E–W-trending depression located above the central part of the salt diapir on central Mors. Marine heterolithic deposits are characterised by shells of *Cardium*, and mounds of oyster (*Ostrea edulis*) beds formed where strong currents cut narrow gaps in the former fjord. A number of distinctive fossil coastal cliffs occur, particularly on northern Mors where raised shorelines are found up to *c.* 5 m above the present sea level. The raised beaches have occasionally dammed coastal lakes. Beach ridges occur along the coastline on southern Mors. Several of these contribute to the closure of small fjords and coastal lakes with peat accumulation. In the past, the coastal plains were larger, but are now subjected to increased erosion along the coastline of Mors.

References

Gry, H. 1940: De istektoniske Forhold i Moleret. Med Bemærkninger om vore dislocerede Klinters Dannelse og om den negative Askeserie. Meddelelser fra Dansk Geologisk Forening **9**, 586–627.

Jørgensen, F., Sandersen, P.B.E., Auken, E., Lykke-Andersen, H. & Sørensen, K. 2005: Contributions to the geological mapping of Mors, Denmark – a study based on a large-scale TEM survey. Bulletin of the Geological Society of Denmark **52**, 53–75.

Larsen, G. & Baumann, J. 1982: Træk af Mors salthorstens udvikling. Dansk Geologisk Forening, Årsskrift for **1981**, 151–155.

Pedersen, G.K *et al.* 2012: Moleområdets geologi – sedimenter, fossiler, askelag og glacialtektonik. Geologisk Tidsskrift **2011**, 41–135.

Pedersen, S.A.S. 2000: Superimposed deformation in glaciotectonics. Bulletin of the Geological Society of Denmark **46**, 125–144.

Pedersen, S.A.S. & Jakobsen, P.R. 2012: Geological map of Denmark, 1:50 000, Mors. Copenhagen: Geological Survey of Denmark and Greenland.

Authors' address

Geological Survey of Denmark and Greenland, Øster Voldgade 10, DK-1350 Copenhagen K, Denmark. E-mail: *sasp@geus.dk*

Assessing urban groundwater table response to climate change and increased stormwater infiltration

Mark T. Randall, Lars Troldborg, Jens Christian Refsgaard and Jacob B. Kidmose

The global climate is expected to show continued warming throughout the coming century. As a direct consequence of higher temperatures, the hydrological cycle will undergo significant changes in the spatial and temporal distribution of precipitation and evapotranspiration. In addition to more frequent and severe droughts and floods, climate change can affect groundwater recharge rates and groundwater table elevation (Bates *et al.* 2008).

Some previous studies of climate change impact on groundwater have suggested alarming reductions in groundwater recharge and lowering of water tables. Other studies, especially those focusing on regions of higher latitudes, have indicated a potential rise in water tables due to increased precipitation and recharge (Scibek & Allen 2006; Woldeamlak *et al.* 2007).

In addition to changes in precipitation patterns, a shift in stormwater infrastructure design may also alter the hydrologic cycle of urban areas. In recent years, there has been a growing trend towards adoption of low-impact development practices managing stormwater runoff. These practices aim to mitigate the impacts of urbanisation such as increased runoff volume, higher peak runoff flows, lowered water tables and reduced water quality (Prince George's County 1999). In contrast to conventional stormwater infrastructure, which is designed to rapidly collect and convey runoff, low-impact development practices are designed to slow runoff, remove pollutants and evapotranspirate and infiltrate runoff locally.

In recent years, numerous modelling studies have investigated the potential impact of stormwater infiltration on groundwater levels. Gobel *et al.* (2004) used a combination of models (GwNeu, HYDRUS-2D, SPRING) to demonstrate that the installation of infiltration practices across an urban catchment area in Germany could raise the groundwater surface by up to 2.3 m in some locations. In another catchment scale study, Maimone *et al.* (2011) used the modelling code DYNFLOW to show that the future groundwater table may eventually stabilise up to 1.5 m higher than its current level in parts of Philadelphia, if the city's plan to alter 40% of its impervious areas into so-called 'green' stormwater recharge areas is completed. Thompson (2010) used HYDRUS-2D to demonstrate that a stormwater infiltration basin could cause up to 1.3 m of localised groundwater mounding. In yet another study, Endreny & Collins (2009) used MODFLOW to show that rain gardens installed throughout a residential catchment area could raise the steady-state groundwater table by up to 1.1 m.

The studies mentioned above have investigated groundwater level response to either changes in climate or stormwater management infrastructure. However, to the authors' knowledge no studies have investigated the concurrent effects of both alterations on the urban hydrologic cycle. In urban areas, it is necessary to determine the potential magnitude of the combined impact, as a steep rise in groundwater level can damage building foundations and subsurface infrastructure due to flooding and buoyancy forces (Gobel *et al.* 2004; Vázquez-Suñé *et al.* 2005). This study aims to assess the potential changes in groundwater response caused by both increased precipitation and widespread instalment of stormwater infiltration infrastructure in the city of Silkeborg, Denmark, using the MIKE SHE model. Change of groundwater level at the planned location of a new motorway in Silkeborg is the focus of this study as portions of the con-

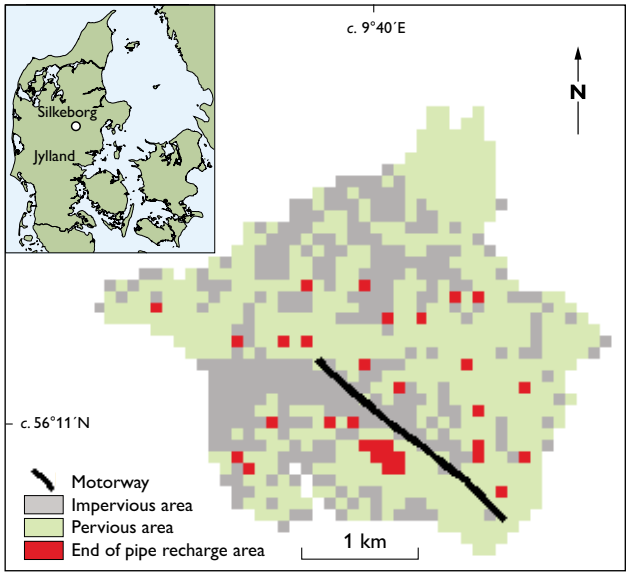

Fig. 1. The Silkeborg study area and the proposed course of the motorway. Inset: the location of Silkeborg in Jylland.

Table 1. Summary of model scenarios

Scenario name	Climate data input	Stormwater infrastructure
CD-2010	Recorded 1991–2010	Conventional drainage to river system
EPR-2010	Recorded 1991–2010	End of pipe infiltration ponds
LAR-2010	Recorded 1991–2010	Local area recharge
CD-2100	Projected 2081–2100	Conventional drainage to river system
EPR-2100	Projected 2081–2100	End of pipe infiltration ponds
LAR-2100	Projected 2081–2100	Local area recharge

struction are expected to come critically close to the present high groundwater table in that area. Knowledge of the magnitude of potential groundwater changes is essential because improved drainage measures and increased use of concrete will significantly raise the costs of the new motorway.

Study area

The city of Silkeborg has a population of *c.* 43 000 inhabitants and is located in the central part of Jylland, Denmark (Fig. 1). The focus of this study is just north of the river Gudenåen, where a portion of the new motorway will be constructed *c.* 6 m below the present terrain surface. The surficial geology is dominated by coarse-grained, postglacial, sandy sediments that form an upper unconfined aquifer with a vertical extent of 10–15 m. The average precipitation in Silkeborg during the period 1961–1990 was 903 mm per year, and the average potential evapotranspiration was 546 mm per year. The average monthly temperature during that period was 15.2°C in July/August and −0.3°C in January/February (Kidmose *et al.* 2013).

Methods

Hydrological models – MIKE SHE is a deterministic, fully-distributed and physically based model software capable of simulating surface and subsurface hydrological processes. The Danish National Water Resources Model (DK-model) is based on MIKE SHE and incorporates national data on geology, soil type, land use, topography, river network geometry, water abstraction and climate. The Silkeborg model is a 100 m grid local model using hydraulic head boundary conditions from the 500 m grid DK-model. A 9.2 km² area within the 103 km² Silkeborg model, which encompasses the new motorway construction and the greater part of the urbanised surroundings, was chosen for the current study (Fig. 1). Details on the development, calibration and validation of the DK-model and the Silkeborg model are found in Højberg *et al.* (2013) and Kidmose *et al.* (2013), respectively. Six different model scenarios have been evaluated (Table 1).

Stormwater infiltration modelling – The Silkeborg study area consists of 65.5% pervious and 34.5% impervious cover. In the scenarios with conventional drainage stormwater infrastructure (i.e. the 'CD' scenarios), 100% of the precipitation on impervious cells was routed directly to the river system (Fig. 2A). Precipitation on impervious cells had one time step (i.e. one day) to infiltrate or evapotranspirate. At the end of the time step, any water in excess of a detention storage of 4.7 mm (based on calibration results) was routed overland to adjacent cells based on topography. It is assumed that the CD-2010 scenario is representative of Silkeborg's current climate and stormwater conditions.

In the end of pipe recharge (EPR) scenarios (Fig. 2B), it was assumed that 10.7% (34 ha) of the city's pervious area has been turned into end of pipe stormwater infiltration ponds (Figs 1, 2). Model cells which were assumed to contain in-

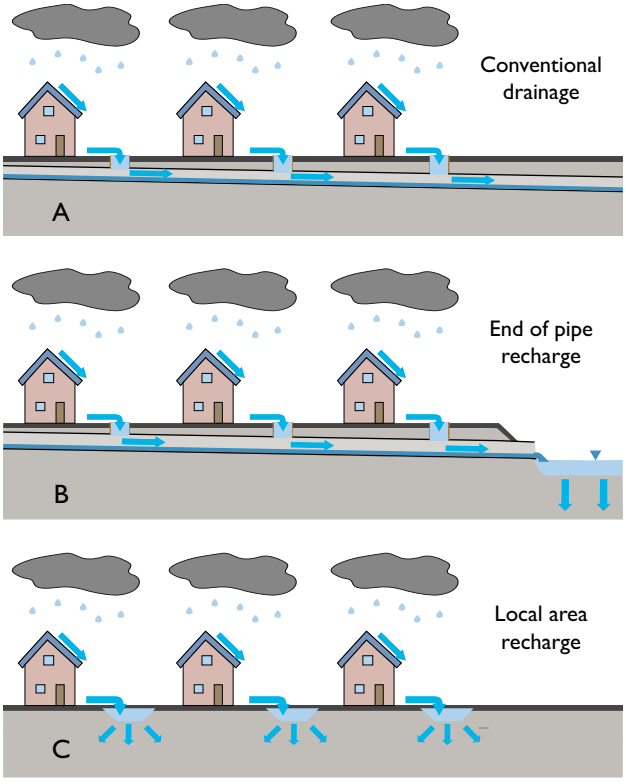

Fig. 2. Three model scenarios for stormwater drainage infrastructure.

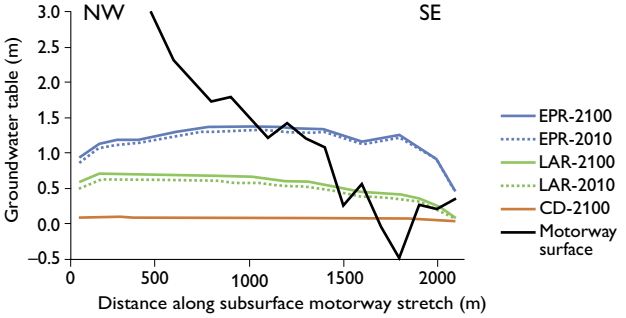

Fig. 3. Average modelled groundwater table elevations along the 2000 m of projected motorway at Silkeborg. The results are relative to CD-2010.

filtration ponds were assigned detention storage of 500 mm to represent the storage depth of the pond. In the EPR scenarios, precipitation which would normally be applied to impervious cells was reduced to zero, and the equivalent volume of precipitation was instead evenly distributed over the infiltration pond cells via an increase in precipitation applied to those cells. In the EPR scenarios there were 9.3 times as much impervious drainage area as infiltration pond area, so the infiltration pond model cells had 1030% (i.e. 100% + 9.3 × 100%) of the actual rainfall applied to them. This method of manipulating precipitation to simulate the collection of stormwater in specialised infiltration areas on a city-wide scale is similar to the modelling strategy used by Holman-Dodds *et al.* (2003).

The local area recharge (LAR) scenarios represent a system where stormwater is managed at the level of individual plots through any combination of infiltration practices, each no more than tens of metres across. It was assumed that infiltration possibilities are numerous and located in close proximity so that at the scale of the model, each cell effectively behaves as a pervious cell. Therefore, all paved areas were given properties identical to the pervious areas with infiltration rates controlled by the underlying soils.

Climate input – Precipitation, temperature and evapotranspiration data from the Danish Meteorological Institute from 1991 to 2010 were used as input to the '2010' model scenarios. The input climate data for the '2100' scenarios were generated by applying correction factors based on nine climate model projections from the ENSEMBLES project (Christensen *et al.* 2009) to present-day climate data. Further information on the Delta Change downscaling method used can be found in Seaby *et al.* (2013). To generate the results for each of the three '2100' infrastructure scenarios, the model was run nine times (once for each of the nine climate model projections), and the results averaged.

Results

Water table elevation – Average groundwater elevations along the area planned for the motorway construction were extracted from the MIKE SHE model results (Fig. 3). Areas where the solid black line (i.e. the motorway surface) drops below the water table indicate portions of the motorway which could be flooded by groundwater.

In the CD-2010 scenario, a stretch of 160 m of motorway is below the average water table. In the CD-2100 scenario, the average groundwater table elevation is raised by 0.08 m, and the length of motorway surface at risk is extended to 180 m. Hundreds of metres of the proposed motorway are potentially flooded in the LAR-2010 and the LAR-2100 scenarios where the average water table rose 0.48 and 0.55 m above CD-2010 levels, respectively. The highest average water tables of 1.15 and 1.19 m above CD-2010 occur in the EPR-2010 and EPR-2100 scenarios, which would both put a stretch of nearly 1 km of the proposed motorway at risk.

The results indicate that the impact of climate change (i.e. the difference between the '2010' and the '2100' scenarios) is small compared to the impact of extensive implementation of either local area or end of pipe stormwater infiltration practices. Only average water tables are presented here to compare the relative impacts of different model scenarios. However, maximum water tables could put much longer sections of the motorway at risk and will therefore be considered in the final design of the motorway.

Water balance – Average yearly volumes of precipitation, evapotranspiration, recharge and overland flow were calculated for the 1991–2010 time period for each stormwater in-

Table 2. Catchment water balances for different stormwater infrastructure scenarios

Model scenario	Mean (mm/year, 1991–2010)				
	Precipitation	Evapotranspiration	Recharge	Overland flow	Baseflow
CD	911	319	304	292	8
LAR	911	441	463	11	15
EPR	911	311	588	19	29

frastructure scenario using MIKE SHE's water balance tool (see Table 2). Evapotranspiration was greater in the LAR scenario, due to the much larger evaporation surface available. Recharge was much higher in both infiltration scenarios than in the CD scenario. Overland flow, or the volume of water which flows directly into the river system, was very small in both the infiltration scenarios in comparison to the CD scenario which routed all water from impervious areas into the nearest stream. Baseflow was highest in the EPR scenario, followed by the LAR scenario and finally the CD scenario, as would be expected based on the relative recharge volumes in these scenarios.

Summary and conclusions

Previous studies have reported groundwater level rise due to either climate change (Scibek & Allen 2006; Woldeamlak *et al.* 2007) or stormwater infiltration practices (Gobel *et al.* 2004; Maimone *et al.* 2011). However, these two changes to the urban hydrologic cycle are typically not assessed in an integrated way as in this study. The modelling results presented in this paper are within the ranges of the above studies, i.e. tens of centimetres due to climate change and potentially more than 1 m due to the widespread adoption of stormwater infiltration practices. However, these results are specific to the Silkeborg motorway and it is expected that the relative magnitude of the impact due to climate change and stormwater infiltration could vary greatly under different climatic and geological regimes.

Stormwater infiltration practices are often regarded as a form of climate change adaptation in the field of stormwater management as they can help to accommodate the higher intensity and larger volume precipitation events expected in the future. However, as the results of this study indicate, these same practices amplify other problems associated with climate change (i.e. groundwater table rise). The study clearly shows the need for integrated research of urban hydrology, and communication between hydrogeologists, stormwater engineers, planners and policy makers.

Acknowledgement

We thank the Danish Road Directorate for funding this study.

References

Bates, B., Kundzewicz, Z., Wu, S. & Palutikof, J. 2008: Climate change and water. Intergovernmental Panel on Climate Change, Technical Paper **6**, 200 pp. Geneva: IPCC.

Christensen, J.H., Rummukainen, M. & Lenderink, G. 2009: Formulation of very-high-resolution regional climate model ensembles for Europe [Research Theme 3]. ENSEMBLES: Climate change and its impacts: summary of research and results from the ENSEMBLES project, 47–58. Exeter, UK: Meteorological Office Hadley Centre.

Endreny, T. & Collins, V. 2009: Implications of bioretention basin spatial arrangements on stormwater recharge and groundwater mounding. Ecological Engineering **35**, 670–677.

Gobel, P. *et al.* 2004: Near-natural stormwater management and its effects on the water budget and groundwater surface in urban areas taking account of the hydrogeological conditions. Journal of Hydrology **299**, 267–283.

Højberg, A.L., Troldborg, L., Stiesen, S., Christensen, B.B.S. & Henriksen H.J. 2013: Stakeholder driven update and improvement of a national water resources model. Environmental Modelling & Software **40**, 202–213.

Holman-Dodds, J.K., Bradley, A.A. & Potter, K.W. 2003: Evaluation of hydrologic benefits of infiltration based urban storm water management. Journal of the American Water Resources Association **39**, 205–215.

Kidmose, J., Refsgaard, J.C., Troldborg, L., Seaby, L.P. & Escrivà, M.M. 2013: Climate change impact on groundwater levels: ensemble modelling of extreme values. Hydrology and Earth System Sciences **17**, 1619–1634.

Maimone, M., O'Rourke, D.E., Knighton, J.O. & Thomas, C.P. 2011: Potential impacts of extensive stormwater infiltration in Philadelphia. Environmental Engineer **14**, 29–39.

Prince George's County 1999: Low-impact development design strategies: an integrated design approach, 150 pp. Prince George's County, MD: Department of Environmental Resources. http://water.epa.gov/polwaste/green/upload/lidnatl.pdf

Scibek, J. & Allen, D. 2006: Comparing modelled responses of two high-permeability, unconfined aquifers to predicted climate change. Global and Planetary Change **50**, 50–62.

Seaby, L.P., Refsgaard, J.C., Sonnenborg, T.O., Stisen, S., Christensen, J.H. & Jensen, K.H. 2013: Assessment of robustness and significance of climate change signals for an ensemble of distribution-based scaled climate projections. Journal of Hydrology, *http://dx.doi.org/10.1016/j.jhydrol.2013.02.015*

Thompson, A., Nimmer, M. & Misra, D. 2010: Effects of variations in hydrogeological parameters on water-table mounding in sandy loam and loamy sand soils beneath stormwater infiltration basins. Hydrogeology Journal **18**, 501–508.

Vázquez-Suñé, E., Sanchez-Vila, X. & Carrera, J. 2005: Introductory review of specific factors influencing urban groundwater, an emerging branch of hydrogeology, with reference to Barcelona, Spain. Hydrogeology Journal **13**, 522–533.

Woldeamlak, S., Batelaan, O. & de Smedt, F. 2007: Effects of climate change on the groundwater system in the Grote-Nete catchment, Belgium. Hydrogeology Journal **15**, 891–901.

Authors' addresses

M.T.R., *Computational Hydraulics International, 147 Wyndham Street North, Suite 202, Guelph, Ontario, N1H 4E9 Canada*. E-mail: *mark@chiwater.com*

L.T., J.C.R. & J.B.K., *Geological Survey of Denmark and Greenland, Øster Voldgade 10, DK-1350 Copenhagen K, Denmark.*

Evaluation of total groundwater abstraction from public waterworks in Denmark using principal component analysis

Brian Lyngby Sørensen and Rasmus Rønde Møller

In Denmark water abstraction data have been collected since the late 1970s. Initially the purpose was to monitor and assess the groundwater resources available for future local water abstraction. For this reason, abstraction data were collected not only from waterworks, but also from irrigation, industry etc. Today water abstraction data are used for several purposes, for instance in water -balance calculations to estimate the available resource to wetlands, streams and lakes or to calculate the flow of chemical substances in the water environment.

The role of climatic changes in the future hydrological cycle is subject to increasing attention. Apart from a small reserve of surface water, all drinking water in Denmark comes from groundwater. When precipitation changes in the future the amount of groundwater available for abstraction will also change. Hence, for reasons of security of supply and environmental impact, it is important to know the amount and trend of abstraction each year.

At national level, it is a statutory objective to abstract groundwater in a way that does not obstruct the general water-environmental objectives outlined in the European Union's Water Framework Directive (The European Parliament and the Council of the European Union 2000). The purpose of this paper is to present a method to evaluate the errors in the overall national groundwater abstraction dataset and describe how to correct erroneous data. For the sake of overview the national data are typically presented as an overall sum in million cubic metres per year (e.g. Thorling *et al*. 2012).

Public groundwater abstraction in Denmark

Drinking water in Denmark comes from approximately 2500 waterworks, abstracting about 400 million m^3 of groundwater per year. There is a pronounced decentralised water supply structure with many small waterworks spread across the country. Approximately 72% of the waterworks each abstract less than 0.1 million m^3 water per year, amounting to a total of 56.5 million m^3 per year. At the other end of the

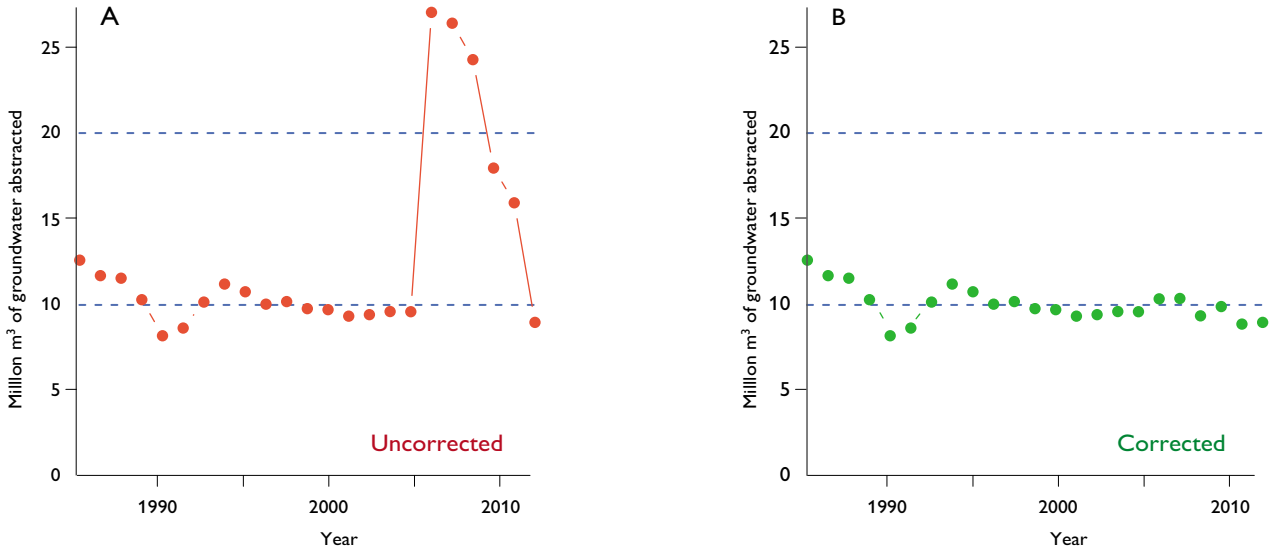

Fig. 1. An example of a time series for a specific municipality before (**A**) and after (**B**) correction of the abstraction data. Data from 2011 are included in the graph for clarity.

Table 1. Typical problems associated with registration of water abstraction data

Problem	Cause	Action
No data	No data were reported at all from the municipality	An expected average was calculated based on data from 1–2 years before and after the year with missing data.
Evidently missing data	No data from one or more waterworks. Typing errors	An expected average was calculated for the individual waterworks, or in case of typing errors a more probable value was estimated.
Evidently too high amount quoted	Double registration from one or more waterworks. Typing errors	Evident double registrations were subtracted from the sum. In case of typing errors a more probable value was estimated.
Other apparent error	Unidentified	No action taken.

scale, 3% of the waterworks each abstract more than 1 million m^3 per year, totalling 154 million m^3 per year.

According to Danish legislation it is mandatory for waterworks and other users abstracting groundwater to report the amount abstracted once a year to the municipalities. The municipalities check for mistyped data and forward them to the national Danish database on geology, groundwater and drinking water (the Jupiter database at the Geological Survey of Denmark and Greenland).

Municipal reform

In 2007, a major municipal reform took place in Denmark. Thirteen former counties (amter) were replaced by five so-called regions and most municipalities (kommuner) were merged into fewer and larger units, resulting in a drop from 271 to 98 municipalities. As part of this reform the new municipalities took over the responsibility to manage the water resources including abstraction licensing. This involved transferring employees from the former counties, new distribution of responsibilities and introduction of new computer systems and new procedures; all of which influenced the overall quality of the abstraction data. For instance, the new municipalities were responsible for submitting the 2006 water abstraction data to Jupiter, although they were not operative before 1 January 2007.

Data preparation

The water abstraction data used in this study were extracted from the Jupiter database for the period 1989–2010. Based on the extracted data, a date table was compiled with the sum of groundwater abstraction per year within each municipality. A time series for each municipality was plotted and visually inspected. At municipality level, small year-to-year changes and thus a smooth curve are expected, because

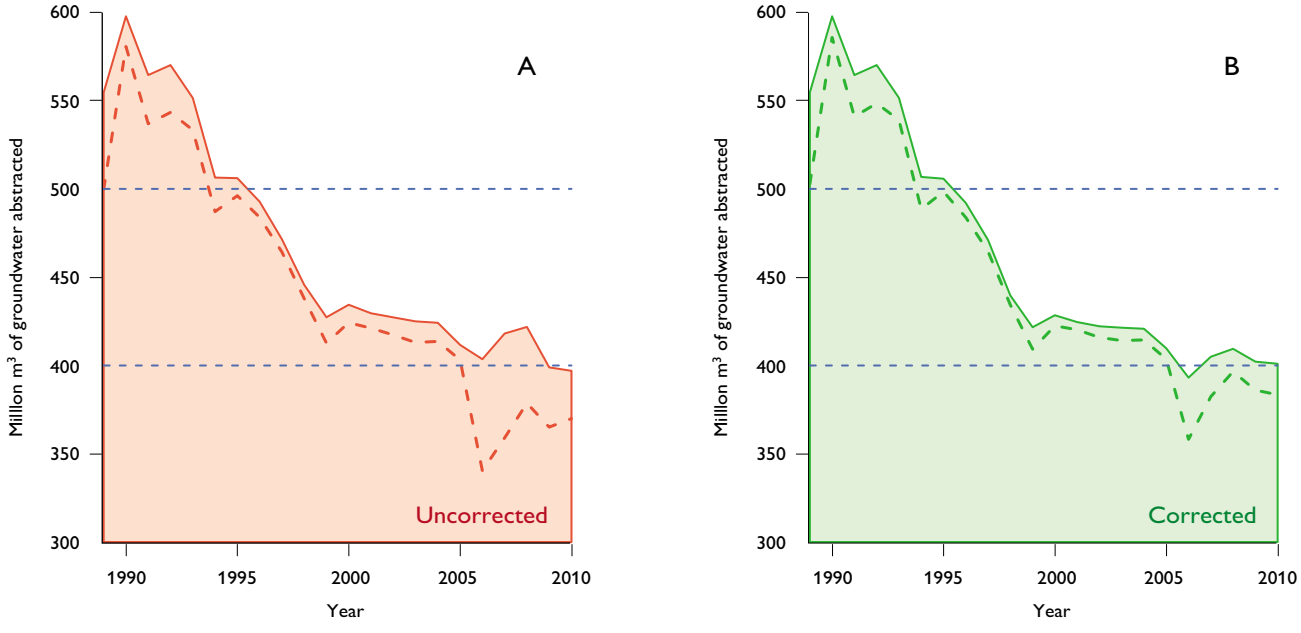

Fig. 2. Total water abstraction in Denmark for uncorrected (**A**) and corrected (**B**) data. The dashed lines show VAR_{exp} – the correlation between the PCA score of the first primary component (PC1) and the input data, expressed in million m^3 per year.

on average the waterworks abstract almost the same amount each year.

After initial inspection, 22 municipalities with unexpected data pattern were selected for detailed examination. Four types of main problems were identified (Table 1); the causes for three of the types could be identified and relevant action taken.

Correction of abstraction data for a single municipality

An example of a time series for a selected municipality is shown in Fig. 1A. The water abstraction from a specific waterworks was erroneously reported three times in the years 2006–2008 and twice in the years 2009–2010. Thus, the water abstraction in the municipality was overestimated by 16.7 and 7 million m^3, respectively, in the two periods. With the extra registrations removed, the time series shows a behaviour similar to what is expected (Fig. 1B). A similar inspection was made of the time series from the 21 other municipalities. Finally, a new data table was compiled by merging the corrected data with the data from the uncorrected time series from the remaining 76 municipalities.

Principal component analysis and Pearson's correlation coefficient

Principal component analysis is a mathematical procedure introduced by Pearson (1901) and widely used to visualise multivariate data by dimension reduction (Garcia & Filzmoser 2011). According to Garcia & Filzmoser, the main problems of multivariate data can be avoided by using the principal component analysis to transform ". . . the original variables into a smaller set of latent variables which are uncorrelated". Each new variable (principal component or PC) can then be interpreted independently.

There are several ways to perform principal component analysis, some of which are described in Wikipedia (2013). The method used here is singular value decomposition (SVD) using the 'prcomp' function of the base package of R (R Core Team 2012).

The time series for the individual municipalities were used as objects (rows) and the years were used as variables (columns). For each year the Pearson's correlation coefficient ρ between the scores of the first principal component (PC1) and the corrected and uncorrected datasets D, was calculated and expressed in terms of million m^3 (VAR_{exp}) using the formula:

$$VAR_{exp} = \rho \times T = cor(PC1, D) \times T$$

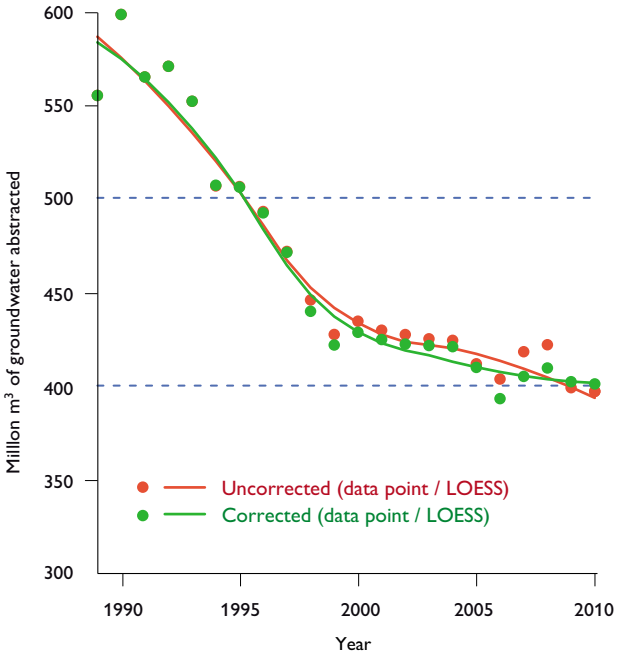

Fig. 3. Locally weighted average (LOESS) of uncorrected and corrected groundwater abstraction data.

where T is the total national abstraction. The correlation was done using the default settings of the 'cor' function of R (R Core Team 2012). The magnitude of ρ shows the strength of the linear dependence between the score of PC1 and D.

Status of water abstraction and comparison of uncorrected and corrected data

Figure 2 shows the total groundwater abstraction from public waterworks in million m^3 per year from 1989 to 2010 with uncorrected and corrected data. Both diagrams show the Pearson's correlation coefficient expressed in million m^3 (VAR_{exp}, dashed lines), according to the formula above. The variance explained ranges between 90 and 98% of the total yearly water abstraction. The remaining 2–10% can be perceived as 'noise' in the sense that this part of the variance is due to errors, short-term but large extra deliveries of water, abrupt changes in water needs, new or closed down waterworks etc. Before the municipal reform (the period from 1989 to 2005) the unexplained variance on average corresponds to 16 million m^3 for the uncorrected data and 12.7 million m^3 for the corrected data. The improvement of the explained variance by correcting the data is thus 3.3 million m^3. After the reform (2006–2010) the unexplained variance on average corresponds to 45.3 million m^3 for the uncorrected data and 20.8 million m^3 for the corrected data, leading

to an average improvement of 24.5 million m^3 by correcting the data.

Because of the errors mentioned above the amount of groundwater abstracted in Denmark by the waterworks is only known with some uncertainty. In Fig. 3 a locally weighted regression (LOESS) is calculated for corrected and uncorrected abstraction data in order to yield a 'best guess' of the total water abstraction. The curves show an overall trend with a large decline in the first half of the 1990s when abstraction decreased *c.* 20% from *c.* 550 million m^3 in 1990 to *c.* 460 million m^3 in 1996. Later, the abstraction dropped to just over 400 million m^3 in 2005. From Fig. 3 it is clear that when corrected data are used, the abstraction flattens out at around 400 million m^3 per year from 2005 onwards. If uncorrected data are used the abstraction level seems to decrease even further to below 400 million m^3 per year over the same period. Therefore the interpretation of trends depends to a large degree on whether the data are corrected or not. The main reasons for the large decline after 1989 are adoption of new legislation, increased water taxes and water saving campaigns (Stockmarr & Thomsen 2006).

Conclusions

After the municipal reform in 2007 water abstraction data reported to the Jupiter database show increased levels of errors due to changes in the way data are treated and reported. This means that national trends and levels are blurred which can lead to misinterpretations. By carefully examining data from the individual waterworks, it is often possible to determine the causes of errors and thereby correct them. The combined use of PCA and Pearson's correlation coefficient is a useful way to provide an overall check on how well the data are corrected. This study shows that after the municipal reform the improvement is on average equivalent to 24.5 million m^3 or *c.* 6%.

On regional and local scales the impact of erroneous data can be severe. The example in Fig. 1 shows that the abstraction can be overestimated by a factor 2.5 if no action is taken to investigate and correct erroneous data. It is crucial to correct and improve such data before they are used in water-balance calculations, hydrological modelling, abstraction licensing and projections of water use in Denmark.

References

Garcia, H. & Filzmoser, P. 2011: Multivariate statistical analysis using the R package chemometrics, 71 pp. Vienna: Vienna University of Technology, Department of Statistics and Probability Theory.

Thorling, L., Hansen, B., Langtofte, C., Brüsch, W., Møller, R.R. & Mielby, S. 2012: Grundvandsovervågning 2012 – Grundvand. Status og udvikling 1989–2011. Teknisk rapport, http://www.geus.dk/publications/grundvandsovervaagning/1989_2011.htm

Pearson, K. 1901: On lines and planes of closest fit to systems of points in space. Philosophical Magazine, series 6, **2**, 559–572.

R Core Team 2012: R: A language and environment for statistical computing. Vienna: R Foundation for Statistical Computing, *http://www.R-project.org/*

Stockmarr, J. & Thomsen, R. 2006: Water supply in Denmark. The Danish action plan for promotion of eco-efficient technologies – Danish lessons, 18 pp. Copenhagen: Miljøstyrelsen.

The European Parliament and the Council of the European Union 2000: Establishing a framework for community action in the field of water policy. *http://eur-lex.europa.eu/LexUriServ/LexUriServ.do?uri=CELEX:32000L0060:EN:HTML*

Wikipedia, the free encyclopedia 2013: Principal component analysis. Accessed 7 February 2013. *http://en.wikipedia.org/wiki/Principal_component_analysis*

Authors' addresses

B.L.S. & R.R.M.* *Geological Survey of Denmark and Greenland, Lyseng Allé 1, DK-8270 Højbjerg, Denmark*. E-mail: *bls@geus.dk*

* Present address: *Horsens Kommune, Rådhustorvet 4, 8700 Horsens, Denmark*.

Seismic activity in Denmark: detection level and recent felt earthquakes

Trine Dahl-Jensen, Peter H. Voss, Tine B. Larsen and Søren Gregersen

The Geological Survey of Denmark and Greenland (GEUS) records seismological data at six locations in Denmark (Fig. 1) and all data from these stations are manually reviewed for events like earthquakes and explosions. The identified events are analysed and located, in many cases using supporting data from stations outside Denmark. Seismic events have been recorded instrumentally in Denmark since 1929, but earthquakes felt in Denmark have been reported as far back as 1515 (Lehmann 1956; Gregersen *et al.* 1998; GEUS 2012). This article reports on the developments in detection level of both man-made events and natural earthquakes within the Danish Exclusive Economic Zone (EEZ) from 2000 to 2012. Changes in detection level are mainly due to the availability of data from new seismic stations in Sweden and Norway as well as from a GEUS test station at Gøttrup in NW Jylland. As a case study, the list of events on and around Bornholm is reviewed. Also described here are the reported intensities at two recent felt events in Denmark (North Sea magnitude 4.3 on 19 February 2010 and Kattegat magnitude 4.1 on 6 August 2012).

Development in detection level and completeness from 2000 to 2012

The events from 2000 to 2012 located within the Danish EEZ (Fig. 1) are divided into known explosions (pink), events recorded only on one or two stations which are typically small events (yellow), events where a magnitude could not be calculated (grey) and events which possibly are earthquakes (red) and recorded on three or more stations. Many of the 'possibly earthquakes' events occur in areas where explosions are known to take place, and many of these events are suspected to have a man-made origin. Many explosions are reported to the Seismological Service at GEUS, and are tagged as such, but many more are not reported and only some are tagged as possible explosions. The North Sea is the only area with no explosions known to the Seismological Service but with many probable earthquakes. For example, the earthquake felt in February 2010, described below, is located in this area. However, earthquakes do occur in other areas of Denmark; for example the felt earthquake that occurred in August 2012 in Kattegat.

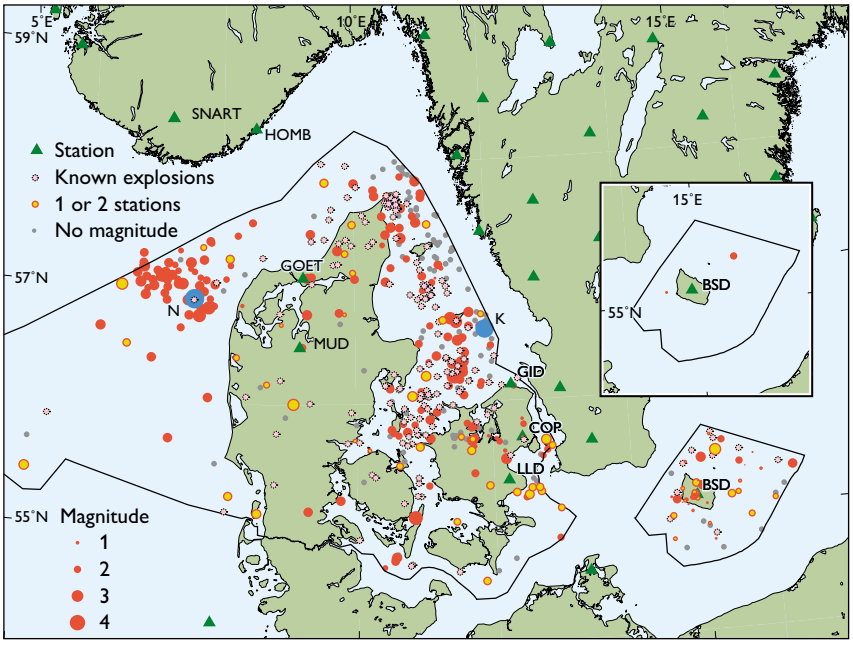

Fig. 1. Seismic events within the Danish Exclusive Economic Zone (EEZ). Among the recorded events are un-identified explosions, particularly in the area where many identified explosions are marked (in pink). The two felt events described in this paper are marked in blue. **K** = Kattegat on 6 August 2012 and **N** = North Sea on 19 February 2010. Seismological stations are green triangles. The events are divided into events seen on three or more stations with defined magnitude (red), events seen on only one or two stations with defined magnitude (yellow), events where no magnitude has been calculated (grey) and known (or probable) explosions (pink). Inset: The EEZ around Bornholm after revision of the database.

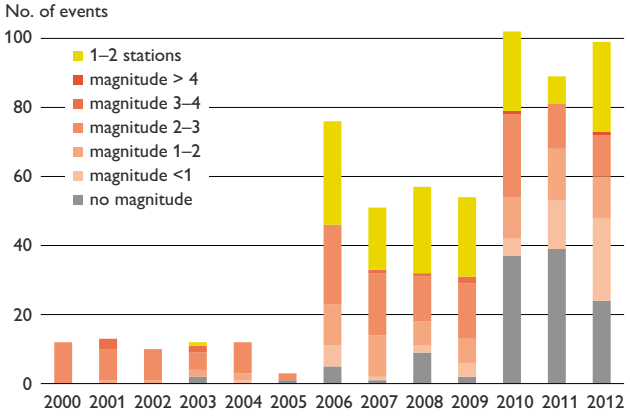

Fig. 2. Statistics on event detection from 2000–2012 within the Danish Exclusive Economic Zone. Known or probable explosions are not included.

In the years 2000–2005, fewer than 15 events (either earthquakes or non-reported explosions) observed on three or more stations were recorded each year, with an additional *c.* 20 known explosions. Only large events were seen outside the Danish network of stations (at the time BSD, COP, MUD, LLD and GID) (Fig. 1). The number of events rose dramatically in 2006 (Fig. 2), as a result of the installation of the Norwegian seismological station SNART (NNSN 2012). The addition of this station has aided in locating events, as it provides a much improved geometry of the station network (Fig. 1). The increase in the number of events recorded is also due to a change in policy in 2006; since then

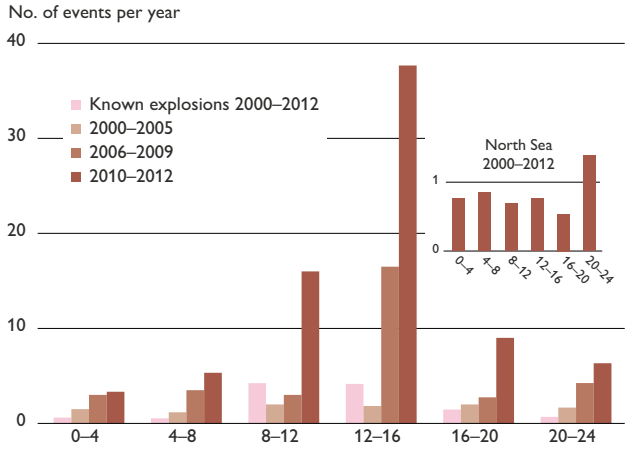

Fig. 3. Seismic events seen on three or more stations sorted by time of day. The events are sorted into 4 hour intervals in UTC time. Denmark is one hour ahead of UTC (two hours in summertime). For each series of years, the number of events within a 4 hour interval is calculated as per year, so the three periods (2000–2005; 2006–2009 and 2010–2012) can be compared. In addition the number of known explosions in the entire period (2000–2012) is sorted in the same manner for comparison. Inset: events in the area in the Danish North Sea with many events recorded but no known explosions.

events located by azimuthal analysis when only one or two stations have recorded the events (Fig. 2) are included. For events seen on three or more stations, the increase is most pronounced for the smaller events, under magnitude 2, but also events with magnitudes between 2 and 3 are more numerous. The next large step up in event detections occurred in 2010 (Fig. 2). This is due to data from the large Swedish network (SNSN 2012) becoming available, and also data from the new Norwegian station HOMB. Many of the additional events, only recorded on the SNSN stations, have no magnitude due to missing calibration information from the new SNSN. In 2012 the number of events with no magnitude declined, while the total number of events is fairly constant, as a result of SNSN becoming established and complete metadata becoming available. In Denmark we added GOET as a test station in 2012, and data came online in November 2012. Together with MUD and the Norwegian stations the azimuth coverage for the many events in the Danish North Sea is highly improved.

Explosions in the database

Far from all activity recorded within the Danish EEZ are natural earthquakes. The Seismological Service at GEUS is frequently notified by the Danish Navy of upcoming or recent blasts. Following World War II, numerous unexploded mines and ammunition are still present in Danish water; the largest neutralised in 2012 was equivalent to 800 kg TNT. The Navy searches for the mines and detonates them on site. Many are seen as signals on the seismic stations, and if known to be explosions they are logged as such in the database. On Fig. 1 the known explosions are marked with pink, and are present in large parts of Danish waters. Known explosions also occur on land – for example in controlled-source scientific projects (Thybo *et al.* 2006) and on rare occasions a house demolition. However, not all explosions are known by the Seismological Service. Natural earthquakes are distributed evenly throughout the 24 hours of the day, while man-made events such as explosions mainly take place during the daytime. The Navy usually blasts in the early afternoon. Figure 3 illustrates the distribution of recorded events sorted by of day, and it is clear that the distribution is heavily skewed towards events in daytime hours. The known explosions are, as expected, concentrated during daytime hours; the exception being urgent blasts when a find of undetonated explosives endangers the surroundings. Scientific blasts often take place during the quiet night hours. In the period 2000–2005 the events are evenly distributed through all 4 hour intervals, while the events in both the 2006–2009 and the 2010–2012 periods have a large overrepresentation in daytime. In total

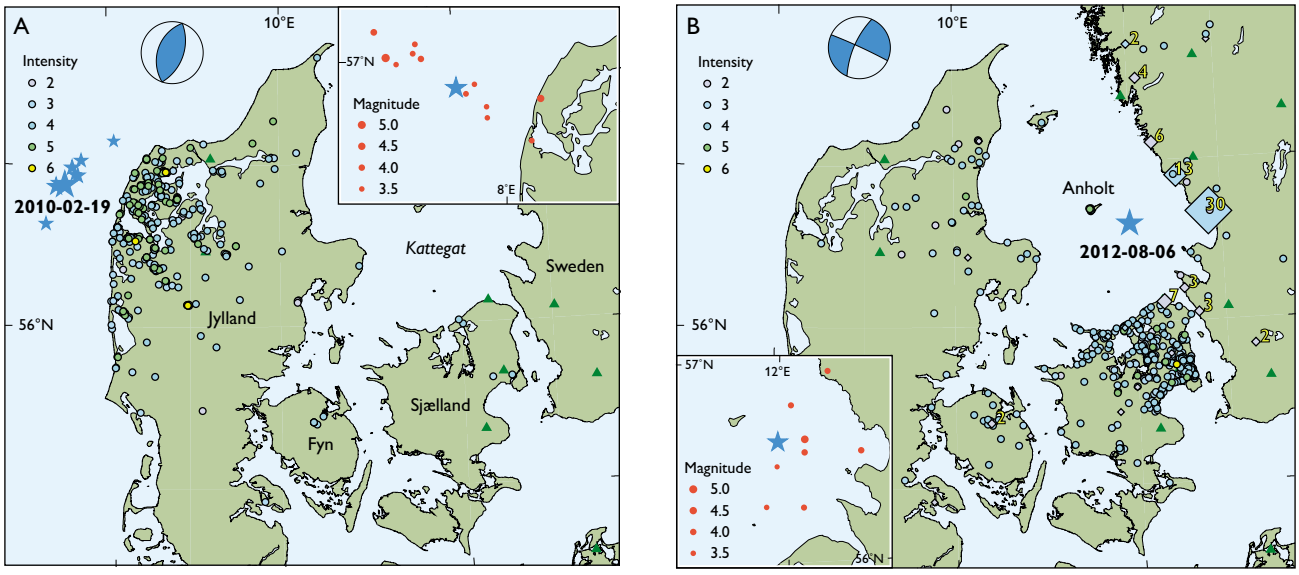

Fig. 4. Reports of observed intensity from the public. The earthquakes are marked by blue stars scaled by size. **A**: North Sea on 19 February 2010 magnitude 4.3. GEUS received 344 reports from people who felt the earthquake. Seven small aftershocks (magnitude 1.9 to 2.8) were observed during four weeks after the main event. **B**: Kattegat on 6 August 2012 magnitude 4.1. In addition to reports received by GEUS (441), we have reports from the United States Geological Survey (in all 76 reports of which more than half are from Sweden (30 in Halmstad and 13 in Falkenberg)) marked with diamonds scaled to the number of individual reports, and from The Swedish National Seismic network (SNSN) (16 reports) – marked with dots in Sweden – are included. The insets in both A and B are all known, instrumentally recorded events over magnitude 3.5 in the two areas.

426 events are included. Assuming that the night-time level of events is correct, and the natural earthquakes are evenly distributed, a simple calculation shows that at least half the events are probably not natural earthquakes. Not all explosions are reported to GEUS, for example explosions carried out by foreign naval vessels participating in exercises in Danish waters or mines or ammunition neutralised by our neighbouring countries but erroneously located into Danish waters. The only area where no known explosions are located is within the group of events in the Danish North Sea. For events in this area there is no concentration in daytime (Fig. 3 – inset), and they are assumed to be natural earthquakes.

Case study Bornholm

A revision of the entire database of seismic events is in its initial phase, and for 2000 to 2012 the revision has been carried out on Bornholm and within the EEZ around the island. Here quarry blasts add to the man-made events recorded, as Bornholm Granit blasts several times a week at set times (Paul Ebbesen, Rønne Granit, NCC, pers. communication). By logging all events known or strongly suspected to be explosions, excluding small events seen only on one or two stations (and with a large uncertainty in location) and events so small that no magnitude could be calculated in spite of all necessary station information, only two events remain as probable natural earthquakes. The original list contained 129 events within the EEZ around Bornholm, of which 25 were seen on three or more stations (of these three without magnitude). The remaining 104 events were seen only on one or two stations, and many with no magnitude. Seventy events are suspected quarry blasts. In all 23 events had a magnitude of 2 or higher. Ten previously known explosions make an original total of 139 events recorded. The two 'surviving' events are marked on the inset on Fig. 1 and are a magnitude 2.0 event in 2006 and a very small magnitude 0.8 event in 2011.

Recent felt earthquakes

It is rare for Denmark to experience an earthquake which can be felt. However, it does happen and the two most recent felt earthquakes are briefly described below.

North Sea, 19 February 2010, magnitude 4.3

At 21:08 UTC (22:08 local time) on 19 February 2010, a magnitude 4.3 earthquake occurred 45 km offshore the north-western Danish coast at a depth of 39 km (Fig. 4A). The focal mechanism indicates a reverse fault overthrusting to the west, in agreement with earlier earthquakes in the area. This is the most active area in Denmark, with many known earthquakes. From the instrumental era, Table 1 lists

Table 1. All instrumentally recorded events over 3.2 on the Richter scale in the areas around the North Sea and Kattegat earthquakes

Y/M/D-T (UTC)	Position (Degree)	Depth (km)	Stations	Magnitude (ML)
North Sea area				
1954/10/18 -16:44	56.85N 8.29E	25.5	4	4.6
1964/07/14 -05:33	57.03N 7.20E	36.0		4.0
1969/04/05 -19:09	57.16N 6.76E	0.1	23	4.2
1975/11/12 -06:00	57.10N 7.14E	40.0	37	3.7
1978/04/26 -12:32	56.75N 7.81E	40.0	18	3.4
1981/09/06 -04:11	57.03N 6.88E	40.0	84	5.2
1981/09/07 -14:03	57.06N 7.12E	30.3	13	3.6
1982/05/24 -03:10	56.64N 8.21E	41.4	25	3.7
1987/03/01 -06:42	57.00N 6.98E	40.1	26	3.5
1997/11/15 -16:11	56.86N 7.62E	6.6	56	3.6
1997/12/04 -22:03	56.91N 7.69E	8.5	48	3.4
2001/06/02 -00:44	56.80N 7.80E	59.3	39	3.5
2010/02/19 -21:08	56.89N 7.52E	22.0	111	4.3
Kattegat area				
1970/03/12 -16:05	56.54N 12.69E	0.0	12	4.0
1980/01/21 -07:41	56.27N 12.16E	10.2	29	3.9
1982/11/01 -02:48	56.28N 11.82E	3.4	17	3.5
1985/06/15 -00:40	56.61N 12.19E	9.1	44	4.7
1986/04/01 -09:56	56.54N 12.18E	7.2	37	4.1
1990/05/24 -09:51	56.48N 11.93E	10.0	15	3.2
1995/10/04 -20:49	56.78N 12.08E	9.9	31	3.8
1997/09/20 -14:21	56.94N 12.42E	15.0	4	3.8
2012/08/06 -02:57	56.60N 11.95E	22.1	31	4.1

earthquakes in the area over magnitude 3.5 (see also inset in Fig. 4 A). Earlier earthquakes are also known historically (Gregersen *et al.* 1991). GEUS received 344 macroseismic reports with observations of the 2010 earthquake from the public. The earthquake was mainly felt in north-western Denmark, with a few reports from northern Sjælland and Fyn. All observations were classified according to the European Macroseismic Scale (Grünthal 1993), and ranged from 2 to 6, including three instances of slight damage to houses in the form of cracks in walls.

Kattegat, 6 August 2012, magnitude 4.1

Early morning at 02:57 UTC (03:57 local time) on 6 August 2012, a magnitude 4.1 earthquake occurred in Kattegat, 26 km from the island of Anholt, at a depth of 22 km. The focal mechanism indicates a dextral strike-slip movement in a NW–SE direction, aligning with the general fault direction in the area including the Tornquist zone. Also in this area earthquakes are known, both historically (Gregersen *et al.* 1991) and instrumentally recorded (events over magnitude 3.5 in Table 1 and inset in Fig. 4B). GEUS received 441 macroseismic reports with observations of the 2012 earthquake from the public. The earthquake was felt mainly in northern Sjælland – where the population density is high, and where many people also experienced the magnitude 4.8 earthquake in southern Sweden in 2008 (Voss *et al.* 2009). But the earthquake was also felt in north-eastern Jylland and northern Fyn – and of course on Anholt. Furthermore, this event was widely felt in Sweden, and on Fig. 4B observations from SNSN (SNSN 2012) and USGS (USGS 2012) in USA are included. All observations were classified according the European Macroseismic Scale (Grünthal 1993), and ranged from 2 to a single occurrence of intensity 6 where small cracks had opened in the façade of a house.

Acknowledgement

Reynir Bodvarsson at University of Uppsala kindly supplied us with the macroseismic reports in Sweden from the Kattegat event.

References

GEUS 2012: Seismological Service. Registrerede jordskælv, http://www.geus.dk/departments/geophysics/seismology/seismo_reg-dk.htm

Gregersen, S., Korhonen, H. & Husebye, E.S. 1991: Fennoscandian dynamics: Present-day earthquake activity. Tectonophysics **189**, 333–344.

Gregersen, S., Hjelme, J. & Hjortenberg, E. 1998: Earthquakes in Denmark. Bulletin of the Geological Society of Denmark **44**, 115–127.

Grünthal, G. (ed.) 1993: European Macroseismic Scale 1992 (updated MSK scale). pp. Luxemborg: European Seismological Commision, Subcommision of Engineering Seismology, Working Group Macroseismic Scales.

Lehmann, I. 1956: Danske jordskælv. Bulletin of the Geological Society of Denmark **13**, 88–103.

NNSN 2012: Norsk Nasjonalt Seismik Nettverk, *http://www.geo.uib.no/seismo/nnsn/index.shtml*

SNSN 2012: Svenska Nationella Seismiska Nätet, *http://snsn.geofys.uu.se/*

Thybo, H., Sandrin, A., Nielsen, L., Lykke-Andersen, H. & Keller, G.R. 2006: Seismic velocity structure of a large mafic intrusion in the crust of central Denmark from project ESTRID. Tectonophysics **420**, 105–122.

USGS 2012: National Earthquake Information Center – NEIC, *http://earthquake.usgs.gov/regional/neic/*

Voss, P.H., Larsen, T.B., Ottemüller, L. & Gregersen, S. 2009: Earthquake in southern Sweden wakes up Denmark on 16 December 2008. Geological Survey of Denmark and Greenland Bulletin **17**, 9–12.

Authors' address

Geological Survey of Denmark and Greenland, Øster Voldgade 10, DK-1350 Copenhagen K, Denmark. E-mail: *tdj@geus.dk*

The norite belt in the Mesoarchaean Maniitsoq structure, southern West Greenland: conduit-type Ni-Cu mineralisation in impact-triggered, mantle-derived intrusions?

Adam A. Garde, John Pattison, Thomas F. Kokfelt, Iain McDonald and Karsten Secher

With the recent discovery of the giant, deeply eroded, 3 Ga Maniitsoq impact structure in southern West Greenland (Garde 2010), an enigmatic, *c.* 75 by 15 km large, curvilinear belt of undeformed norite intrusions with Ni-Cu mineralisation was re-interpreted as representing crustally contaminated melts derived from the mantle in the wake of the impact (Fig. 1; Garde *et al.* 2012). The norite belt (Nielsen 1976; Secher 1983) was discovered in the early 1960s by the mining and exploration company Kryolitselskabet Øresund A/S, and more than one hundred shallow exploration holes were drilled by the company in the period 1965–1971. The mineralisation has subsequently been investigated by Cominco Ltd., Falconbridge Ltd. and NunaMinerals A/S. In 2011, the re-interpretation of the norite belt, and recent availability of improved airborne geophysical exploration tools, prompted the Canadian company North American Nickel Inc. (NAN) to resume exploration.

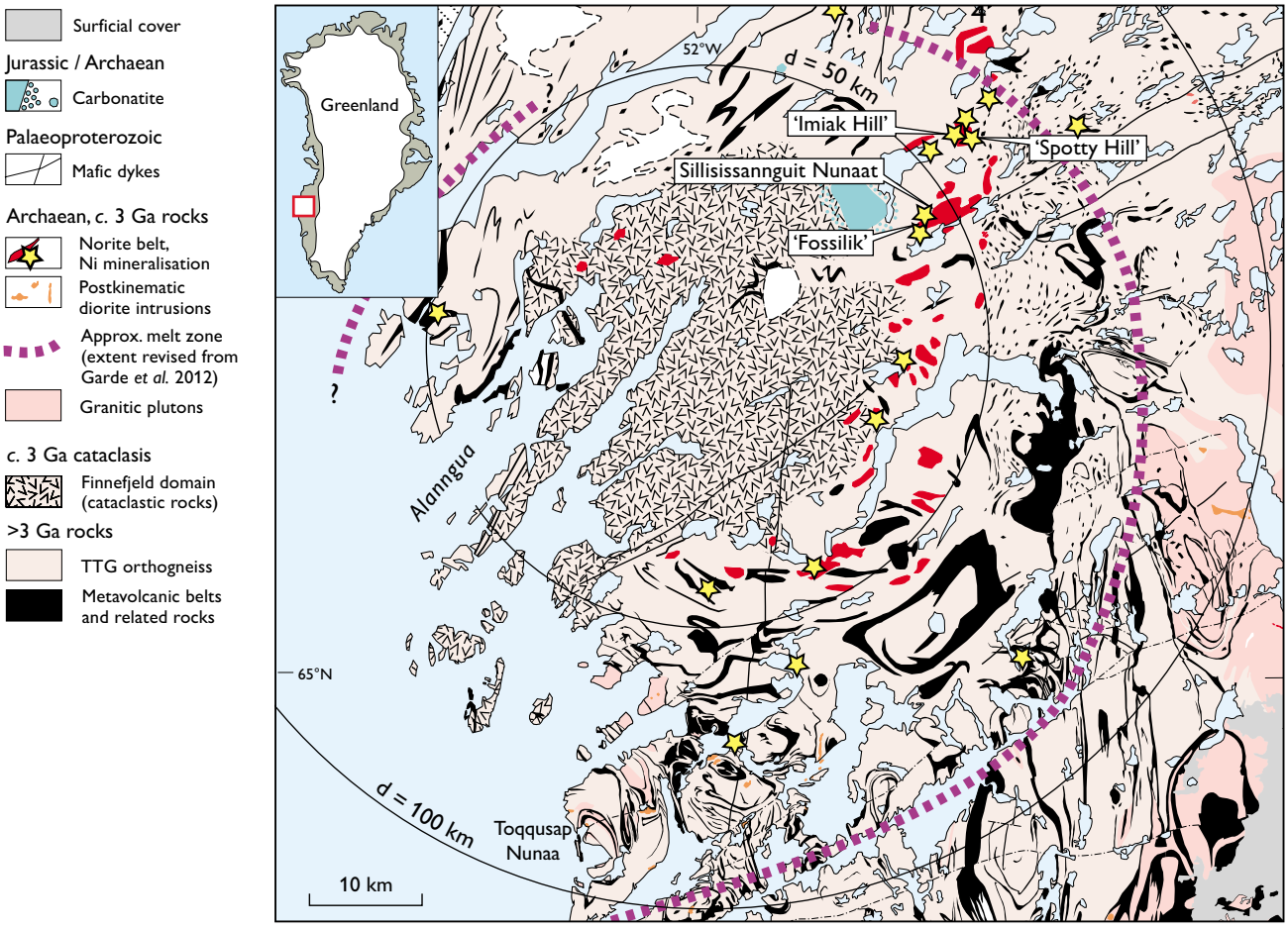

Fig. 1. Geological map of the central part of the Maniitsoq impact structure with the cataclastic Finnefjeld domain in its centre, currently known distribution of norites and postkinematic diorites, and three labelled diamond drilling sites from 2012. Reference circles with 50 and 100 km diameters are shown.

Fig. 2. Typical homogeneous, undeformed norite outcrop with diffuse, hybridised contact zones to quartzo-feldspathic orthogneiss. From Garde *et al.* (2012).

This contribution gives a short description of the norite belt, outlines its Ni-Cu mineralisation and presents a preliminary interpretation. It is well known that the 1.85 Ga Sudbury impact structure in Canada hosts a group of world-class Ni-Cu deposits at the base of the impact melt sheet (Eckstrand & Hulbert 2007). The Ni-Cu mineralisation of the norite belt in West Greenland is profoundly different as it is located in lower-crustal mafic intrusions, but we suggest here that also this was governed by impact-related magmatic processes.

The Maniitsoq structure

The Maniitsoq structure (Garde *et al.* 2012) constitutes the deeply eroded, deep-crustal remains of a giant extraterrestrial impact that struck an active magmatic arc 3 Ga ago in the north-central part of the North Atlantic craton (Fig. 1). The visible remains of the structure comprise a core measuring 35 by 50 km of thoroughly crushed, mechanically mixed and subsequently welded fragments of orthogneiss and amphibolite (together constituting the Finnefjeld domain), surrounded by an up to *c.* 75 km wide, annular melt zone variably affected by both crushing and melting, and a peripheral, less damaged zone with a diameter of approximately 150 km. Large parts of the entire structure have been affected by intense hydrothermal alteration and related, fluid-induced, partial melting. These features, and their large geographical extent, suggest that the original Maniitsoq crater was larger than all previously known terrestrial impact structures.

Fig. 3. Proto-orbicular texture in norite, with rounded, skeletal plagioclase crystals and interstitial hypersthene. The hammer is 45 cm long.

The norite belt and postkinematic diorites

The norite belt (see above) and associated postkinematic diorites in the southern part of the impact structure (Berthelsen 1960; Garde 1991) collectively comprise numerous mafic to ultramafic intrusions ranging in size from small dykes to inclined, elongate bodies up to several square kilometres in outcrop size, hosted by Mesoarchaean orthogneisses and mafic, metavolcanic belts. They were emplaced close to 3.0 Ga ago (see Garde *et al.* 2012), and their undeformed state and occasional xenoliths of crushed orthogneiss and fluidised microbreccia document that they post-date the impact. The intrusions are locally cut by few centimetres thick, white, undeformed pegmatites. Most intrusions display inclined host-rock contacts, and the exposed bodies may thus represent open-ended magma conduits. The hybridised contact zones are diffuse, up to about 10 m wide and commonly hydrated (Fig. 2). The known extent of the norite belt is shown on Fig. 1, but at least a few additional, unmapped bodies are known to occur east and west of the main belt. The postkinematic diorites have a more random distribution and extend up to *c.* 70 km south and east of the centre of the impact structure. They have only been mapped systematically south of 65°N.

The noritic and dioritic rocks typically form dark brown, crumbly weathering, medium- to coarse-grained, mostly structureless masses. They largely consist of variable proportions of orthopyroxene and andesine plagioclase with medium- to coarse-grained, granular textures. Rhythmic magmatic layering is rare, but has been observed, e.g. at Sillisissannguit Nunaat (Fig. 1; Secher 1983). Both small and large intrusions locally display proto-orbicular quench textures comprised of skeletal, rounded to ellipsoidal plagioclase crystals up to about 10 cm in size, and interstitial orthopyroxene (Fig. 3), and locally display metre-scale layering. Bulk compositions cover a large range from dioritic to

noritic, but display a broadly uniform trace element distribution pattern; high MgO, Cr and Ni contents (≤21 wt%, 3685 ppm and 909 ppm, respectively) coupled with low Nb and Ta suggest an ultramafic precursor affected by abundant crustal contamination (Garde 1991; Garde *et al.* 2012).

Ni-Cu mineralisation

More than 50 sulphide-mineralised norite localities with uniform characteristics have been investigated over time (Nielsen 1976; unpublished company reports). In typical, two-dimensional outcrops, the mineralised rocks form isolated, rusty weathered spots and lenses that rarely exceed 25 m in length (Secher 1983). The sulphide paragenesis in fresh samples is almost invariably pyrrhotite-pentlandite-chalcopyrite-pyrite, with accessory magnetite and ilmenite. The sulphide minerals form interconnected, semi-massive networks with inclusion-bearing, breccia-like textures characterised by rounded, centimetre-sized and larger lumps of the host rock (Fig. 4). These textures closely resemble those found in magmatic, conduit-type Ni deposits such as Noril'sk in Russia and Lynn Lake and Voisey's Bay in Canada (Eckstrand & Hulbert 2007).

All significant nickel occurrences discovered to date at Maniitsoq are entirely contained within norite intrusions. Based on NAN's diamond drilling, combined with historical drill-hole information and three-dimensional modelling of airborne geophysical and down-hole electromagnetic data, the mineralisation can typically be described as steeply to vertically dipping pipe- and sheet-like bodies comprised of heavily disseminated to near massive sulphide, often with abundant 0.2–5.0 cm subangular to subrounded inclusions of norite. In most cases, strongly mineralised zones are surrounded by a broad halo of weaker, disseminated mineralisation; however, in some places the contact between near solid sulphide and barren norite host rock is extremely sharp.

Diamond drilling in 2012 was performed at 'Imiak Hill', 'Spotty Hill' and 'Fossilik II' (cf. Fossilik in Fig. 1); the following, generalised figures of metal contents are solely intended to characterise the type of mineralisation without addressing economic aspects. The mineralisation has a high, uniform Ni tenor averaging 6–9% Ni recalculated to 100% sulphide, both at localities previously drilled by Kryolitselskabet Øresund A/S and also in new cores drilled by NAN at 'Imiak Hill' and 'Spotty Hill' in 2012. Typical Ni contents in wt% of the total rock vary between 1 and 2% over several to many metres, with additional 0.1–0.6% Cu, 0.01–0.07% Co, up to 0.2 ppm Pt and Pd, and Au in the ppb range (data from *www.northamericannickel.com* and Secher 2001). These relatively low platinum-group element tenors are similar to the Voisey's Bay deposit (Lightfoot *et al.* 2012).

Fig. 4. Inclusion-bearing, breccia-like texture of Ni-Cu mineralisation at 'Imiak Hill' (North American Nickel Inc. 2012 drill core MQ-12-002 at 66.55 m).

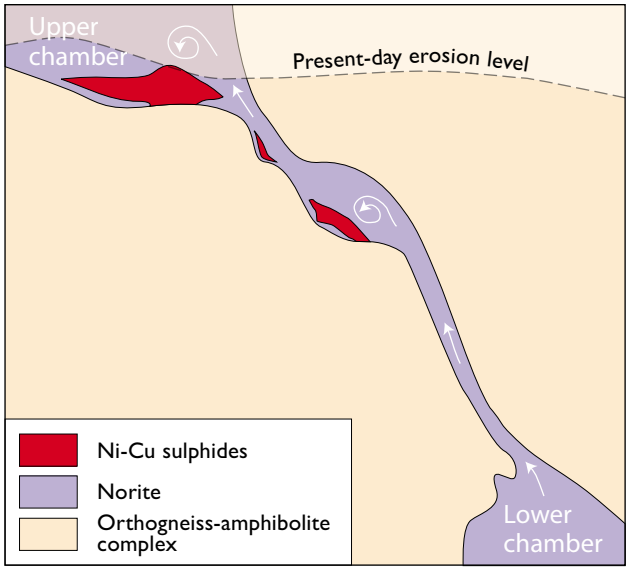

Fig. 5. Magmatic open-conduit model for the Ni-Cu mineralisation in the norite belt. Schematic vertical section. Modified from Maier *et al.* (2001).

Discussion and interpretations

Origin of the noritic and dioritic intrusions

Garde (1991) and Garde *et al.* (2012) interpreted the noritic and almost all of the dioritic intrusions as highly unusual, mantle-derived, crustally contaminated ultrabasic melts. This interpretation is based on (1) the wide, hybrid contact zones and (2) proto-orbicular interior textures of skeletal plagioclase and orthopyroxene, showing that the magmas were chilled by their hosts and crystallised rapidly (and thus indicating a very high emplacement temperature), (3) highly variable chemical compositions combined with (4) broadly similar overall element spectra consistent with mantle-crust mixtures, (5) ultramafic trace element signatures with very high Cr, Ni and V contents, and (6) mantle-like, strongly suprachondritic Ru/Ir, Rh/Ir, Pt/Ir and Pd/Ir ratios similar to high-Mg basalts.

Interpretation of the Ni-Cu (-PGE) mineralisation

Magmatic Ni-Cu-PGE deposits are governed by several different factors (e.g. Li *et al.* 2001; Maier *et al.* 2001) including a fertile source (typically the mantle), where a significant Ni contribution comes from interstitial sulphide minerals in addition to olivine. A high degree of melting is also required in order to ensure a complete dissolution of the sulphides with their metals into the primary magma. On the ascent of the magma, segregation of immiscible, sulphidic melt from the silicate melt must then occur in order to recapture the chalcophile elements of interest. In general terms, such segregation in response to sulphur saturation can be brought about by either fractional crystallisation in large magma chambers (potentially leading to PGE-dominated deposits), or by crustal contamination in dynamic magma channels of restricted volume, potentially leading to Ni-Cu-dominated deposits (Li *et al.* 2001). In the latter case, a suitable physical mechanism to separate and concentrate the exsolved, high-density sulphide liquid from the flowing magma is also required.

The essential features of the sulphide occurrences in the norite belt are all compatible with an interpretation as magmatic, open-source mineralisation systems. These features include high-temperature ultramafic host rock melts, abundant field and chemical evidence of crustal contamination, inclusion-bearing, breccia-like textures in the mineralised rocks, a high Ni tenor in the sulphides, and Ni/Cu and (Ni + Cu)/PGE ratios characteristic of this type of mineralisation. The three-dimensional shapes of the mineralised volumes and mechanism(s) of physical extraction of the exsolved sulphide melt phase are currently poorly known, but a schematic section of a possible scenario is shown in Fig. 5.

Concluding remarks

Widespread ultramafic magmatism, such as in the norite belt, does not belong in convergent orogenic systems (Garde 1991; Garde *et al.* 2012), although ultramafic intrusions can occur under special plate-tectonic circumstances of ridge subduction or delamination of the lower crust, for which there is no evidence at Maniitsoq. Furthermore, the proto-orbicular textures and very high degrees of contamination in the norite belt and postkinematic diorites are highly unusual even for ultramafic melts.

The possibility of impact-induced mantle melting associated with giant impacts has previously been discussed in the literature (Jones *et al.* 2002), but no examples have been found prior to the case at Maniitsoq (see Garde *et al.* 2012). We conclude that the Ni-Cu occurrences in the norite belt are likely an impact-induced mineralisation. However, unlike Sudbury they are not part of a differentiated impact melt sheet, but constitute a special variety of open-conduit systems, which are otherwise known from magmatic settings of non-impact origin.

References

Berthelsen, A. 1960: Structural studies in the pre-Cambrian of western Greenland. II. Geology of Tovqussap nunâ. Bulletin Grønlands Geologiske Undersøgelse **25**, 223 pp.

Eckstrand, O.R. & Hulbert, L.J. 2007: Magmatic nickel-copper-platinum group element deposits. In: Goodfellow, W.D. (ed.): Mineral deposits of Canada: a synthesis of major deposit types, district metallogeny, the evolution of geological provinces, and exploration methods. Geological Association of Canada Special Publication **5**, 205–222.

Garde, A.A. 1991: Post-kinematic diorite intrusions in Archaean basement rocks around outer Fiskefjord, southern West Greenland. Bulletin of the Geological Society of Denmark **39**, 167–177.

Garde, A.A. 2010: The 2975 Ma Maniitsoq impact structure in West Greenland: the oldest and most deeply exposed meteorite crater on Earth. Abstracts and Proceedings of the Geological Society of Norway **1**, 57–58.

Garde A.A., McDonald, I., Dyck, B. & Keulen, N. 2012: Searching for giant, ancient impact structures on Earth: the Mesoarchaean Maniitsoq structure, West Greenland. Earth and Planetary Science Letters **337–338**, 197–210.

Jones, A.P., Price, G.D., Price, N.J., De Carli, P.S. & Clegg, R.A. 2002: Impact induced melting and the development of large igneous provinces. Earth and Planetary Science Letters **202**, 551–561.

Li, C., Maier, W.D. & de Waal, S.A. 2001: Magmatic Ni-Cu versus PGE deposits: contrasting genetic models and exploration implications. South African Journal of Geology **104**, 309–318.

Lightfoot, P.C., Keays, R.R., Evans-Lamswood, D. & Wheeler, R. 2012: Saturation history of Nain Plutonic Suite mafic intrusions: origin of the Voisey's Bay Ni-Cu-Co sulfide deposit, Labrador, Canada. Mineralium Deposita **47**, 23–50.

Maier, W.D., Li, C. & de Waal, S.A. 2001: Why are there no major Ni-Cu sulfide deposits in large layered mafic–ultramafic intrusions? Canadian Mineralogist **39**, 547–556.

Nielsen, B.L. 1976: Economic minerals. In: Escher, A. & Watt, W.S. (eds): Geology of Greenland, 460–487. Copenhagen: Geological Survey of Greenland.

Secher, K. 1983: Noritic rocks and associated nickel-copper-sulphide occurrences in Sukkertoppen district, central West Greenland. Rapport Grønlands Geologiske Undersøgelse **115**, 30–34.

Secher, K. 2001: The Pd+Pt dispersion in noritic and undifferentiated mafic rocks of the Archaean craton east of Maniitsoq, southern West Greenland. Danmarks og Grønlands Geologiske Undersøgelse Rapport **2001/123**, 22 pp.

Authors' addresses

A.A.G., T.F.K. & K.S., *Geological Survey of Denmark and Greenland, Øster Voldgade 10, DK-1350 Copenhagen K, Denmark*. E-mail: *aag@geus.dk*

J.P., *North American Nickel Inc., 301–260 W. Esplanade, North Vancouver, BC V7M 3G7, Canada.*

I.McD., *School of Earth and Ocean Sciences, Cardiff University, P.O. Box 914, Cardiff CF10 3YE, UK.*

Geochemistry and petrology of gold-bearing hydrothermal alteration zones on Qilanngaarsuit, southern West Greenland

Martin Koppelberg, Annika Dziggel, Denis Martin Schlatter, Jochen Kolb and Franz Michael Meyer

During field work in 2008, the Geological Survey of Denmark and Greenland investigated the gold potential of hydrothermal vein systems in the Nuuk region of the Archaean North Atlantic craton. A new gold occurrence was discovered on the island of Qilanngaarsuit, 35 km south of Nuuk. Two cross sections through hydrothermal alteration zones, that locally contain up to 672 ppb Au, were mapped and sampled in detail. In this study, we present petrological and geochemical data in order to constrain the conditions for ore formation and transport of elements during fluid–rock interaction.

Geological setting

Qilanngaarsuit in southern West Greenland (Fig. 1) is situated in the Godthåbsfjord gold province, a *c.* 20 km by 150 km wide, NE-trending sector along the Ivinnguit fault system. Several gold occurrences such as Storø, Qussuk, Bjørneøen and SW Isua have been described from this sector (Garde *et al.* 2012; Scherstén *et al.* 2012; Kolb *et al.* 2013). The Ivinnguit fault, situated north of the island, is a deep-crustal shear zone, which formed during terrane amalgamation and it represents the border between the Færingehavn and Akia terranes (Nutman & Friend 2007). Qilanngaarsuit island is dominated by Eoarchaean tonalite-trondhjemite-granodiorite (TTG) gneisses of the Færingehavn terrane, which are overlain by amphibolites and aluminous cordierite-orthoamphibole gneisses that originated from *c.* 2840 Ma old protoliths (Nutman & Friend 2007). Four deformation events can be distinguished, involving north-vergent thrusting, isoclinal folding and the formation of late, upright, open to tight folds (e.g. Kolb *et al.* 2013). The gold-bearing quartz veins are hosted by amphibolites in the central part of the island and surrounded by approx. 8 m wide hydrothermal alteration zones. The foliation-parallel, *c.* 10–20 cm wide, quartz veins can be followed over several hundred metres along strike. Structural data indicate that they formed in response to flexural, slip folding during the late-tectonic evolution of the region (Kolb *et al.* 2013). One sample from a hydrothermal alteration zone surrounding the veins contains up to 672 ppb Au and several other vein and alteration zone samples have elevated Au contents (> 20 ppb Au; Kolb *et al.* 2009).

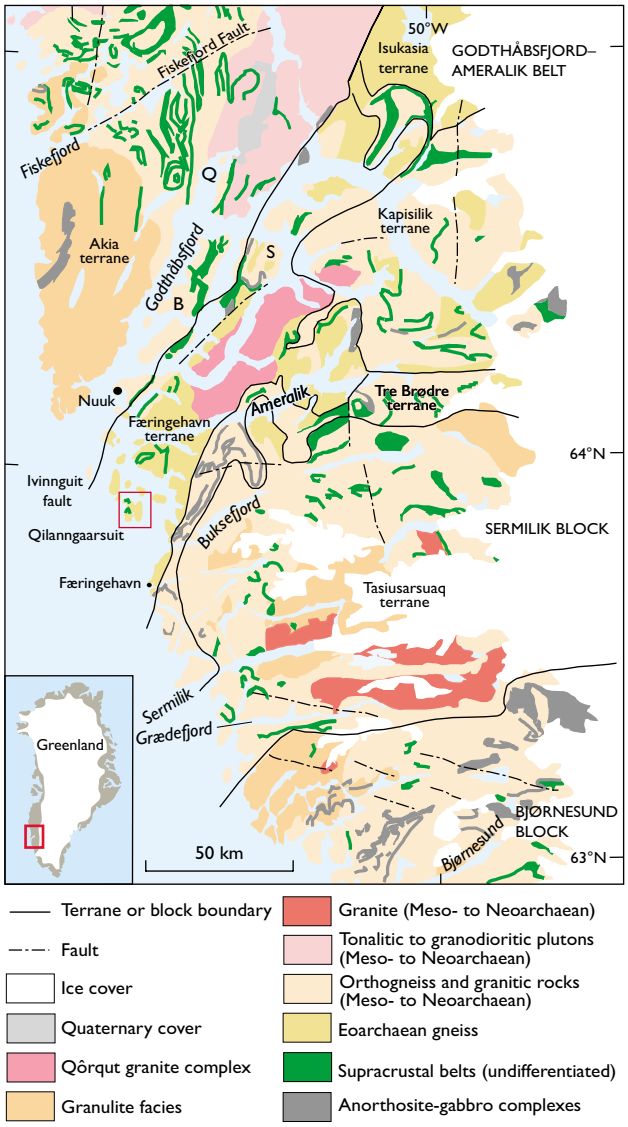

Fig. 1. Geological map of the Nuuk region (modified from Allaart 1984). **B**: Bjørneøen, **Q**: Qussuk, **S**: Storø.

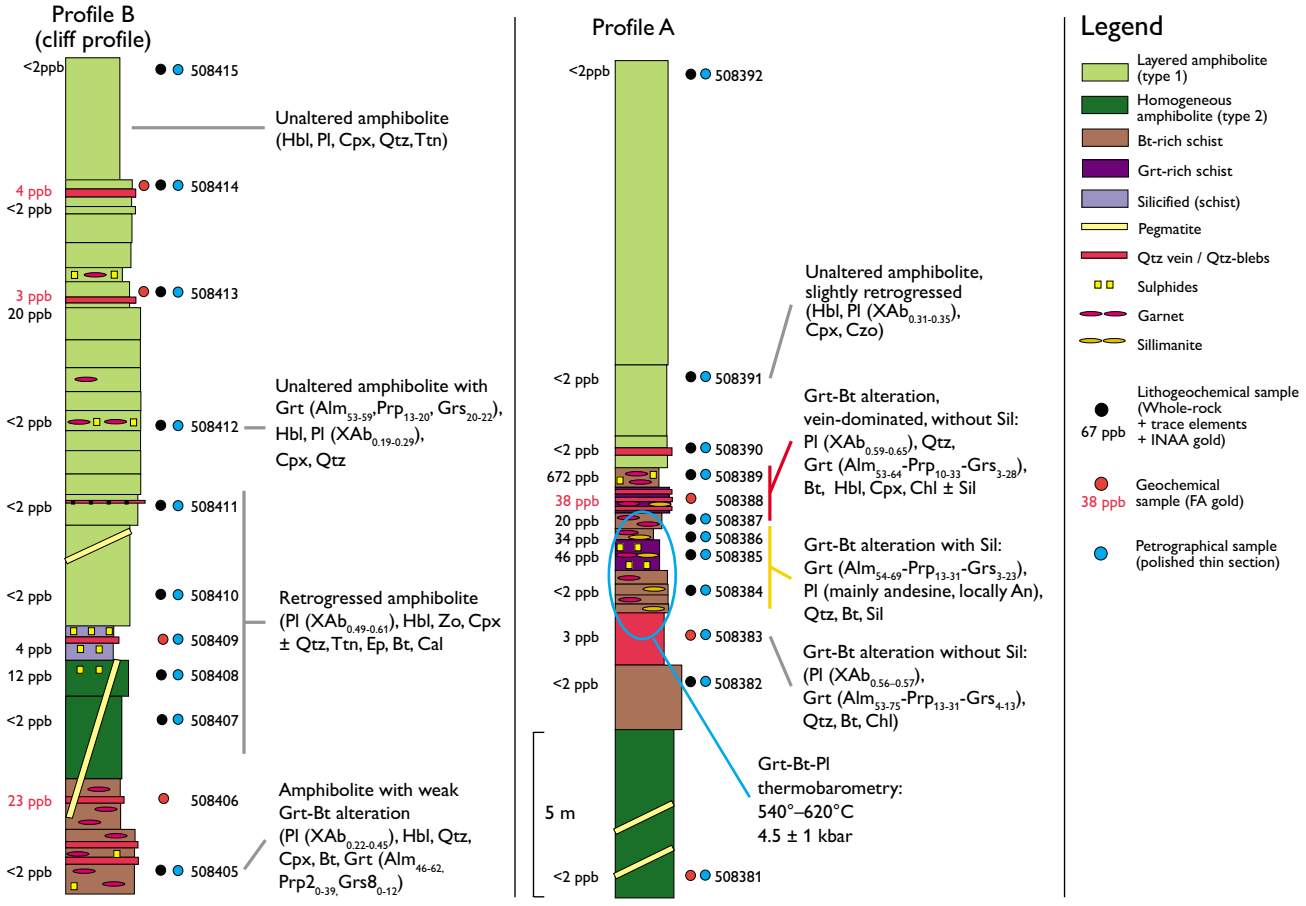

Fig. 2. Lithological logs of profiles **A** and **B** (modified from Schlatter 2009).

Petrology and geochemistry

Two profiles from the unaltered wall rocks through the hydrothermal alteration zones were investigated (Fig. 2). Two types of amphibolite can be distinguished: homogeneous amphibolite in the footwall and compositionally layered amphibolite in the hanging wall of the hydrothermal vein system. Their protoliths were low-K tholeiites depleted in light rare-earth elements (LREE), geochemically similar to other amphibolites in the Buksefjord region (Chadwick 1981). Generally, the amphibolites are fine- to medium-grained and consist of hornblende (40 vol.%), plagioclase (30 vol.%), clinopyroxene (20 vol.%) and clinozoisite/zoisite/epidote (10 vol.%). Metamorphic garnet is locally present in the layered amphibolite. Retrogression is indicated by the transformation of plagioclase to a fine-grained assemblage of zoisite and quartz, and by the replacement of amphibolite and clinopyroxene by epidote and clinozoisite.

Within the alteration zone, the amphibolite-facies mineral assemblages are replaced by a high temperature alteration assemblage of garnet, quartz, plagioclase, biotite, and sillimanite (Figs 2, 3). In contact with the veins, the hydrothermal alteration zone consists of up to 50 vol.% garnet, 15 vol.% plagioclase, 15 vol.% quartz, 10 vol.% biotite and 10 vol.% sillimanite (Fig. 2). Relict amphibole facies minerals such as hornblende and clinopyroxene are locally preserved, indicating that these minerals formed during regional metamorphism prior to the mineralisation. Ore minerals make up ≤1 vol. % of the rocks; they include pyrite, pyrrhotite and chalcopyrite. Mass-balance calculations based on whole-rock, major- and trace- element data (Kolb *et al.* 2009; Koppelberg 2011) and using the method of Gresens (1967) indicate that the ore fluid was enriched in Si, K, LREE, Au, Cr, Cu, Zn, Mo and As (Fig. 4). In Si-rich, vein-dominated samples, the hydrothermal overprint was associated with a volume increase of 14–62%. In contrast, the sillimanite-bearing samples record a significant volume loss of 15–50%, and are depleted in Si (Fig. 4). This suggests that at least some of the Si in the quartz veins was leached from the surrounding wall rocks.

Garnet in the alteration zones is rich in almandine (Koppelberg 2011). Most grains are essentially unzoned and have

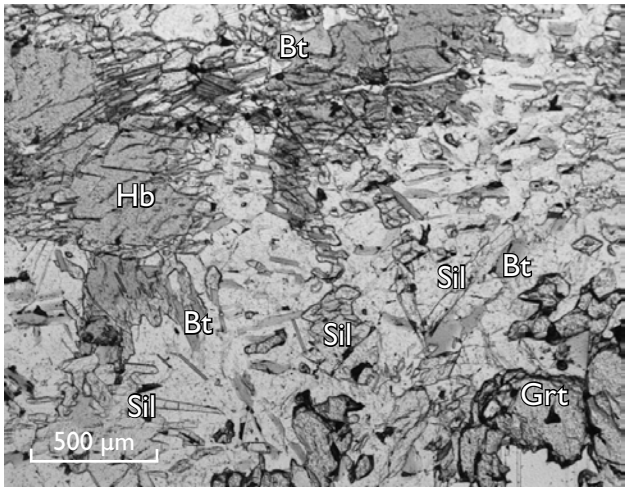

Fig. 3. Photomicrograph illustrating the replacement of the regional metamorphic amphibolite facies mineral assemblages by hydrothermal garnet, biotite and sillimanite in sample GGU 508405.

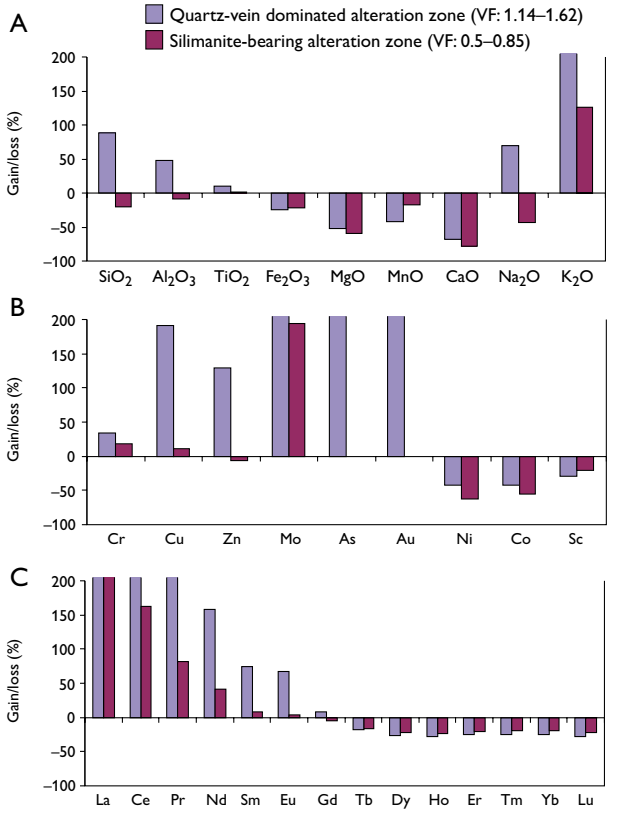

Fig. 4. Results of mass-balance calculations for quartz-vein dominated and sillimanite-bearing alteration zones. **VF**: volume factor – the change of volume of altered rock relative to unaltered rock. **A**: major elements, **B**: trace elements, **C**: rare-earth elements (REE).

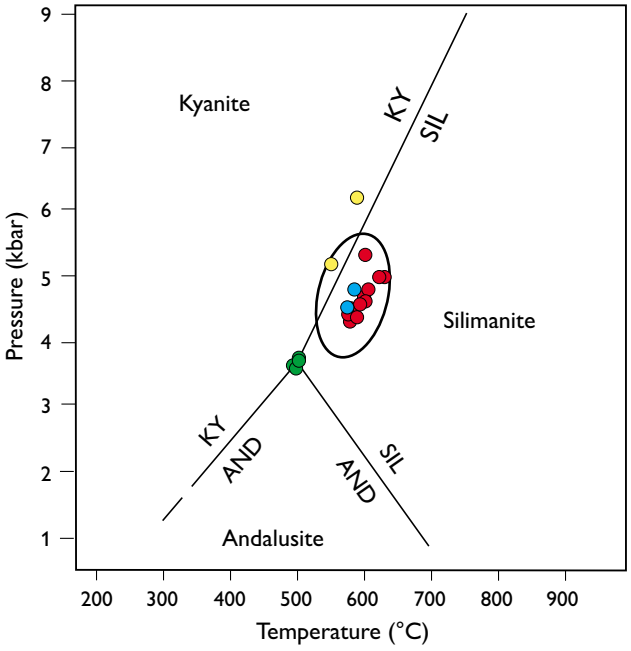

Fig 5. Thermobarometry results (see main text). The Al2SiO5 diagram is from Holdaway & Mukhopadhyay (1993). Red: sample GGU 508384, green: 508385, blue: 508386, yellow: 508405. The Al2SiO5 triple point is at 500°C and 3.75 kbar.

a composition of Alm_{53-69}, Prp_{21-31}, Grs_{3-12}, depending on bulk composition. In some of the larger grains, the rims have slightly higher Fe concentrations (Alm_{62-72}, Prp_{20-25}, Grs_{3-10}). Metamorphic garnet in the unaltered wall rocks is unzoned and enriched in grossular (Alm_{53-59}, Prp_{13-20}, Grs_{17-21}). Both types of garnet have very low REE contents (<2 ppm), and are depleted in LREE. Biotite in the alteration zone has Al^{IV} contents between 2.4 and 2.65 atoms per formula unit and Mg/(Fe+Mg) ratios between 0.25 and 0.45. The composition of plagioclase from the amphibolites varies from andesine to anorthite; most grains can be classified as labradorite and bytownite. Plagioclase in the hydrothermal alteration zone is depleted in Ca and is mostly andesine.

In order to achieve reliable pressure–temperature (*P–T*) estimates, only mineral cores of neighbouring minerals were used for geothermobarometry. Due to the presence of retrograde reaction rims in some of the garnet grains, it was assumed that the mineral cores reflect the equilibrium mineral composition and were not altered by retrograde processes. *P–T* estimates on the alteration assemblage using the garnet-biotite-plagioclase-quartz geothermobarometer of Wu *et al.* (2004) give conditions of *c.* 540–620°C and 4.5 ± 1 kbar (Fig. 5). *P–T* pseudosection models using the computer program PeRpLeX developed by Connolly (1990) confirm these conditions (Koppelberg 2011).

Discussion and conclusion

The majority of the world's gold deposits formed in the Archaean (*c.* 2.7 Ga) as a result of crust-forming processes during collision events of converging continental plates (Groves *et al.* 2005). These epigenetic deposits are called orogenic gold deposits, and occur in metamorphic terranes that mainly show greenschist facies metamorphism (Groves *et al.* 1998). Other orogenic deposits are known to have formed at amphibolite-facies metamorphic grades, and these are termed hypozonal deposits (Groves *et al.* 1998). The replacement of regional, metamorphic, amphibolite-facies mineral assemblages by hydothermal minerals surrounding the gold-bearing quartz veins as well as the late timing of quartz-vein formation by ductile, flexural slip folding (Kolb *et al.* 2009), indicate that the gold mineralisation and associated hydrothermal alteration formed late in the metamorphic evolution on Qilanngaarsuit. The low-pressure amphibolite-facies metamorphism in the surrounding amphibolites has been dated to *c.* 2715 Ma (Nutman & Friend 2007), while the mineralisation probably occurred between 2660 and 2600 Ma (Kolb *et al.* 2013). The Qilanngaarsuit mineralisation is, therefore, interpreted to represent a new example of hypozonal orogenic gold mineralisation in the Godthåbsfjord gold province. The origin of other gold prospects (Storø, Qussuk) is still a matter of debate, and both metamorphosed epithermal and orogenic models have been proposed (Garde *et al.* 2012; Scherstén *et al.* 2012; Kolb *et al.* 2013). The alteration systematics, timing and conditions of the gold mineralisation on Qilanngaarsuit are, however, similar to those of other gold occurrences, in particular Storø, in the Godthåbsfjord gold province. The deposits are spatially closely associated with a major terrane boundary, the Ivinnguit fault, suggesting that this shear zone may have acted as a major pathway for the gold-bearing fluids between *c.* 2660–2600 Ma.

Acknowledgements

The Professor Dr. Karl-Heinrich Heitfeld-Stiftung is thanked for financial support. The work benefited from valuable comments and discussions with Susan Giffin and Nicolas Stoltz.

References

Allaart, J.H. 1982: Geological maps of Greenland 1:500 000. Map sheet no. 2, Frederikshåb Isblink – Søndre Strømfjord. Copenhagen: Geological Survey of Denmark and Greenland.

Chadwick, B. 1981: Field relations, petrography and geochemistry of Archaean amphibolite dykes and Malene supracrustal amphibolites, northwest Buksefjorden, southern West Greenland. Precambrian Research **14**, 221–259.

Connolly J.A.D. 1990: Multivariable phase diagrams: an algorithm based on generalised thermodynamics. American Journal of Science **290**, 666–718.

Garde, A.A., Whitehouse, M. & Christensen, R. 2012: Mesoarchean epithermal gold mineralisation preserved at upper amphibolite-facies grade, Qussuk, southern West Greenland. Economic Geology **107**, 881–908.

Gresens, P.L. 1967: Composition-volume relationships of metasomatism. Chemical Geology **2**, 47–65.

Groves, D.I., Goldfarb, R.J., Gebre-Mariam, M., Hagemann, S.G. & Robert, F. 1998: Orogenic gold deposits: a proposed classification in the context of their crustal distribution and relationship to other gold deposit types. Ore Geology Reviews **13**, 7–27.

Groves, D.I., Condie, K.C., Goldfarb, R.J., Hronsky, J.M.A. & Vielreicher, R.M. 2005: Secular changes in global tectonic processes and their influence on the temporal distribution of gold-bearing mineral deposits. Economic Geology **100**, 203–224.

Holdaway, M.J. & Mukhopadhyay, B. 1993: A re-evaluation of the stability relations of andalusite: thermochemical data and phase diagram for the aluminum silicates. American Mineralogist **78**, 298–315.

Kolb, J., Stensgaard, B.M., Schlatter, D.M. & Dziggel, A. 2009: Controls of hydrothermal quartz vein mineralization and wall-rock alteration between Ameralik and Sermilik, southern West Greenland. Danmarks og Grønlands Geologiske Undersøgelse Rapport **2009/25**, 76 pp.

Kolb, J., Dziggel, A. & Schlatter, D.M. 2013: Gold occurrences of the Archean North Atlantic Craton, southwestern Greenland: a comprehensive genetic model. Ore Geology Reviews **54**, 29–58.

Koppelberg, M. 2011: Geochemische und petrologische Charakterisierung einer goldführenden hydrothermalen Alterationszone auf der Insel Qilanngaarsuit, SW Grönland, 70 pp. Unpublished Diploma thesis, Institut of Mineralogy and Economic Geology, RWTH Aachen University.

Nutman, A.P. & Friend, C.R.L. 2007: Adjacent terranes with *c.* 2715 and 2650 Ma high-pressure metamorphic assemblages in the Nuuk region of the North Atlantic Craton, southern West Greenland: complexities of Neoarchaean collisional orogeny. Precambrian Research **155**, 159–203.

Scherstén, A., Szilas, K., Creaser, R.A., Næraa, T., van Gool, J.A.M. & Østergaard, C. 2012: Re-Os and U-Pb constraints on gold mineralisation events in the Meso- to Neoarchaean Storø greenstone belt, Storø, southern West Greenland. Precambrian Research **200-203**, 149-162.

Schlatter, D.M. 2009: Petrographic and lithogeochemical surface data from the new gold occurrence on Qilanngaarsuit Island, southern West Greenland. In: Kolb, J & Kokfelt, T.: Annual workshop on the geology of southern West Greenland realted to field work: abstract volume 1, GEUS Rapport **2009/94**, 18–21.

Wu, C.-M., Zhang, J. & Ren, L.-D. 2004: Empirical garnet-biotite-plagioclase-quartz (GBPQ) geobarometry in medium- to high-grade metapelites. Journal of Petrology **45**, 1907–1921.

Authors' addresses

M.K., A.D., F.M.M., *Institute of Mineralogy and Economic Geology, RWTH Aachen University, Wüllnerstraße 2, 52056 Aachen, Germany;*
E-mail: *koppelberg@iml.rwth-aachen.de*

D.M.S., *Helvetica Exploration Services GmbH, Carl Spitteler Strasse 100, CH-8053 Zürich, Switzerland.*

J.K., *Geological Survey of Denmark and Greenland, Øster Voldgade 10, DK-1350 Copenhagen K, Denmark.*

Fingerprinting of corundum (ruby) from Fiskenæsset, West Greenland

Nynke Keulen and Per Kalvig

Since the late 1960s, it has been known that pink and red corundum occur in the area near Fiskenæsset (Qeqertarsuatsiaat) in southern West Greenland. Corundum is hosted in the Fiskenæsset complex, which is part of the Archaean basement of the North Atlantic Craton. To date, *c.* 40 corundum localities with a wide range of quality are known in the area – a few localities yield stones of gem quality. The most promising locality, Aappaluttoq, is likely to be mined in the foreseeable future by the Canadian company True North Gems (Figs 1, 2A). Red corundum of gem quality is called ruby; gem quality corundum of other colours (e.g. pink, yellow or blue) is called pink sapphire, yellow sapphire etc., while the blue gem corundum is sapphire. Red, pink and blue corundum are also known in smaller quantities from other areas in Greenland.

The Fiskenæsset complex

The Fiskenæsset complex (Fig. 1) comprises a series of intrusive sheets of anorthosite, leucogabbro, gabbro and ultramafic rocks (Myers 1985), and is interpreted as derived from a supra-subduction setting, while the associated amphibolites stem from a mid-oceanic ridge to island arc basalt precursor (Polat *et al.* 2009). The greater Fiskenæsset region was metamorphosed *c.* 2.85–2.80 Ga ago at mid- to upper amphibolite-facies temperatures and pressures, reaching granulite facies conditions near the village of Fiskenæsset (McGregor & Friend 1992; Schumacher *et al.* 2011). At least one generation of the *c.* 2.71 Ga felsic pegmatite sheets cuts the anorthosite, ultramafic rocks, amphibolite and gneisses and created reaction zones that developed aluminium-rich mineral assemblages derived from the aluminium in the anorthosite rocks (Schumacher *et al.* 2011; Fig. 2B). These reaction zone assemblages, associated with pegmatitic felsic sheets and the ultramafic bodies, include very coarse-grained, radial anthophyllite ± green pargasite ± green or red spinel ± sapphirine ± cordierite (up to 30 cm single crystals) ± pink corundum, and ± phlogopite (Schumacher *et al.* 2011).

This study is a first attempt to find geochemical and mineralogical characteristics that can be used to tie the Greenlandic rubies to their area of origin. This may have practical implications if an operation of rubies and pink sapphires is established in Greenland. Here, we present Laser Ablation Inductively Coupled Plasma Mass Spectrometry (LA-ICP-MS) trace-element geochemical and oxygen isotope data of samples from the Fiskenæsset area and other known localities in Greenland (Storø, Maniitsoq, Kapisillit and Nattivit).

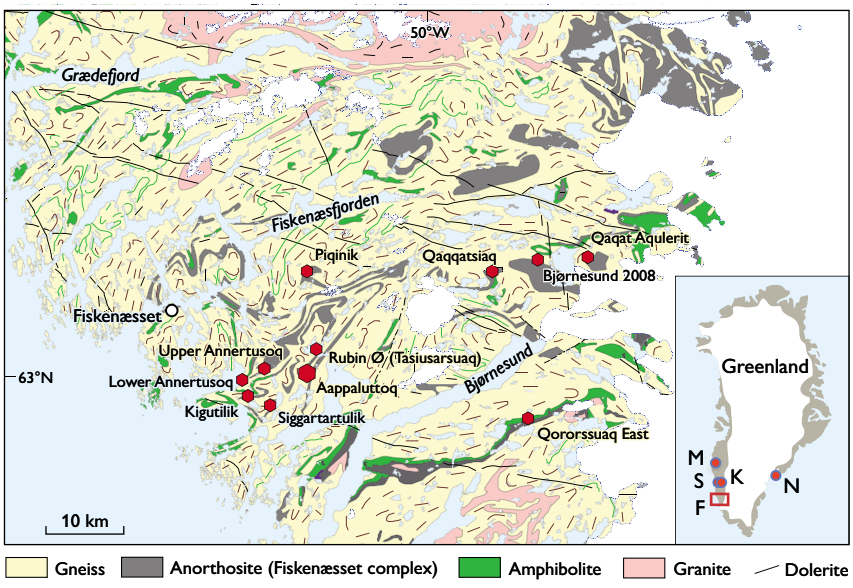

Fig. 1. Simplified geological map of the Fiskenæsset area in southern West Greenland showing the investigated pink and red corundum (ruby) localities in the Fiskenæsset complex. Map after Keulen & Kokfelt *et al.* (2011). **M:** Maniitsoq, **S:** Storø, **K:** Kapisillit, **F:** Fiskenæsset, **N:** Nattivit.

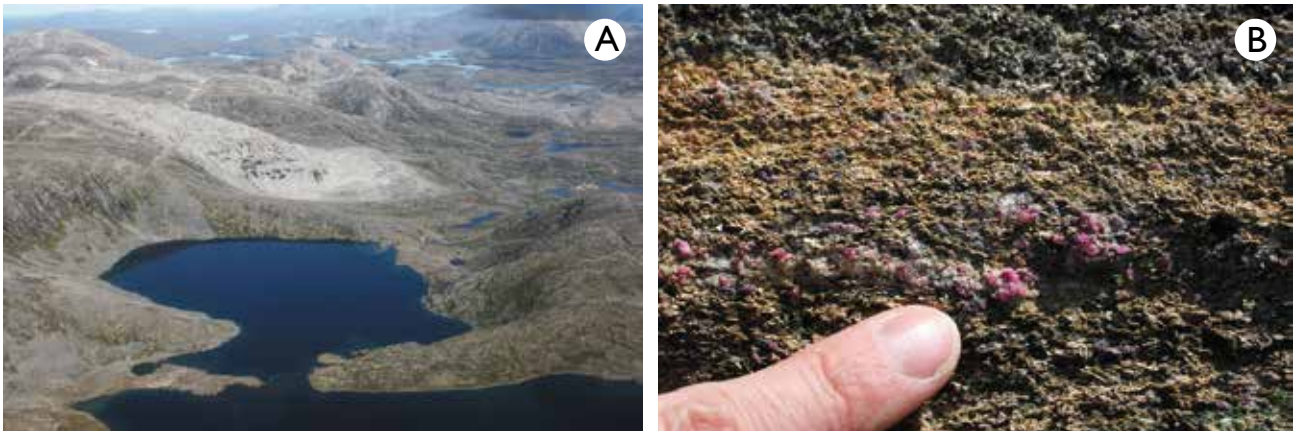

Fig. 2. **A**: Aappaluttoq, Fiskenæsset, seen from a helicopter towards the north. The white-grey rock is anorthosite. **B:** Rubies in their host rock at Tasiussarsuaq, Fiskenæsset, Greenland.

Trace-element geochemistry

Corundum has the chemical formula Al_2O_3 and like most other minerals usually includes very small quantities of other elements in its crystal structure. The amounts of these trace elements and their ratios may depend on the geological conditions during the formation of the corundum and therefore usually vary between individual corundum deposits. Twenty-four different elements were analysed for by means of LA-ICP-MS; however most of them were not detected, including Sn, Nb, and Ta. Our investigations of the Greenlandic corundum were concentrated on the elements Mg, Si, Ti, V, Cr, Fe, and Ga, as these elements are present in significant amounts and are also the most widely documented. We used

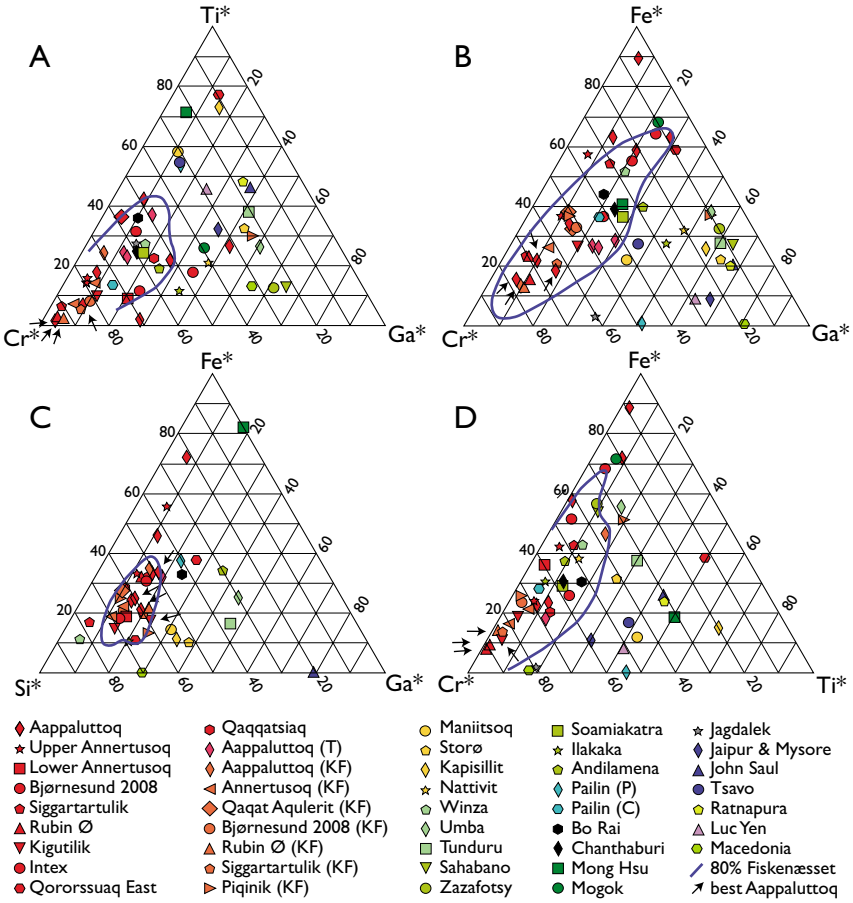

Fig. 3. Normalised trace-element distributions for **A**: Ti-Cr-Ga, **B**: Fe-Cr-Ga, **C**: Fe-Si-Ga and **D**: Fe-Cr-Ti in corundum from Fiskenæsset. The data are compared with data on international and Greenlandic corundum occurrences (Calligaro *et al*. 1999; del Castillo *et al*. 2009; Kalvig & Frei 2010; Pornwilard *et al*. 2011; Rakontondrazafy *et al*. 2008; Schwarz *et al*. 2008; Thirangoon 2008). Different colours show different countries. Initials of the authors' names were used where more than one study of the same locality exist. Diagrams were created with WxTernary (Keulen & Heijboer 2011).

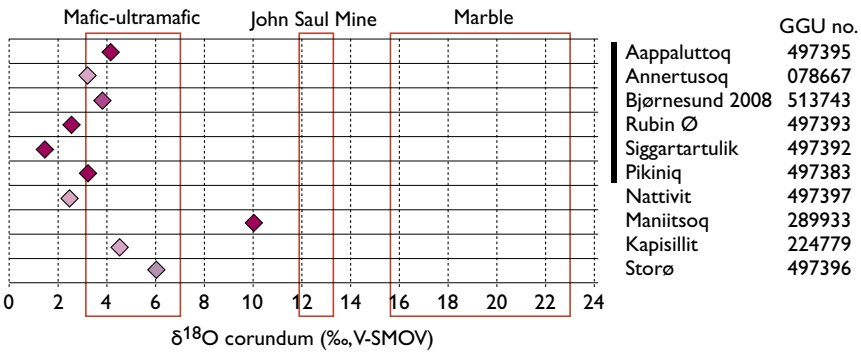

Fig. 4. $\delta^{18}O$ values for six samples from Fiskenæsset and four other localities in Greenland. The values are relative to VSMOW (Vienna standard mean ocean water). Colours indicate the approximate colour of the stones. Red boxes and classification as mafic-ultramafic, John Saul mine, and marble after Giuliani *et al.* (2007).

the Laser Ablation Sector-Field Inductively Coupled Plasma Mass Spectrometer (LA-SF-ICP-MS) at the Geological Survey of Denmark and Greenland (Frei & Gerdes 2009), employing an ELEMENT 2 instrument from Thermo-Fisher Scientific and a UP213 frequency-quintupled Nd:YAG solid state laser system from New Wave Research. Data reduction and determination of concentrations were calculated off-line through the software Iolite using the Trace_Elements_IS routine (Hellstrom *et al.* 2008). Further details on the methods are found in Keulen & Kalvig (2013).

Results on the trace-element investigations of corundum grains separated from 21 hand specimens from ten localities in the Fiskenæsset complex are shown with red symbols in the ternary diagrams of Fig. 3. The data for corundum from the Fiskenæsset complex are in good concordance with earlier data from the area (Kalvig & Frei 2010; Thirangoon 2008). In Fig. 3 they are compared with data from other localities in Greenland and from internationally, well-known, ruby occurrences. Samples from Fiskenæsset show a considerably higher amount of Cr (up to 14000 ppm) than samples from other areas in Greenland and most international samples. The Fiskenæsset rubies are relatively rich in Fe and Si, but relatively poor in Ti and Ga, while V and Mg do not show very distinctive values compared to samples from other areas (Kalvig & Keulen, 2011).

In order to use trace-element investigations as a fingerprinting tool for rubies it is necessary to investigate the amount of overlap between samples from Fiskenæsset and other localities. The blue lines in Fig. 3 include 80% (26 out of 32) of the samples from the Fiskenæsset area, based on sample distribution density contouring. Most samples from other localities plot outside the blue line, but an overlapping chemistry is found with samples from Soamiakatra, Ilakaka, and Andilamena in Madagascar, Bo Rai and Chanthaburi in Thailand, Pailin in Cambodia and Winza in Tanzania. Rubies from all these localities are hosted by ultramafic to mafic rocks or are found as placer deposits. This indicates that the trace elements in the rubies derive from the ultramafic rocks that are associated with the anorthosite.

However, if only the four handspecimens with the most transparent and most intensively red-coloured corundum grains from Aappaluttoq, Fiskenæsset, are taken into account, no overlap between these handspecimens and samples from other known ruby occurrences is seen. Corundum from these handspecimens is closest in transparency and colour to the stones that would be sold from a potential mine and therefore represent the Aappaluttoq signature. As these corundum grains have a distinct composition, it can be concluded that trace-element geochemistry with ICP-MS is a helpful tool in fingerprinting rubies from Greenland.

Oxygen isotope geochemistry

Oxygen isotopic composition measurements were performed on ten samples from Greenland at the University of Lausanne, Switzerland using an isotope ratio mass spectrometer, employing a method similar to that described by Kasemann *et al.* (2001), see Kalvig & Keulen (2011) for details.

Six of the samples come from the Fiskenæsset complex. Their $\delta^{18}O$ values vary between 1.62 and 4.20‰ for the Fiskenæsset area, which is low compared to the other areas in Greenland (up to 10.03‰ for Maniitsoq) with the exception of one sample from Nattivit (2.41‰; Fig. 4). The $\delta^{18}O$ values are also low compared to most other investigated corundum deposits worldwide (Giuliani et al. 2007). The lowermost values ($\delta^{18}O$ <3‰) are nearly diagnostic for the Fiskenæsset area – worldwide only the placer deposits at Andilamena and Ilakaka in Madagascar and gem-corundum in a cordieritite from Iankaroka, Madagascar have lower reported $\delta^{18}O$ values. Low $\delta^{18}O$ values (≤4‰) generally reflect rock types such as mafic rocks, mafic gneiss, basalts, and desilicated pegmatite in mafic rocks (Giuliani et al. 2005), which is in excellent agreement with the mafic to ultramafic setting of the Fiskenæsset rubies. The values for samples from Nattivit, Kapisillit and Storø are also low (2.4, 4.5 and 6.0‰ respectively) and also plot in the mafic–ultramafic field. Unfortunately, no further geological information is available for these specimens and the data can thus not be validated

against field observations. The value for Maniitsoq with $\delta^{18}O$ =10.03‰ is typically related to skarns in marble, or to biotitite in gneiss related to shear zones with high fluid activity. The rubies in the investigated sample are assumed to stem from sapphirine-bearing hornblendite. The hornblendite was probably formed in a shear zone with high fluid activity (like the biotitites in Madagascar).

The low $\delta^{18}O$ values are a potentially useful tool for fingerprinting Greenlandic rubies, especially the very low values for the Fiskenæsset complex and Nattivit, as only few other international occurrences have such low values.

Conclusions

High confidence fingerprinting of rubies requires a combination of independent analytical methods such as trace-element analyses, oxygen isotope analyses and other studies. The two methods discussed here are efficient in characterising the Fiskenæsset rubies. The ongoing research focuses on optical and physical characteristics, spectroscopy methods and scanning XRF.

Acknowledgements

This study is part of a collaboration project between the Bureau of Minerals and Petroleum in Nuuk, Greenland and the Geological Survey of Denmark and Greenland. The authors wish to thank Kerstin Bauer and Torsten Vennemann for help with the oxygen isotope analyses.

References

Calligaro, T., Poirot, J.-P. & Querré, G. 1999: Trace element fingerprinting of jewellery rubies by external beam PIXE. Nuclear Instruments and Methods in Physics Research B **150**, 628–634.

Calvo del Castillo, H., Deprez, N., Dupuis, T., Mathis, F., Deneckere, A., Vandenabeele, P., Calderón, T. & Strivay, D. 2009: Towards the differentiation of non-treated and treated corundum minerals by ion-beam-induced luminescence and other complementary techniques. Analytical and Bioanalytical Chemistry **394**, 1043–1058.

Frei, D. & Gerdes, A. 2009: Precise and accurate *in situ* U-Pb dating of zircon with high sample throughput by automated LA-SF-ICP-MS. Chemical Geology **261**, 261–270.

Giuliani, G., Fallick, A.E., Garnier, V., France-Lanord, C., Ohnenstetter, D. & Schwarz, D. 2005: Oxygen isotope composition as a tracer for the origins of rubies and sapphires. Geology **33**, 249–252, http://dx.doi.org/10.1130/G21261.1.

Giuliani, G. *et al*. 2007: Oxygen isotope systematics of gem corundum deposits in Madagascar: relevance for their geological origin. Mineralium Deposita **42**, 251–270.

Hellstrom, J., Paton C., Woodhead J. & Hergt J. 2008: Iolite: software for spatially resolved LA- (quad and MC) ICPMS analysis. In: Sylvester P. (ed.): Laser ablation ICP–MS in the earth sciences: current practices and outstanding issues, 343–348. Mineralogical Association of Canada short course series **40**, 343–348.

Kalvig, P. & Frei, D. 2010: Testing the use of geochemical characteristics of corundum from Greenland as a tool for geographical typing. Danmarks og Grønlands Geologiske Undersøgelse Rapport **2010/68**, 36 pp.

Kalvig, P. & Keulen, N. 2011: Aktiviteter i rubinprojektet 2011 – samarbejdsprojekt med Råstofdirektoratet. Danmarks og Grønlands Geologiske Undersøgelse Rapport **2011/138**, 41 pp.

Kasemann, S., Meixner, A., Rocholl, A., Vennemann, T., Schmitt, A. & Wiedenbeck M. 2001: Boron and oxygen isotope composition of certified reference materials NIST SRM 610/612, and reference materials JB-2G and JR-2G. Geostandards Newsletter **25**, 405–416.

Keulen, N. & Heijboer, T. 2011: The provenance of garnet: semi-automatic plotting and classification of garnet compositions. Geophysical Research Abstracts **13**, EGU 2011-4716.

Keulen, N. & Kalvig, P. 2013: Report of the activities in the ruby project 2012 – a joint project with the Bureau of Minerals and Petroleum. Danmarks og Grønlands Geologiske Undersøgelse Rapport **2013/09**, 25 pp.

Keulen, N., Kokfelt, T.F. & the homogenisation team 2011: A 1:100 000 seamless, digital, internet-based geological map of South-West and southern West Greenland, 61°30′–64°N, *http://geuskort.geus.dk/gis-farm/gis_svgreenland.jsp*. Copenhagen: Geological Survey of Denmark and Greenland.

McGregor, V.R. & Friend, C.R.L. 1992: Late Archean prograde amphibolite- to granulite-facies relations in the Fiskenæsesset region, southern West Greenland. The Journal of Geology **100**, 207–219.

Myers, J.S. 1985: Stratigraphy and structure of the Fiskenæsset Complex, southern West Greenland. Bulletin Grønlands Geologiske Undersøgelse **150**, 72 pp.

Polat A., Appel, P.W.U., Fryer, B., Windley, B., Frei, R., Samson, I.M. & Huang, H. 2009: Trace element systematics of the Neoarchean Fiskenæsset anorthosite complex and associated meta-volcanic rocks, SW Greenland: evidence for a magmatic arc origin. Precambrian Research **175**, 87–115.

Pornwilard, M.-M., Hansawek, R., Shiowatana, J. & Siripinyanond, A. 2011: Geographical origin classification of gem corundum using elemental fingerprint analysis by laser ablation inductively coupled plasma mass spectrometry. International Journal of Mass Spectrometry **306**, 57– 62.

Rakontondrazafy, A.F.M. *et al*. 2008: Gem corundum deposits of Madagascar: a review. Ore Geology Reviews **34**, 134–154.

Schumacher, J.C., van Hinsberg, V.J. & Keulen, N. 2011: Metamorphism in supracrustal and ultramafic rocks in southern West Greenland and South-West Greenland 64°–61.5°N. Danmark og Grønlands Geologiske Undersøgelse Rapport **2011/6**, 29 pp.

Schwarz, D. *et al*. 2008: Rubies and sapphires from Winza, Central Tanzania. Gems & Gemology **44**, 322–347.

Thirangoon, K. 2008: Ruby and pink sapphire from Aappaluttoq, Greenland. Status of on-going research. Unpublished report for True North Gems Co. (In archives of Geological Survey of Denmark and Greenland, GEUS Report File **23642**, 18 pp.).

Authors' address

Geological Survey of Denmark and Greenland, Øster Voldgade 10, DK-1350 Copenhagen K, Denmark. E-mail: *ntk@geus.dk*

Lineament mapping and geological history of the Kangerlussuaq region, southern West Greenland

Knud Erik S. Klint, Jon Engström, Andrew Parmenter, Timo Ruskeeniemi, Lillemor Claesson Liljedahl and Anne Lehtinen

How could future ice ages affect deep nuclear waste repositories in crystalline basement rocks? Deep repositories may be affected by a number of glacially induced processes including, but not limited to, (1) fault activation or re-activation and associated seismicity, (2) changing hydraulic and chemical groundwater dynamics and (3) enhanced erosion. Such processes are likely to affect not only man-made barriers in spent fuel repositories such as copper canisters and bentonite clay buffers, but also the rock masses that contain and isolate the repositories. In order to increase our understanding of this problem, an international study (the Greenland Analogue Project) was set up in 2008. The aim of the study was to use crystalline bedrock at the margin of the Inland Ice near Kangerlussuaq airport in West Greenland as an analogue for future nuclear fuel waste repositories affected by glaciation in Fennoscandia and Canada. Accordingly, a wide range of field surveys were conducted for the analogue project (Fig. 1). This paper describes a detailed structural investigation of lineament zones and the establishment of an event succession for fault and fracture zone evolution in central parts of the study area (Figs 1B, 2), as well as an interpretation of the distribution of fracture and fault zones with potentially increased permeability. Three deep holes were drilled in the study area, and instruments were installed in two of them for subsequent down-hole sampling and monitoring of groundwater to a depth of *c.* 600 m. The cores were used to compare the subsurface fracture patterns with those established on the basis of surface mapping.

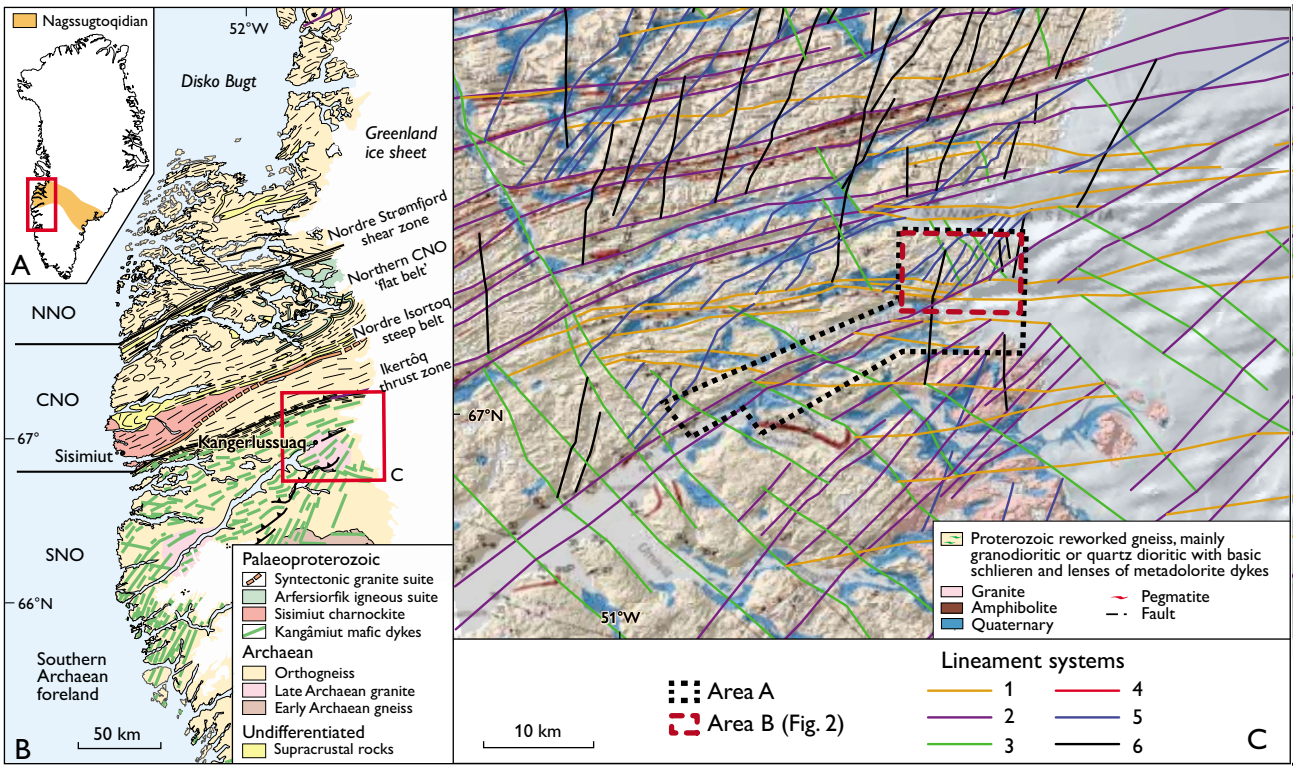

Fig. 1. **A**: Map of Greenland showing the extent of the Nagssugtoqidian orogen and the location of Fig. 1B (rectangle). **B**: Regional geology of southern West Greenland, modified from Garde & Hollis (2010) and Garde & Marker (2010). **CNO**, **NNO** and **SNO** are central, northern and southern Nagssugtoqidian orogen, respectively. **C**: Lineament map of the area around Kangerlussuaq airport. Areas A and B were mapped in detail.

Geological setting

The Kangerlussuaq area is located close to the southern margin of the *c.* 1.85 Ga old collisional Nagssugtoqidian orogen (van Gool *et al.* 2002). The study area covers a 100 × 50 km large area in front of and below the western margin of the Inland Ice (Fig. 1). Detailed geological mapping was carried out along a transect from Kangerlussuaq airport to the margin of the Inland Ice, and of a smaller area around the three drilling sites in the valley in front of the Inland Ice (Fig. 2).

The bedrock is mainly reworked Archaean orthogneiss with minor Palaeoproterozoic metavolcanic amphibolite and metasedimentary rocks that were deformed under high-grade metamorphic conditions during the Nagssugtoqidian orogeny (van Gool *et al.* 2002). The Nagssugtoqidian structures are generally ductile and include a penetrative gneissic fabric, macroscale folds and pronounced shear zones. Occasional, deformed mafic dykes also occur, mainly members of the rift-related Nagssugtoqidian Kangâmiut dyke swarm that preceded the Nagssugtoqidian orogeny (Mayborn & Lesher 2006). Brittle structures such as faults and fractures are abundant and were probably formed in a younger, shallower, colder and hence more rigid environment.

Regional lineament mapping and geology of the study area

Most lineaments in crystalline rocks represent structural features such as faults and shear zones, rock fabrics and lineaments that were created at discontinuities due to differences in rheology or competence. Our lineament mapping comprised four steps. First, lineaments were identified using remotely sensed GIS-data compiled from aerial photographs,

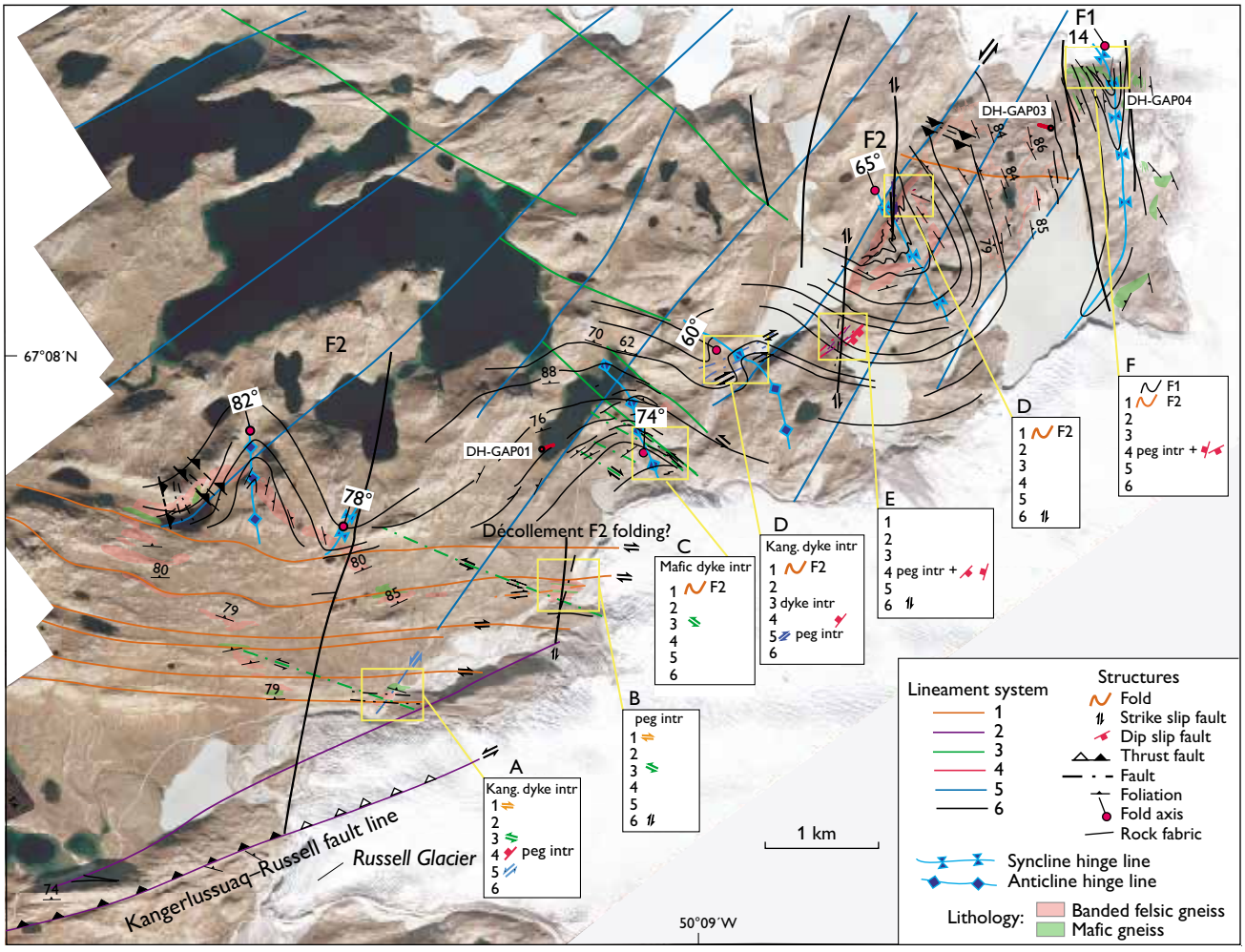

Fig. 2. Aerial image of area B (Fig. 1C) with mapped and inferred rock fabric (foliation), rock types and structural elements. Local event stratigraphic models were developed for locations A–F. The macro-scale structures outline large-scale ductile folds overprinted by various shear and fault zones. Three deep holes were drilled (DH-GAP01, DH-GAP03 and DH-GAP04).

Table 1. Event succession of the Kangerlussuaq area compared with the general history of central West Greenland*

Age	General tectonic events in central West Greenland	Correlation to the Kangerlussuaq area
>2.5 Ga (Archaean)	Formation of 'banded gneiss' protoliths	F1 folding + multiple healed structures
c. 2.04 Ga	Continental rifting coupled with mafic dyke intrusions	Intrusion of Kangâmiut mafic dykes
1.92–1.75 Ga	Nagssugtoqidian orogen. Continental collision. Reworking, folding and thrusting of gneiss/mafic rocks followed by peak metamorphism and large-scale folding during N–S contraction. Finally formation of steep belts with sinistral movements	System 1 dextral, strike-slip shear and F2 folding System 2 WSW–ENE-trending faulting (K–R fl†) Reactivation of Kangerlussuaq–Russell fault sinistral strike slip System 3 sinistral strike-slip shear zones
c. 1.78 to present day	Various stress conditions. Formation and reactivation of open mode fractures at more shallow depths during 20–25 km uplift	System 4 normal faults with shallow dip towards SE and NW accompanied by pegmatite intrusions
1.2 Ga	Diamond-bearing, ultramafic lamprophyre intrusions S and W of Kangerlussuaq	
600 Ma	Kimberlite intrusions S and W of Kangerlussuaq	
100–50 Ma	Faulting related to sea-floor spreading during the opening of Labrador Sea and Baffin Bay. NNE–SSW sinistral strike-slip faulting and conjugate dextral strike-slip faulting	System 5 sinistral strike-slip faults trending NE–SW System 6 dextral strike-slip faults trending N–S
At least the last 2 Ma	Repeated glaciations resulting in erosion, glacier-induced reactivation of fractures during glacial subsidence and rebound of the basement	Reactivation of existing fault zones

* based on van Gool *et al.* (2002) and Garde & Hollis (2010)
† Kangerlussuaq–Russell fault line

topographical and geological maps and geophysical data. The second step was a descriptive and kinematic field analysis of the remotely detected lineaments. In the third step, a local event succession model was developed by determination of overprinting relationships. Finally, the local geological history of the Kangerlussuaq area was interpreted and correlated with the regional geological evolution (van Gool *et al.* 2002; Garde & Hollis 2010).

In order to provide an overview of the geological framework of the study area, the measured and interpreted structures (foliation, fold hingeline, fault and shear zone traces) are shown on a high-resolution aerial image (Fig. 2). Close to the margin of the Inland Ice in the north-eastern part of the area, the bedrock is characterised by folded mafic gneiss that defines an open, NNW-trending and shallowly plunging (*c.* 14°) F1 fold structure. This structure gradually turns into a tight to isoclinal fold that can be traced southward and westward around an open, steeply-plunging, kilometre-scale F2 fold structure with a NW- to N-trending axial surface (Figs 1C, 2).

Five general lineament systems were outlined from the GIS analysis, and a sixth, subhorizontal system was identified by the field work, during which also the curvilinear nature of the foliation traces became apparent and highlighted the superposition of the F1 and F2 fold phases. On a regional scale, system 1 lineaments are generally distributed between the system 2 steep belts (Fig 1). These lineaments dominate in some parts of the southern study area and consist of ductile, E–W-trending, 10–100 m wide, foliation-parallel, steeply inclined and steeply N-dipping dextral shear zones (Figs 1C, 2). These shear zones may have acted as décollement planes for the F2 folding (see below).

System 2 lineaments constitute the most pronounced linear feature and represent regional, SW-trending shear zones, including the zone outlining Søndre Strømfjord itself and especially the northern margin of Sandflugtdalen that extends from Kangerlussuaq to Russell Glacier, hereafter named the Kangerlussuaq–Russell fault line. Other lineaments farther north with similar orientations (Fig. 1B) comprise the Ikertôq zone (van der Molen 1984), the Nordre Isortoq steep belt and the Nordre Strømfjord shear zone (van Gool *et al.* 2002). Along the Kangerlussuaq–Russell fault line this lineament is dominated by sinistral strike-slip movement overprinting elements of thrust faulting dipping towards the north. Large boudins of deformed Kangâmiut mafic dykes (Mayborn & Lesher 2006) are included in this zone, which is therefore younger than the intrusion of the Kangâmiut dykes.

System 3 lineaments are a major NW-trending system along pronounced valleys and extend all the way up to Aassiaat and Disko Bugt (Fig. 1A). Locally within the study area they form semi-brittle, sinistral strike-slip fault zones that displace the system 1 shear zones.

System 4 lineaments form oblique to sub-horizontal fracture systems trending NNE and are not represented by any pronounced topographic lineaments. These structures may also be related to a population of normal faults and younger,

NNE-trending pegmatites orientated parallel with the normal faults. They overprint the system 1 and 3 lineaments, but no cross-cutting relations to system 2 lineaments have been noticed.

System 5 lineaments are semi-brittle, sinistral, strike-slip faults trending NE and dipping to the NW. This system outlines the pronounced escarpment in the central to north-eastern part of the study area (Fig. 2). Local zones of WSW-striking thrust faults with both northerly and southerly dips are regarded as representing local transpression in a wrench fault system related to the overall system 5 lineaments.

System 6 lineaments consist of N–S-trending, brittle, dextral, strike-slip faults. This system may be conjugate with system 5. Lineaments with this orientation near the outer coast of central West Greenland have been related to the rifting between Greenland and Canada during the last 100 Ma (Wilson *et al.* 2006).

Preliminary geological history

As demonstrated by its structural complexity (Fig. 2), the study area has undergone several episodes of deformation. These episodes have been compiled into a local event history that recognises seven types of structural overprint (Table 1). Two stages of folding (F1 and F2) are identified. F1 may be of Archaean age, while F2 seems to be Nagssugtoqidian and contemporary with the system 1 shear zones, since the Kangâmiut dykes were folded during this event. The Kangerlussuaq–Russell fault line of system 2 lineaments has been reactivated with sinistral, strike-slip movement, during which the Kangâmiut dykes were deformed, but a clear, cross-cutting relation with systems 1 and 3 has not yet been documented. The system 3 lineaments clearly overprint system 1 and the F2 folds. The normal faulting and NNE-trending pegmatites of system 4 either indicate a general, extensional stress regime or local transtension during strike-slip movements. The timing of this event is highly speculative. The youngest geological events are related to the type 5 and 6 lineaments that form two, generally brittle, strike-slip fault systems. These are also regarded as the primary hydraulic zones in the Kangerlussuaq area.

The absolute ages of the different types of ductile and brittle deformation are uncertain because of lack of radiometric ages. However, in relative terms, it is suggested that the Kangerlussuaq–Russell fault line and most other semi-ductile shear zones are ancient features related to the Nagssugtoqidian orogeny (van Gool *et al.* 2002). The system 3 and 4 semi-brittle lineaments may be of intermediate ages related to postorogenic tectonic events, whereas the youngest and most brittle deformations may be related to the opening of the North Atlantic Ocean, the Labrador Sea and the Baffin Bay over the last 100 Ma (Wilson *et al.* 2006).

Acknowledgement

The study was funded by the Swedish, Finnish and Canadian nuclear waste management organisations.

References

Garde, A.A. & Hollis, J.A. 2010: A buried Palaeoproterozoic spreading ridge in the northern Nagssugtoqidian orogen, West Greenland. Geological Society Special Publications (London) **338**, 213–234.

Garde, A.A. & Marker, M. 2010: Geological map of Greenland, 1:500 000, Søndre Strømfjord – Nuussuaq. Copenhagen: Geological Survey of Denmark and Greenland.

Mayborn, K.R. & Lesher, C.E. 2006: Origin and evolution of the Kangâmiut mafic dyke swarm, West Greenland. In: Garde, A.A. & Kalsbeek, F. (eds): Precambrian crustal evolution and Cretaceous–Palaeogene faulting in West Greenland. Geological Survey of Denmark and Greenland Bulletin **11**, 61–86.

van Gool, J.A.M., Connelly, J.N., Marker, M. & Mengel, F.C. 2002: The Nagssugtoqidian orogen of West Greenland: tectonic evolution and regional correlations from a West Greenland perspective. Canadian Journal of Earth Sciences **39**, 665–686.

van der Molen, I. 1984: Dykes and deformation in the Ikertôq zone of the Nagssugtoqidian at Søndre Strømfjord Airport, West Greenland. Bulletin of the Geological Society of Denmark **32**, 101–106.

Wilson, R.W., Klint, K.E.S., van Gool, J.A.M., McCaffrey, K.J.W., Holdsworth, R.E. & Chalmers, J.A. 2006: Faults and fractures in central West Greenland: onshore expression of continental break-up and seafloor spreading in the Labrador – Baffin Bay Sea. Geological Survey of Denmark and Greenland Bulletin **11**, 185–204.

Authors' addresses

K.E.S.K., *Geological Survey of Denmark and Greenland, Øster Voldgade 10, DK-1350 Copenhagen K, Denmark*. E-mail: *kesk@geus.dk*

J.E. & T.R., *Geological Survey of Finland, P.O. Box 96, SF-02151 Espoo, Finland.*

L.C.L., *Swedish Nuclear Fuel and Waste Management Co, Box 250, SE-101 24, Stockholm, Sweden.*

A.P., *Nuclear Waste Management Organization, 22 St. Clair Avenue East, Sixth Floor, Toronto, M4T 2S3, Canada.*

A.L., *Posiva Oy Olkiluoto, SF-27160 Eurajoki, Finland.*

Calibration of spectral gamma-ray logs to deltaic sedimentary facies from the Cretaceous Atane Formation, Nuussuaq Basin, West Greenland

Gunver Krarup Pedersen, Niels H. Schovsbo and Henrik Nøhr-Hansen

Gamma-ray logs are widely used as a lithology indicator in wells as part of standard petrophysical interpretations. In cored wells, gamma-ray logs should always be calibrated to the lithology in order to correct the petrophysical model. Gamma radiation is emitted from three elements, K, Th and U (potassium, thorium and uranium) which occur in minerals such as feldspar, mica, glauconite, clay minerals, zircon, titanite and apatite as well as in organic complexes. Organic-rich mudstones usually have high gamma-radiation values and quartz-rich sandstones low values. In many places, upward-coarsening successions are recognisable from the gamma log. The gamma log records the sum of radiation from K, Th and U, and their relative contributions are measured in a spectral gamma-ray log. The present case study focuses on spectral gamma-ray characterisation of the deltaic Atane Formation which shows well-developed, upward-coarsening delta-front deposits in outcrops (Fig. 1C).

Geological setting

The Nuussuaq Basin is a rift basin, which contains the only exposures of Cretaceous and Paleocene sediments along the west coast of Greenland. The siliciclastic sediments are overlain by a thick pile of volcanic rocks (Chalmers *et al*. 1999; Dam *et al*. 2009). During Late Cretaceous, Greenland was characterised by a warm and probably humid climate. The sediments range from alluvial fans overlying deeply weathered Precambrian basement through marginally marine deposits to marine deep-water deposits, all referred to the Nuussuaq Group (Dam *et al*. 2009). The floodplains and delta plains had a rich flora, recorded in well-preserved plant

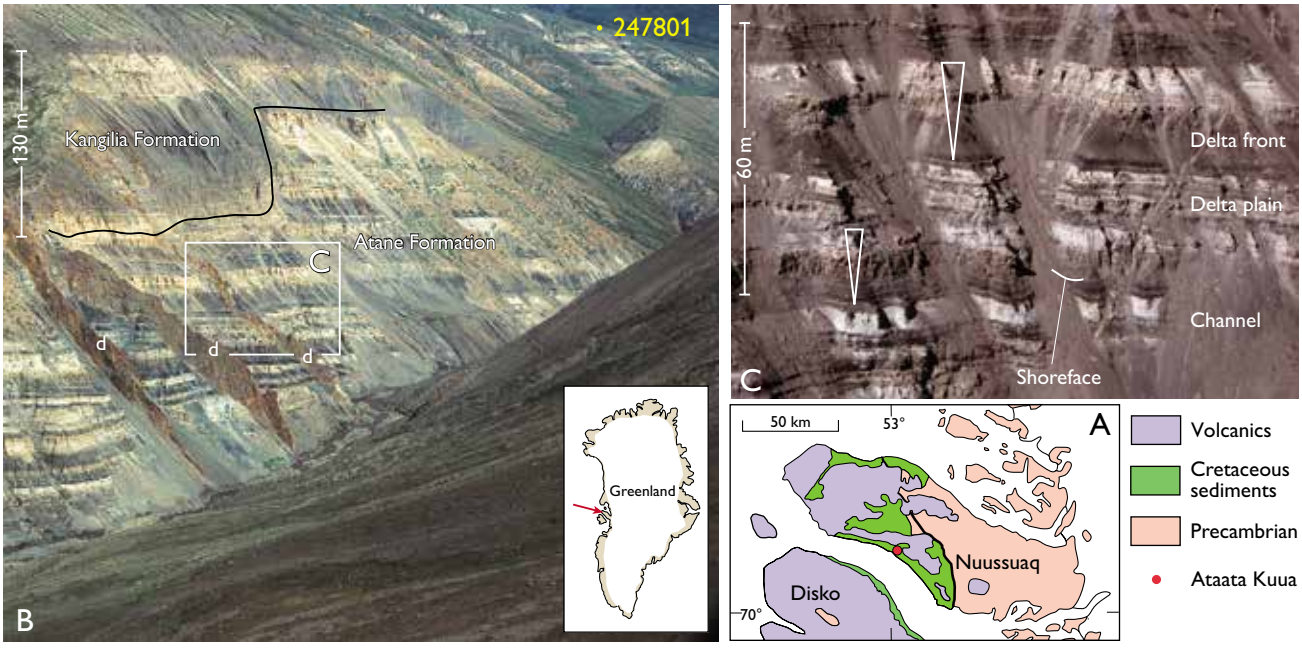

Fig. 1. **A:** Geological map of central West Greenland showing the location of Ataata Kuua on the south coast of Nuussuaq. **B:** The Atane Formation is erosionally overlain by the Kangilia Formation in the western slope of Ataata Kuua. The yellow dot marks the drilling site of borehole 247801, **d**: dyke. Height of section *c.* 500 m. The frame shows the position of Fig. 1C. **C:** The Atane Formation with depositional environments indicated. Note the distinct coarsening-upward successions (triangles). Height of section *c.* 100 m.

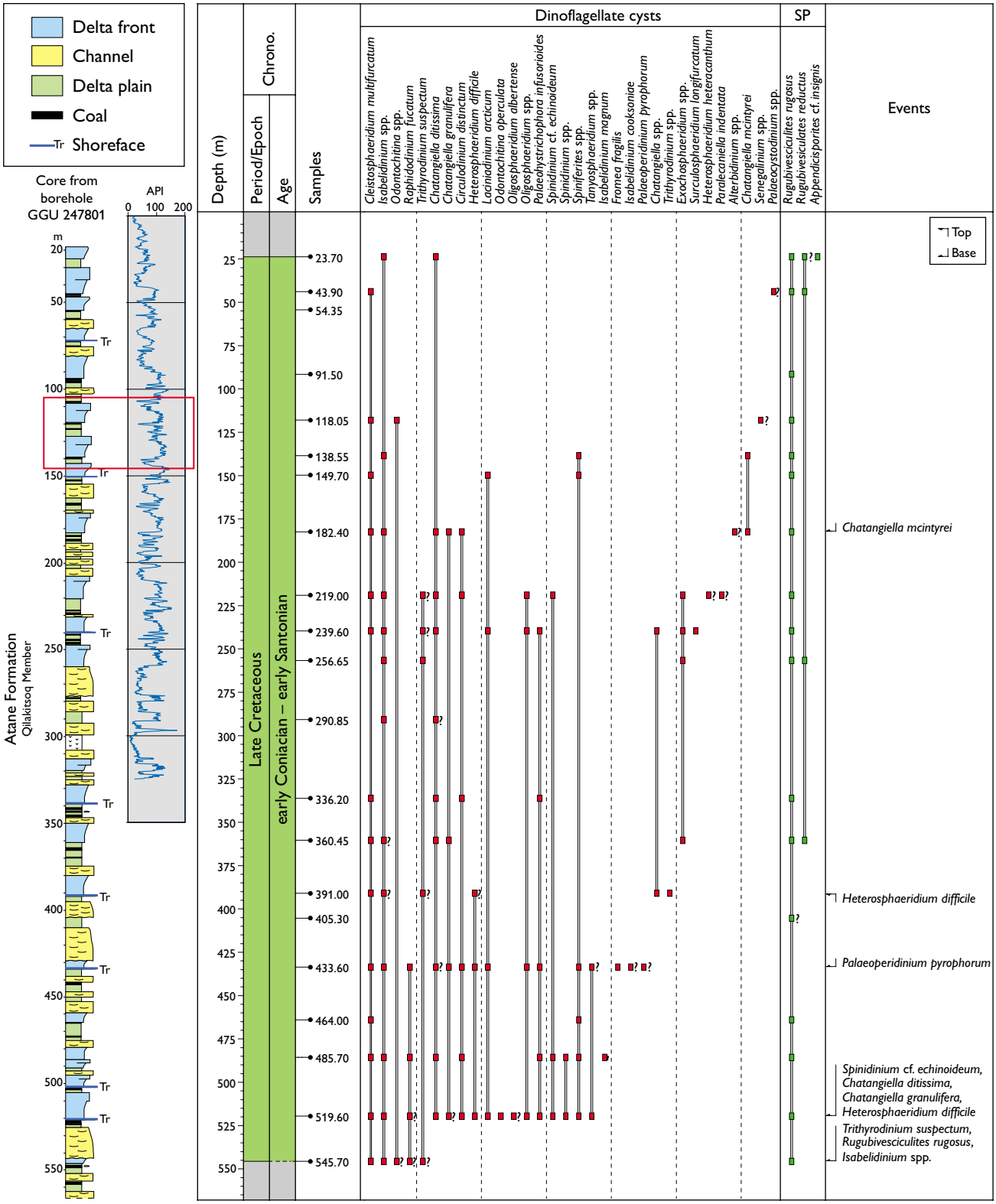

Fig. 2. Data from borehole 247801: a simplified sedimentological log of the entire core (566 m), a gamma log measured in the borehole to a depth of 320 m, and the new range chart for the dinoflagellate cysts in core samples. **API:** American Petroleum Institute units. GGU 247801 is located at 70°19.87′N, 52°55.8′W. The framed interval is shown in Fig. 3. The drill site is shown in Fig. 1B.

macrofossils and abundant comminuted plant debris. A huge volume of non-marine to shallow marine deposits constitutes the Cretaceous Atane Formation, which is well exposed along 65 km of the south coast of Nuussuaq from sea level to altitudes of 500–800 m. Seismic data indicate a minimum thickness of 3000 m for the formation (Dam *et al*. 2009).

Ataata Kuua – A narrow fluvial valley at Ataata Kuua, on the south coast of Nuussuaq (Fig. 1), shows the deltaic Atane Formation erosively truncated and overlain by the turbiditic, Paleocene Kangilia Formation (Dam *et al*. 2009). In 1980, the Geological Survey of Greenland drilled a 566 m deep borehole (GGU 247801) at Ataata Kuua as part of a regional study of the composition and distribution of coal in the Atane Formation. The entire succession was cored, with 100% recovery, and a gamma log was measured in the upper 320 m of the borehole. This gamma log as well as a simplified sedimentological log of the entire core are shown adjacent to the new biostratigraphical range chart in Fig. 2.

Biostratigraphy – In recent studies of 21 delta-front mudstone samples from core 247801, palynomorphs have been examined (Fig. 2). The diversity and density of dinoflagellate cysts, spores and pollen are very low, but the presence of *Chatangiella granulifera*, *Heterosphaeridium difficile* and *Spinidinium* cf. *echinoideum* in the lower part and *Chatangiella mcintyrei* and *Spinidinium* cf. *echinoideum* in the middle to upper part indicates an early Coniacian age or younger. An early Santonian minimum age of the upper part of the core is indicated by the presence of *Rugubivesciculites* spp., the absence of Campanian marker species and by the presence of *Heterosphaeridium difficile, Laciniadinium arcticum* and *Spinidinium* cf. *echinoideum* in a sample from the Ataata Kuua 2004-3 section situated immediately above the site of borehole 247801. The relatively uniform dinoflagellate assemblage recorded throughout the core (Fig. 2) supports the interpretation of a relatively high sedimentation rate.

Sedimentology – The delta deposits of the Atane Formation represent four depositional environments: delta front, distributary channel, delta plain and shoreface (Figs 1C, 2, 3). The delta-front deposits include mudstones, heterolithic sandstones with wave-generated sedimentary structures and well-sorted sandstones, all with comminuted plant debris. The distributary channel deposits are mostly cross-bedded, medium- to coarse-grained sandstones with some feldspar grains. The delta-plain mudstones are interbedded with coal beds or thin sandstone beds. The thin shoreface sandstones contain abundant marine trace fossils and overlie erosive surfaces. The delta-front deposits and the overlying fluvial sandstones form distinctly upward-coarsening units (Figs 1C, 2, 3), interpreted as formed during delta progradation. The shoreface sandstones are interpreted as deposited during a transgression. A detailed log of the core is shown in Dam *et al*. 2009 (fig. 43).

The dominant minerals in the mudstones are quartz and kaolinite, neither of which contain more than traces of K. Small amounts of K-feldspar and mica result in a K content about 1.3–1.8% K_2O, significantly lower than the 2.7% K_2O of average mudstones (Rider 1990). All mudstones and many sandstones in the Atane Formation contain comminuted debris from higher land plants. Total organic carbon (TOC) values of the non-marine delta-plain mudstones range from 3 to 15% and include thin coal beds with 50–65% TOC (Pedersen *et al*. 2006). The marine delta-front mudstones contain 6–14% TOC, with the highest values in the fine-grained, lower part, which includes a flooding surface and had a low sedimentation rate. Despite this, marine organic particles, such as dinoflagellate cysts, only form a small part compared to terrestrial organic matter.

The gamma log obtained in the borehole shows, as expected, low values for the fluvial sandstones whereas the mud-dominated delta-front and delta-plain deposits are difficult to identify from the gamma log alone (Fig. 2). In order to document the contributions of K, Th and U to the total gamma radiation we measured the spectral gamma radiation (Fig. 3). K is mainly located in feldspar, mica and glauconite; Th and U are hosted in zircon, titanite, and apatite. Clay minerals may contain small amounts of Th, and organic complex compounds may contain U.

Spectral gamma-ray characterisation

Core scanning – The core interval was scanned at the core laboratory at the Geological Survey of Denmark and Greenland using a set-up which allows simultaneous spectral gamma-ray and density measurements. The spectral gamma-ray analysis is carried out using two 15 cm NaI (Tl) crystals and the bulk density is determined using a caesium source. The scanning speed was 1 cm/min., corresponding to a vertical resolution of approximately 2 cm for the density log. The scanning data thus supply high resolution data to support sedimentary and geochemical data from the core, as exemplified in Fig. 3.

Results – The upward-coarsening successions, which are clearly seen in the field and in the core (Figs 1C, 2, 3), are difficult to identify on the total readings of the spectral gamma log (Fig. 3). The grain-size trends are, however, reflected in the Th and K logs, which are negatively correlated. The mudstones have high Th and low K contents, whereas the sandstones have high K and low Th contents. No distinct

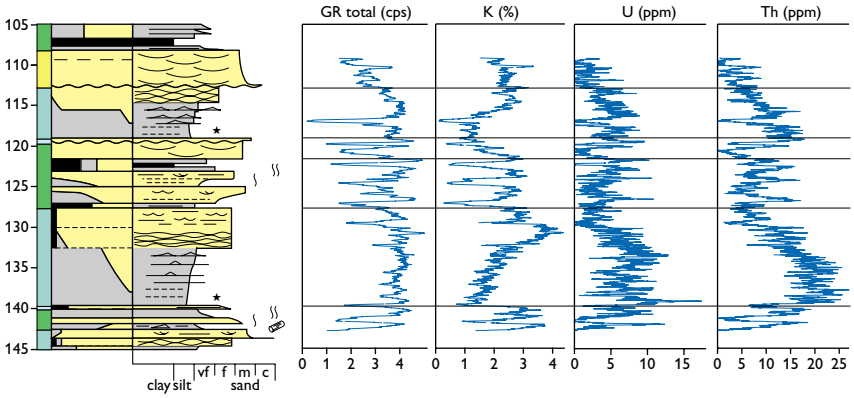

Fig. 3. Spectral gamma logs from 40 m of the core from borehole 247801. Note the difficulty in interpreting the total gamma radiation log, the negative correlation between K and Th content, and the absence of maxima on the U log. The core section is located in Fig. 2. Yellow: sandstone, grey: mudstone, black: coal or plant debris, black stars: pyrite. **cps**: counts per second. The total gamma radiation (**GR**) may be compared to the radiation measured in the borehole (Fig. 2).

relationship between high U content and mudstone grain-size is seen.

Ruffell *et al*. (2003) presented a model for the flux of K, U and Th in different weathering systems at basin scale. One of their scenarios is a basin with a low-relief hinterland and a humid climate, which applies to the depositional setting of the Atane Formation. The model predicts that chemical weathering dominates and that K and U are removed in solution to sea water, while Th is concentrated in detrital clay. This model may explain the relatively high Th radiation in the detrital mudstones of the Atane Formation. K-feldspar is a minor constituent of the sandstones but contributes significantly to the K-radiation in the sandstones. The model further predicts that K and U are enriched in authigenic minerals in the basin. Such enrichment of U is not observed in the Atane Formation, possibly due to the relatively high sedimentation rate. The low U content may also reflect the predominance of land plants (type III kerogen) that generally contain small amounts of U in organic complexes compared to marine organic material. A comparison of sedimentological logs from delta-front successions with their total gamma radiation in a case study from Ireland also indicates that the delta-front successions are difficult to identify from the gamma log alone (Davies & Elliott 1996).

Summary

The present study demonstrates the importance of calibrating petrophysical logs to core data. The cyclicity which characterises the Atane Formation in outcrops and cores (Figs 1, 2), and which would be a means of identifying the Atane Formation in an un-cored well, is obscured in the total gamma-ray log. This fails to resolve the grain-size variation in the Atane Formation because the presence of K-poor kaolinite, despite enrichment by Th, provides a 'cleaner' signature of the mudstones while the presence of sand-sized K-feldspar gives a 'dirtier' signature of the sandstones. The Th log can, to some degree, resolve the lithological variation but the energy is too small to be reflected in the total gamma-ray signal. The high sedimentation rate and the predominance of terrestrial organic material precluded the development of a characteristic U signature in the marine mudstones. The gamma log thus shows the variations in elements which occur in small amounts, because the bulk of the sediment (quartz, kaolinite and terrestrial coal debris) contributes very little to the gamma-ray radiation.

References

Chalmers, J.A., Pulvertaft, T.C.R., Marcussen, C. & Pedersen, A.K. 1999: New insight into the structure of the Nuussuaq Basin, central West Greenland. Marine and Petroleum Geology **16**, 197–224.

Dam, G., Pedersen, G.K., Sønderholm, M., Midtgaard, H.M., Larsen, L.M., Nøhr-Hansen, H. & Pedersen, A.K. 2009: Lithostratigraphy of the Cretaceous–Paleocene Nuussuaq Group, Nuussuaq Basin, West Greenland. Geological Survey of Denmark and Greenland Bulletin **19**, 171 p.

Davies, S.J. & Elliott, T. 1996: Spectral gamma ray characterisation of high resolution sequence stratigraphy: examples from Upper Carboniferous fluvio-deltaic systems, County Clare, Ireland. In: Howell. J.A. & Aitken, J.F. (eds): High resolution sequence stratigraphy: innovations and applications. Geological Society (London), Special Publications **104**, 25–35.

Pedersen, G.K., Andersen, L.A., Lundsteen, E.B., Petersen, H.I., Bojesen-Koefoed, J.A. & Nytoft, H.P. 2006: Depositional environments, organic maturity and petroleum potential of the Cretaceous coal-bearing Atane Formation at Qullissat, Nuussuaq Basin, West Greenland. Journal of Petroleum Geology **29**, 3–26.

Rider, M.H. 1990: Gamma-ray log shape used as a facies indicator: critical analysis of an oversimplified methodology. In: Hurst, A., Lovell, M.A. & Morton, A.C. (eds): Geological applications of wireline logs. Geological Society Special Publications (London) **48**, 27–37.

Ruffell, A.H., Worden, R.H. & Evans, R. 2003: Palaeoclimate controls on spectral gamma-ray radiation from sandstones. International Association of Sedimentologists Special Publication **34**, 93–108.

Authors' address

Geological Survey of Denmark and Greenland, Øster Voldgade 10, DK-1350 Copenhagen K, Denmark. E-mail: *gkp@geus.dk*

A new seamless digital 1:500 000 scale geological map of Greenland

Mikael Pedersen, Willy L. Weng, Nynke Keulen and Thomas F. Kokfelt

For around 40 years, the Geological Survey of Greenland (GGU) and later the Geological Survey of Denmark and Greenland (GEUS) conducted systematic geological overview mapping of Greenland, leading to the production of 14 printed map sheets on a scale of 1:500 000 which covers the entire country (Fig. 1). The mapping was completed in 1999 and the map sheets were published between 1971 and 2004. Revised 2nd editions of two of the sheets have been published (Table 1).

As a result of the development of the Internet, the publication platform for geological maps has increasingly moved from traditional paper sheets to digital publications for most geological surveys worldwide. This tendency has changed the requirements to the underlying production, storage and publication platforms for map data. For the same reason, it has over the past decade been a strategy of GEUS to bring the 1:500 000 geological maps of Greenland together as a seamless, digital product with a homogeneous legend. This has been further motivated by the increasing number of Geographic Information System (GIS) and web applications to which such a map would provide a valuable background, as well as to many international projects such as OneGeology. The harmonisation of the geological maps was carried out by a project team at GEUS comprising both geological and GIS expertise. The first version of the new seamless map was finished in 2012 and will be released in various web applications in 2013.

Digitisation

The production of a seamless, digital product makes new demands on the underlying map data. Most importantly, all data have to be in vector form in a GIS environment. Only the three most recent of the 14 original map sheets mentioned above were produced digitally (sheets 6, 9, and 11; Fig. 1, Table 1). As part of the project Thematic maps and data of North and Northeast Greenland: geology, mineral occurrences and hydrocarbons (Mikkelsen *et al*. 2005; Christoffersen & Jepsen 2007) four of the printed map sheets (sheets 7, 8, 10 and 12) were vectorised. Of the remaining seven sheets, two sheets (1 and 3) were up for revision, and new editions were produced digitally in 2007 and 2010. The last five (sheets 2, 4, 5, 13 and 14) were vectorised in order to create full digital coverage.

The vectorisation was done from scanned versions of the published maps. In this process, the geological information was taken from the maps and integrated with the best available topographic base-map data, which in most cases were photogrammetric data derived from 1:150 000 aerial photographs (based on aerotriangulations of varying quality). Some of the topography from printed maps was taken from *G/250 Vektor* data from the Danish Geodata Agency and used in map sheets 1, 4 and 5. Due to the nature of the mapping technique and the geodetic control, the old geological paper maps had a much better local than absolute accuracy: the geometric relations between a geological feature and

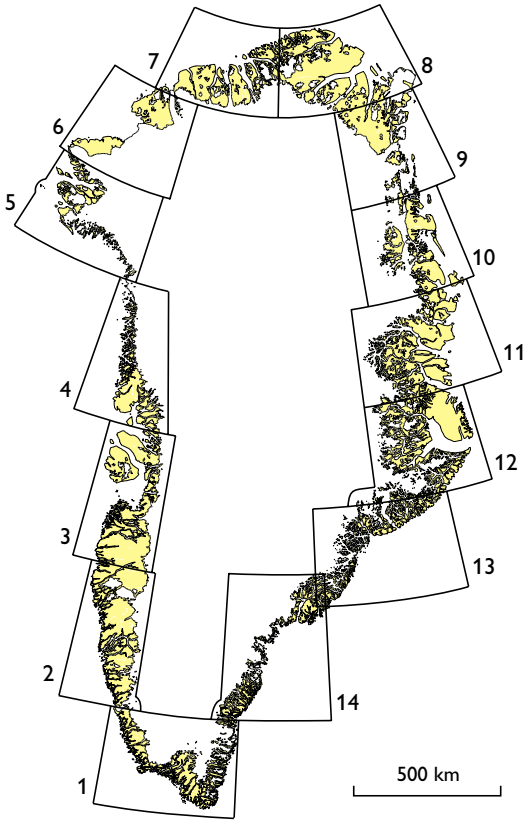

Fig. 1. Index map of Greenland showing the boundaries of the 14 geological map sheets on a scale of 1:500 000 covering Greenland.

Table 1. Data on the Greenlandic bedrock maps 1:500 000

No	Name	Compilers	Published	Edition	Cartographic technique	Topography source
1	Sydgrønland	A.A. Garde	2007	2	Digital	Mixed
2	Frederikshåb Isblink – Søndre Strømfjord	J.H. Allaart	1982		Analog	Photogr.
3	Søndre Strømfjord – Nuussuaq	A.A. Garde & M. Marker	2010	2	Digital	Photogr.
4	Upernavik Isfjord	J.C. Escher	1985		Analog	Paper map
5	Thule	P.R. Dawes	1991		Analog	Paper map
6	Humboldt Gletscher	P.R. Dawes & A.A. Garde	2004		Digital	Photogr.
7	Nyeboe Land	N. Henriksen	1989		Analog (D)	Photogr.
8	Peary Land	H.-J. Bengaard & N. Henriksen	1986		Analog (D)	Photogr.
9	Lambert Land	H.F. Jepsen	2000		Digital	Photogr.
10	Dove Bugt	N. Henriksen	1997		Analog (D)	Photogr.
11	Kong Oscar Fjord	J.C. Escher	2001		Digital	Photogr.
12	Scoresby Sund	H.-J. Bengaard & N. Henriksen	1984		Analog (D)	Photogr.
13	Kangerdlugssuaq	J.S. Myers, P.R. Dawes & T.F.D. Nielsen	1988		Analog	Photogr.
14	Skjoldungen	J.C. Escher	1990		Analog	Photogr.

D: vectorised as a part of the project *Thematic maps and data of North and Northeast Greenland* (Mikkelsen *et al.* 2005; Christoffersen & Jepsen 2007)

the nearby topographic features, such as shore lines and rivers, are usually correct even if the location of such features is quite wrong (as indicated for example by the geographic grid). During vectorisation in the GIS environment, it was therefore constantly necessary to shift the scanned geological map in order to fit the printed map topography to the new digital topography, which in some cases was rather different from that on the printed map.

The digitisation included boundaries between exposed geological units and structural elements, all of which were attributed with type and source information. Subsequent to the vectorisation, polygons were formed and encoded according to their geological type. As the GIS data were stored in a single seamless database, geometric ambiguities across map-sheet boundaries had to be corrected.

The geometric quality of the final map varies substantially. In areas with well-defined topographic features and the best possible photogrammetry, mean errors around 50 m can be expected. However, in areas where topography from paper maps was used as reference during digitisation, errors

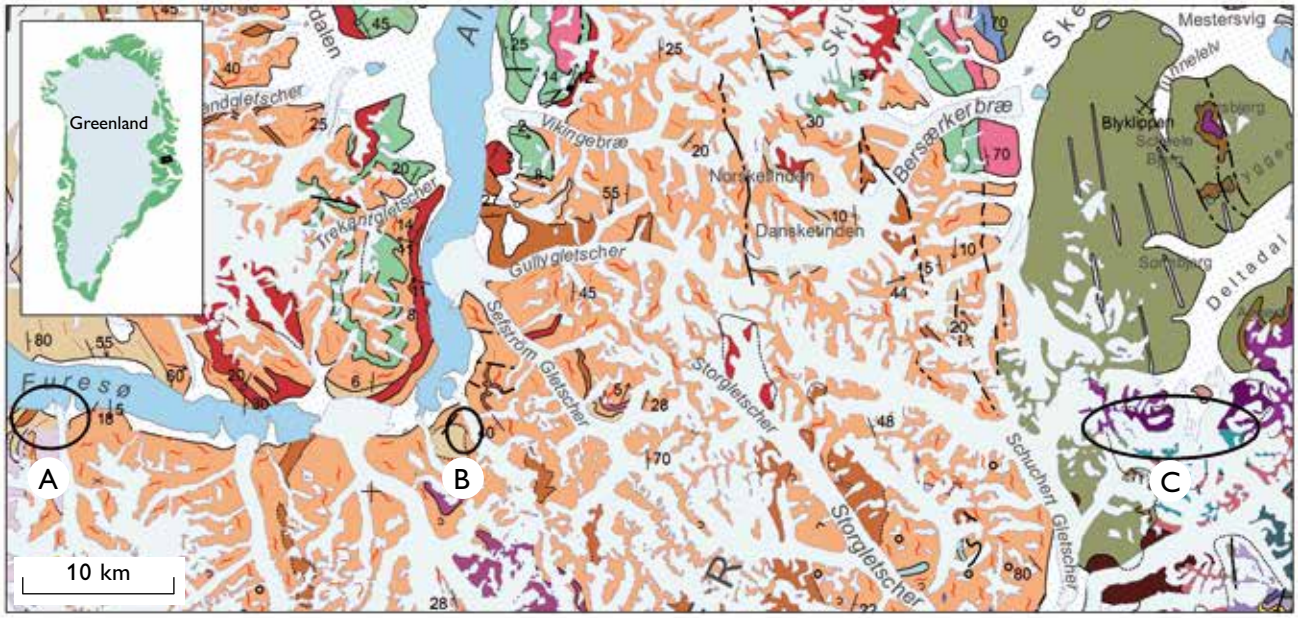

Fig. 2. Geological map of the Mestersvig area in central East Greenland. **A**, **C**: examples of how mapping inconsistencies between two printed map sheets are displayed, where the same unit is shown with different colours across the former map-sheet boundary. **B**: an example of a geometrical problem where a boundary between two units shows a 'jump'. These small inconsistencies remain on the new digital map.

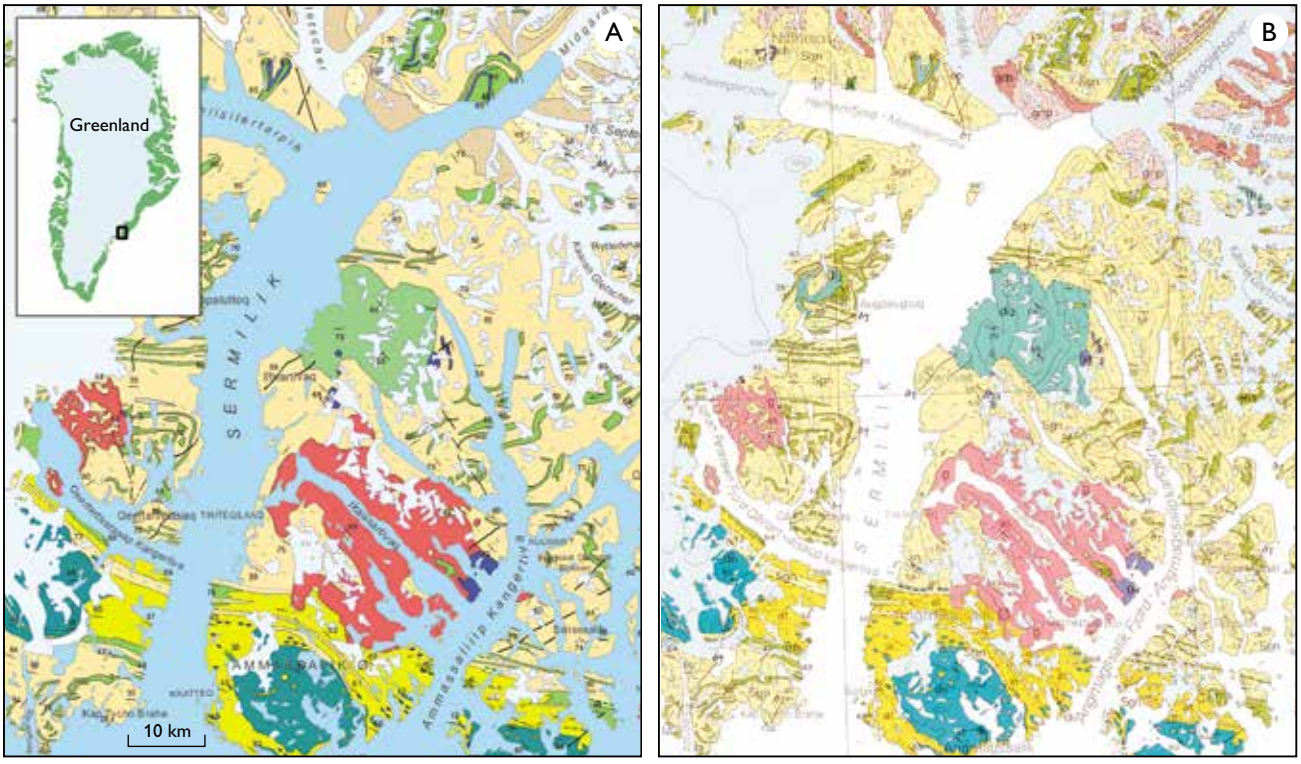

Fig. 3. The colours on the digital map follow the colour scheme of the original 1:500 000 scale maps, but have been updated to modern standards where necessary. An example from South-East Greenland (map sheet 14). **A:** The new digital map. **B:** The same area on the printed version that was published in 1990 (Table 1).

are probably around 250 m. The position of the ice margin shown on the paper maps is even worse. In the Baffin Bay region for example, the ice-margin position in the 1950s is used.

Another important part of the geographic data set is the place names. Although not all of the place names on the printed maps have been digitised yet, the current data set already contains more than 2500 place names.

The concept of map scale also remains when data are being used digitally. The target 1:500 000 scale has governed the selection of features and their degree of detail; it also applies to the base topography that was duly generalised, typically from 1:100 000 originals.

Geological harmonisation

The 14 map sheets that form the basis of the new seamless 1:500 000 scale map were published between 1982 and 2010. The original maps all have their own way of presenting the geology, depending on the map compilers and the individual mapping geologists. The maps vary greatly in degree of detail reflecting the amount of time spent during the original mapping, and the availability of helicopter support in the different areas. Furthermore, the maps show an evolution in the understanding of the geology, and changes in mapping philosophy from older to younger maps.

An important issue was to implement a uniform geological nomenclature to the entire map, so that a single, harmonised legend for all of Greenland could be developed. Since no geological remapping was done, the level of detail displayed in different areas remains uneven. Therefore, boundaries between mapping areas of individual mapping parties, both within former map areas and across former map boundaries, to a large extent remain visible. An example of this is shown in Fig. 2.

The homogenised legend for the *Thematic maps of North and Northeast Greenland* at 1:250 000 (Christoffersen & Jepsen 2007) was used used as a basis for further harmonisation; the harmonisation process was started by combining the adjacent four map sheets (sheet 5, 6, 12 and 13), where similar geological units occur, into a common legend.

The north-western, northern, north-eastern and eastern parts of Greenland largely consist of Palaeoproterozoic to Paleogene sedimentary basins. The sediments are divided into groups, formations and members described in variable, although generally high degrees of detail. The western, southern and south-eastern parts of Greenland mainly consist of metamorphosed Archaean and Palaeoproterozoic

basement rocks. In line with the original, printed 1:500 000 maps, the rock units in these parts of Greenland are mainly divided by their age and petrography. In cases where Archaean rocks have undergone later reworking, e.g. Archaean gneisses deformed and metamorphosed in the Palaeoproterozoic, the entry in the legend is placed under the time of formation and not under the time of reworking, as on the original paper map sheets. The legends of most of the printed map sheets contain a number of rock types with generic names such as orthogneiss, amphibolite, mica schist, granite and ultramafic rocks. These units have been pooled into broader units that cover all of the corresponding rock types of similar age. However, if the original map sheet showed similar rock units with special features as separate types (e.g. the well-described, pyroxene-bearing Ilivertalik granite), these have been retained in order not to loose information compared with the original map sheets.

Legend

The link between geological features on a digital geological map and the corresponding legend is ensured by the use of codes. Each polygon on the map has a code, which is translated into a colour and a descriptive text by the GIS program. In the course of geological harmonisation, the codes from the various input maps were translated into a new, homogeneous encoding scheme so that, e.g. an 'undifferentiated gneiss' in one area got the same code as a corresponding unit in another area. This work was carried out using a combination of translation tables and Python scripts, and resulted in a total list of 443 unique codes each representing a geological unit.

The geological units were subsequently compiled in a legend organised by age and region. Rock units that belong to a supergroup, a sedimentary basin, an igneous province or a metamorphic complex have been grouped together, even if they cover more than one time period. The grouping by age starts with Quaternary deposits and ends with Eoarchaean rocks of the Isua complex. Each original 1:500 000 map sheet legend had its own style, therefore a harmonisation of rock descriptions was also necessary. Where the nomenclatures are obsolete, rock names have been adopted to modern nomenclature. We mainly followed the principles by the British Geological Survey (Gillespie & Styles 1999; Hallsworth & Knox 1999; Robertson 1999).

A data set containing as many different feature types as described requires careful symbolisation. The one currently used tries to stay as close as possible to the tradition of the printed maps of GGU and GEUS. However, some colours – mainly for igneous rocks – have been adapted to colours that are more common on modern maps (Fig. 3).

The new digital compilation is to a large degree intended for viewing on a computer screen. For that reason, the first version of the new map has only been assigned RGB colours. Another colour scheme for map-sheet printing using CMYK colours will be developed at a later stage.

Publication platforms

Compared to a printed map, a digital geological map has more potential applications. First of all, it is well suited for GIS work where users can zoom in on areas of interest and examine the geology e.g. by clicking on geological features and receive detailed information from the underlying databases. The new seamless map has been integrated in such a Web-GIS application which can be found at http://data.geus.dk/map2/geogreen.

The seamless map is furthermore an important GEUS contribution to the global OneGeology portal (http://portal.onegeology.org). This portal aims to put geological maps from all countries in the world together on a scale of 1:1 million or better, by using distributed web map services (WMS). The geological map of Greenland on this portal is currently a 1:2 500 000 scale map. The new 1:500 000 map will fulfil GEUS' participation in this important international initiative.

References

Christoffersen, M. & Jepsen, H.F. 2007: Geological maps of North and North-East Greenland 1:250 000. Copenhagen: Geological Survey of Denmark and Greenland.

Gillespie, M.R. & Styles, M.T. 1999: BGS rock classification scheme 1. Classification of igneous rocks. British Geological Survey Research Report **RR 99-06**, 52 pp.

Hallsworth, C.R. & Knox, R.W.O'B. 1999: BGS rock classification scheme. Classification of sediments and sedimentary rocks. British Geological Survey Research Report **RR 99-03**, 44 pp.

Mikkelsen, N., Jepsen, H.F., Ineson, J.R., Piasecki, S., von Platen-Hallermund, F., Schøjth, F., Thomassen, B. & Weng, W.L. 2005: Thematic maps and data of North and Northeast Greenland: geology, mineral occurrences and hydrocarbons. Danmarks og Grønlands Geologiske Undersøgelse Rapport **2005/28**, 56 pp.

Robertson, S. 1999: BGS rock classification scheme 2. Classification of metamorphic rocks. British Geological Survey Research Report **RR 99-02**, 24 pp.

Authors' address

Geological Survey of Denmark and Greenland, Øster Voldgade 10, DK-1350 Copenhagen K, Denmark; E-mail: *mp@geus.dk*

Darkening of the Greenland ice sheet due to the melt-albedo feedback observed at PROMICE weather stations

Dirk van As, Robert S. Fausto, William T. Colgan, Jason E. Box and the PROMICE project team*

The Greenland ice sheet is losing mass (Barletta *et al.* 2012) and at least half of this loss is caused by an increase in surface melt (e.g. Tedesco *et al.* 2013). The other part is caused by increased dynamic mass loss, as marine-terminating glaciers lose resistive stresses (Nick *et al.* 2009) due to both retreat and meltwater lubrication at the bed (Sasgen *et al.* 2012).

In 2007, the Programme for Monitoring of the Greenland Ice Sheet (PROMICE) was initiated with the aim of gaining an insight into the causes of the ice-mass budget changes based on quantitative observations. This is primarily done by assessing how much mass is gained as snow accumulation on the surface versus how much is lost by calving and surface ablation (Ahlstrøm *et al.* 2008). PROMICE monitors the surface mass balance by means of automatic weather stations (AWSs) designed to quantify accumulation and ablation, as well as the specific energy sources contributing to ablation. These observations are vital to interpreting the physical mechanisms for ice-sheet response to climate change and for the calibration and validation of both satellite observations and climate models.

In the wake of several record-breaking warm summers – increasing surface melt rate and extent (Nghiem *et al.* 2012) – interest in Greenland's surface mass balance has increased (Tedesco *et al.* 2013). Observations of net ablation at PROMICE stations provided *in situ* confirmation of extreme mass-loss events in 2010 (Fausto *et al.* 2012) and 2012, primarily documented by other workers through satellite data. In this paper, we present atmospheric temperatures and surface solar reflectivity (known as albedo) of the Greenland ice sheet in the PROMICE period. Albedo modulates the absorption of solar radiation, which is the primary source of melt energy. It is reported to be decreasing in Greenland in recent years (Box *et al.* 2012), causing the monitoring of albedo variability to be increasingly important. Air temperatures, besides being strongly correlated to surface melt rates, affect surface albedo by controlling the rate of snow-grain metamorphism and the fraction of summer precipitation falling as rain versus snow. To elucidate the so-called melt-albedo feedback, whereby increased melt darkens the ice sheet and further enhances melt, the relationship between albedo and air temperature, observed at PROMICE stations, is examined in this study.

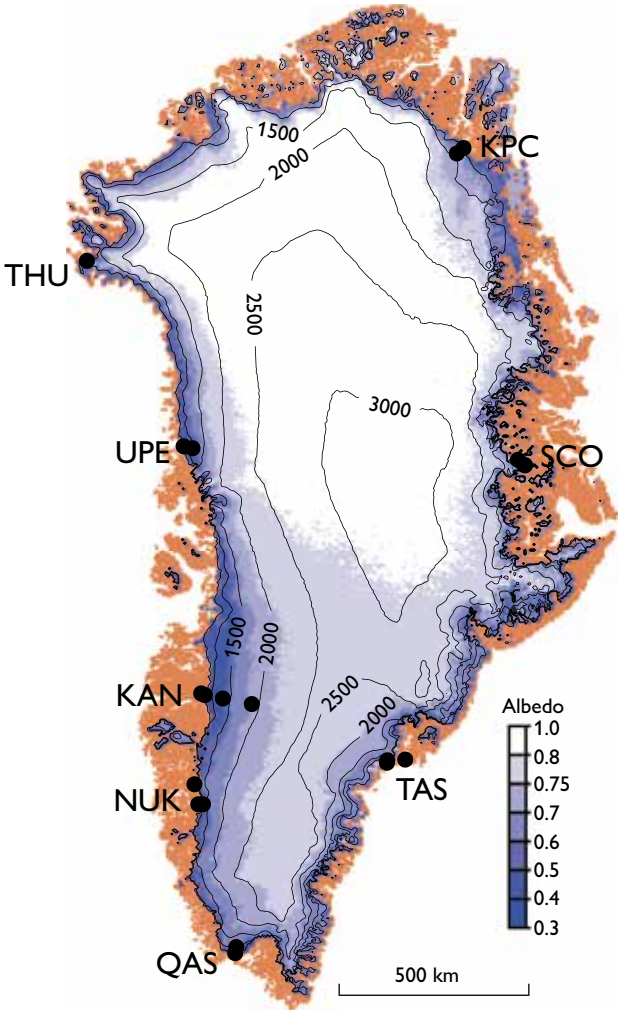

Fig. 1. Map of Greenland showing the locations of the 21 PROMICE weather stations in eight regions. The blue colours show mean satellite (MODIS) derived albedo for the months of June, July and August for 2008–2012. The contour lines show elevations (m) of the ice-sheet surface.

* Andreas P. Ahlstrøm, Signe B. Andersen, Morten L. Andersen, Charalampos Charalampidis, Michele Citterio, Karen Edelvang, Trine S. Jensen, Signe H. Larsen, Horst Machguth, Søren Nielsen, Martin Veicherts and Anker Weidick

PROMICE measurements

The original PROMICE network consisted of 14 AWSs in the regions Kronprins Christian Land (KPC), Scoresbysund (SCO), Tasiilaq (TAS), Qassimiut (QAS), Nuuk (NUK), Upernavik (UPE) and Thule (THU), each region monitored with a lower (L) and an upper (U) station in the ablation area (Fig. 1). PROMICE has both contributed to and received contributions from other projects in the Kangerlussuaq, Nuuk and Tasiilaq regions, leading to the installation of seven additional stations. The PROMICE study regions were selected to best complement the spatial distribution of existing ice-sheet weather stations, such as in the Greenland Climate Network (Steffen *et al.* 1996), by providing data from the under-represented ablation area (Ahlstrøm *et al.* 2008).

The PROMICE AWSs measure meteorological variables including air temperature (at *c.* 2.7 m above the surface), pressure and humidity, wind speed, downward and upward solar (shortwave) and terrestrial (longwave) radiation. The AWSs also record temperature profiles in the upper 10 m of the ice, GPS-derived location and diagnostic parameters such as station tilt angles. A pressure transducer and two sonic rangers measure snow and surface-height change associated with ablation and accumulation (Fausto *et al.* 2012). Most variables are measured every ten minutes, with the data stored locally awaiting collection during maintenance visits. Hourly averages of the most transient variables are transmitted via satellite between days 100 and 300 of each year, while the remaining variables are transmitted at six-hour intervals. Transmissions have a daily frequency in the remaining (winter) period. All data and metadata including sensor specifications are archived in the PROMICE database and made freely available for display and download at *www.promice.dk*.

In this study, we present monthly mean measurements of air temperature and surface albedo. To obtain the temperature averages, we first calculate daily mean air temperatures for all days in which data coverage of hourly mean values exceeds 80%. Subsequently, we calculate monthly mean air temperature for all months in which data coverage of daily mean values exceeds 24 days. To calculate surface albedo, we divide instantaneous values of upward shortwave radiation by the downward component before averaging. However, instrument tilt induces significant errors in the measurement of shortwave radiation (van den Broeke *et al.* 2004), which is a common problem in the ice-sheet ablation area due to irregular melting of the ice surface on which the AWS stands. Therefore we employ the tilt correction method as described by van As (2011) that uses the measured AWS tilt to correct downward shortwave radiation. In contrast to the temperature averaging, a minimum of one successful hourly mean albedo is sufficient to produce a daily mean, provided that the direct solar radiation (which occurs when skies are not overcast) hits the upper dome of the radiometer at angles exceeding 30°, where measurements are more precise. The low sun angle in winter prevents calculation of albedo values.

Atmospheric temperature

All PROMICE sites record a distinct annual cycle in air temperature (Fig. 2A). As is common for Arctic climates, temporal variability is largest in winter due to a more vigorous atmospheric circulation. The amplitude in the annual air temperature cycle is largest for stations at high latitudes or high elevations since above-freezing temperatures and thus a melting ice surface capable of local thermo-regulation, are least common at these stations. The more northerly stations also show a larger annual temperature cycle due to the increasing contrast in the lengths of polar day and night with increas-

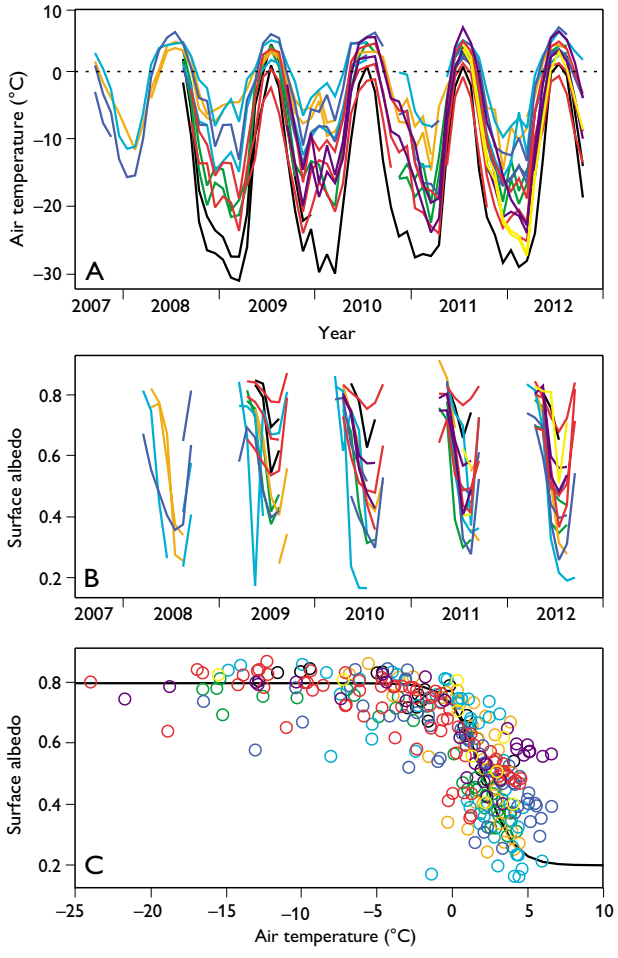

Fig. 2. **A**: Monthly mean air temperatures at the 18 PROMICE sites installed on the ice sheet and before 2012. **B**: Same but for albedo. **C**: Albedo versus temperature. Black lines: KPC stations, green: SCO, orange: TAS, light blue: QAS, dark blue: NUK, red: KAN, purple: UPE, yellow: THU.

ing latitude. The smallest amplitude in the annual temperature cycle is seen at QAS_L, the most southerly PROMICE site. Here, free-atmospheric temperatures can exceed 20°C, leading to strong melt. In 2010, the large heat content of the atmosphere, low summer albedo and anomalously low winter accumulation combined to yield a long net-ablation season and the largest ever recorded ablation in Greenland in a single melt season (9 m of ice; Fausto *et al.* 2012).

As the greater part of mass loss by melt takes place during the summer, we calculated the four- or five-year trends in combined mean air temperature for the months of June, July and August, for eight stations with a sufficiently long coverage. Given the relatively short PROMICE record length, these trends are not free from the influence of inter-annual, natural climatic variability and thus not climatological trends. The data show that at all except two sites the summers have become warmer over the PROMICE period. Most noteworthy is that the warming is most pronounced (*c.* 0.6°C/year) at the high latitude/elevation sites, where the influence of a melting ice surface is spatially and temporally limited. At the sites that experience the highest temperatures and strongest melt, inter-annual variability of free-atmospheric temperatures has had limited effect on air temperatures over the nearly permanently melting ice-sheet surface in summer.

The inter-annual temperature variability is shown in an anomaly plot (Fig. 3A). It is seen that 2010 was a warm year, especially in West Greenland, and mostly early and late in the year, with anomalies exceeding 5°C. The widespread and large melt in 2012 (Nghiem *et al.* 2012) was the result of high temperatures in July, as seen from positive air temperature anomalies at all PROMICE sites.

The record-warm years/summers of 2010 and 2012 (e.g. Tedesco *et al.* 2013), following the warmest decade in Greenland's instrumental temperature record, are consistent with persistent warming observed globally, but are suggested to be a consequence of North Atlantic Oscillation variability affecting atmospheric heat transport (Fettweis *et al.* 2013). Atmospheric warming has been reported to be highest in South and West Greenland. This is confirmed by the PROMICE observations in West Greenland, but observations at KPC_U in north-eastern Greenland show a similar rate of short-term warming. These observations provide *in situ* indications that the atmospheric warming may be spatially pervasive.

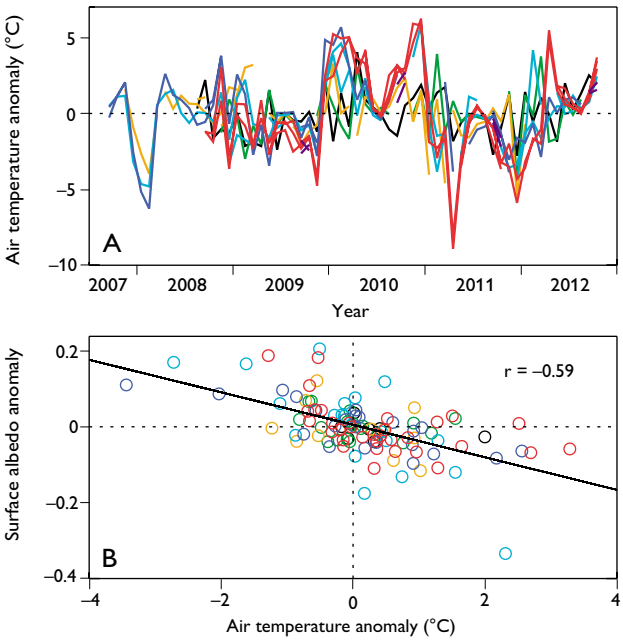

Fig. 3. **A**: Monthly mean air temperature anomalies, i.e. after subtracting the mean annual cycle for stations with data series spanning a minimum of three years. **B**: Albedo versus temperature anomalies plotted for months with mean temperatures exceeding −2°C in order to extract melt-season values only.

Darkening ice-sheet surface

The surface albedo is generally high in the cold, snow-covered interior of the ice sheet (>0.75), and lower along the ice-sheet margin where melting occurs in summer (Fig. 1). In winter, the ice sheet is fully snow covered except where wind erosion dominates. Depending on the location of each AWS in the ablation area, snow melt starts in April or May as seen from air temperatures and decreasing albedo (Fig. 2B). Thereafter, albedo drops throughout the melt season until snowfall occurs in autumn, yielding a distinct annual cycle which is largest at the high-melt sites. Surface melt causes this annual darkening of the ice-sheet surface as snow undergoes heat-driven metamorphosis, or completely melts to expose darker bare ice. The ice-sheet surface may also darken as impurities collect on the ice surface or supraglacial meltwater-filled features become more abundant. We find that on average surface albedo drops below fresh snow values as monthly mean temperatures exceed *c.* −2°C (Fig. 2C). The hyperbolic shape of the scatter plot is primarily a consequence of the annual cycle in albedo (α) and can be approximated by

$$\alpha = \frac{\alpha_{max} + \alpha_{min}}{2} - \frac{\alpha_{max} - \alpha_{min}}{2}\left(\frac{1 - e^{\frac{T - T_0}{C}}}{1 + e^{\frac{T - T_0}{C}}}\right)$$

where T is near-surface air temperature and maximum (α_{max}) and minimum albedo (α_{min}) are prescribed as 0.8 and 0.2, respectively. T_0 and C, taken as 2 and 1°C respectively, are empirical constants characterising a melting point offset and the exponential scaling length of α(T).

Though there are exceptions, taken as a whole the PROMICE data indicate that albedo has decreased over the past five years while temperature has increased. This is most notable at the higher-elevation sites; the lower sites are completely snow-free in every summer and thus exhibit little change. By calculating the temporal correlations between temperature and albedo for all individual stations for the months of June, July and August separately (minimum four-year time series), we isolate the inter-annual variability by eliminating the annual cycle. We observe 36 out of 39 correlation coefficients to be negative, implying a widespread association of temperature-induced melt with surface albedo on the ice sheet. Mean correlation is strongest in June (-0.76 ± 0.28), followed by August (-0.54 ± 0.39) and July (-0.43 ± 0.45).

The surface albedo at most AWSs was relatively low in 2010 and 2012, coincident with the warm summers of the past years. In order to assess the impact of atmospheric warming on ice-sheet darkening at any given site on the Greenland ice sheet, we plot the albedo anomalies versus the temperature anomalies in Fig. 3B for monthly temperatures exceeding –2°C, hereby isolating the melt season. The correlation of –0.59 between the plotted variables is statistically significant. A linear fit yields that one degree of warming in the near-surface air temperature will lead to an average albedo reduction of 0.043. This value is sensitive to the temperature cut-off value (here taken at –2°C) and will become more accurate with longer AWS time series. Since the PROMICE stations measure close to the ice surface where temperature variability is dampened over a melting surface, a stronger correlation could be expected between albedo and local free-atmospheric temperatures, although the regions with low temperature variability are also associated with low albedo variability (Fig. 3B).

As mentioned, this darkening is likely due to an increase in surface melt, which cannot be linked to changes in solar radiation in recent years and thus may very well be directly and indirectly caused by changes in air temperature. Although absorbed solar radiation is the primary source of melt energy, the melt-albedo feedback is initiated by the energy fluxes that respond to changes in temperature, such as downward longwave radiation and the turbulent heat fluxes. Since both atmospheric warming and ice-sheet darkening increase surface melt intensity and melt area, the anticipated future warming will result in a self-reinforcing ice sheet mass-loss contribution from the melt-albedo feedback. While increased surface melt is a primary mechanism for ice loss in Greenland, an increase in meltwater may also enhance mass loss due to ice dynamics, through processes such as basal lubrication and warming of the ice matrix.

Acknowledgements

PROMICE is funded by the Danish Ministry of Climate, Energy and Building. The AWSs in the Kangerlussuaq region are funded by the Greenland Analogue Project, while partner AWSs in the Nuuk region are co-funded by the Greenland Climate Research Centre. Several other projects also contributed to PROMICE.

References

Ahlstrøm, A.P. & the PROMICE project team 2008: A new programme for monitoring the mass loss of the Greenland ice sheet. Geological Survey of Denmark and Greenland Bulletin **15**, 61–64.

Barletta, V.R., Sørensen, L.S. & Forsberg, R. 2012: Variability of mass changes at basin scale for Greenland and Antarctica. The Cryosphere Discussions **6**, 3397–3446.

Box, J.E., Fettweis, X., Stroeve, J.C., Tedesco, M., Hall, D.K. & Steffen, K. 2012: Greenland ice sheet albedo feedback: thermodynamics and atmospheric drivers. The Cryosphere **6**, 821–839.

Fausto, R.S., van As, D. & the PROMICE project team 2012: Ablation observations for 2008–2011 from the Programme for Monitoring of the Greenland Ice Sheet (PROMICE). Geological Survey of Denmark and Greenland Bulletin **26**, 73–76.

Fettweis, X., Hanna, E., Lang, C., Belleflamme, A., Erpicum, M. & Gallée, H. 2013: Important role of the mid-tropospheric atmospheric circulation in the recent surface melt increase over the Greenland ice sheet. The Cryosphere **7**, 241–248.

Nghiem, S.V., Hall, D.K., Mote, T.L., Tedesco, M., Albert, M.R., Keegan, K., Shuman, C.A., DiGirolamo, N.E. & Neuman, G. 2012: The extreme melt across the Greenland ice sheet in 2012. Geophysical Research Letters **39**, L20502, *http://dx.doi.org/10.1029/2012GL053611*.

Nick, F.M., Vieli, A., Howat, I. & Joughin, I. 2009: Large-scale changes in Greenland outlet glacier dynamics triggered at the terminus. Nature Geoscience **2**, 110–114.

Sasgen, I., van den Broeke, M.R., Bamber, J.L., Rignot, E., Sørensen, S.L.S., Wouters, B., Martinec, Z., Velicogna, I. & Simonsen, S.B. 2012: Timing and origin of recent regional ice-mass loss in Greenland. Earth and Planetary Science Letters **333**, 293–303.

Steffen, K., Box, J.E. & Abdalati, W. 1996: Greenland climate network: GC-Net. In: Colbeck, S.C. (ed.): Glaciers, ice sheets and volcanoes: a tribute to Mark F. Meier. CRREL Special Report **96-27**, 98–103.

Tedesco, M., Fettweis, X., Mote, T., Wahr, J., Alexander, P., Box, J. & Wouters, B. 2013: Evidence and analysis of 2012 Greenland records from spaceborne observations, a regional climate model and reanalysis data. The Cryosphere **7**, 615–630.

van As, D. 2011: Warming, glacier melt and surface energy budget from weather station observations in the Melville Bay region of northwest Greenland. Journal of Glaciology **57**(202), 208–220.

van den Broeke, M., van As, D., Reijmer, C. & van de Wal, R. 2004: Assessing and improving the quality of unattended radiation observations in Antarctica. Journal of Atmospheric and Oceanic Technology **21**, 1417–1431.

Authors' address

Geological Survey of Denmark and Greenland, Øster Voldgade 10, DK-1350 Copenhagen K, Denmark. E-mail: *dva@geus.dk*

Titanium minerals in Cameroon

Christian Knudsen, Joseph Penaye, Martin Mehlsen, Roger K. McLimans and Feiko Kalsbeek

The mineral rutile (TiO_2) is a major ore of titanium, which is used in products such as white pigment and titanium metal. The global consumption of titanium minerals in 2011 was *c.* 6.7 million tonnes of which 0.7 million tonnes were rutile and 6 million tonnes ilmenite ($TiFeO_3$). Rutile is almost pure TiO_2 and therefore more valuable than ilmenite (*c.* 1500 $/t and 300$/t, respectively). Compared with ilmenite, rutile can be processed with lower consumption of chemicals and yields less waste products. Rutile was mined in Cameroon between 1935 and 1955 when a total of 15 000 tonnes of rutile were extracted from alluvial deposits. The French Bureau de Recherches Géologiques et Minières conducted a drilling programme in Cameroon in the 1980s which identified *c.* 2.6 million tonnes of rutile in discontinuous occurrences with concentrations of *c.* 1%. Most of the occurrences are located in small- to medium-sized riverbeds with a thickness of 1.5–4.5 m. The main alluvial rutile area is located around the town of Akonolinga, 80 km east of Yaoundé, the capital of Cameroon (Fig. 1). The rutile in the alluvial deposits was derived from the bedrock by weathering, and at some sites major, residual rutile deposits are reported from Quaternary lateritic deposits.

The Geological Survey of Denmark and Greenland conducted a project together with the Institut de Recherches Géologiques et Minières in Cameroon to gain a better understanding of how rutile formed in the bedrock before it was weathered out and try to tie the rutile in the alluvial deposits to its source rocks. This is done by studying the compositional variation of the rutile in the alluvial deposits and comparing it with possible bedrock sources. The compositional variation of ilmenite and monazite ($(La,Ce)PO_4$) and the age distribution of zircon ($ZrSiO_4$) in alluvial sand and bedrock were also investigated. The chemical compositions of minerals in the sediments are used to infer the bedrock source of the minerals. This has particular application in many areas of Cameroon, such as the southern part of the country which is characterised by low relief and dense rain forest with bedrock outcrops that are sparse and difficult to find.

Cameroon is a country in west central Africa (Fig. 1) and is called 'Africa in miniature' because of its cultural, geological and landscape diversity. The landscape includes beaches, deserts, mountains, rain forests and savanna. The highest point is the active volcano Mount Cameroon (4095 m), and the country is home for over 200 different linguistic groups with French and English as the official languages. Compared with other African countries, Cameroon is politically and socially stable. The country covers an area of 475 442 km^2 with a population of *c.* 20 million of which 70% are Christians and 20% Muslims.

Geochronology of the Yaoundé Group

Stendal *et al.* (2006) suggested that the rutile in southern Cameroon is associated with the Neoproterozoic Yaoundé Group that primarily consists of garnet-bearing metamorphosed sediments such as shale and sandstone. These

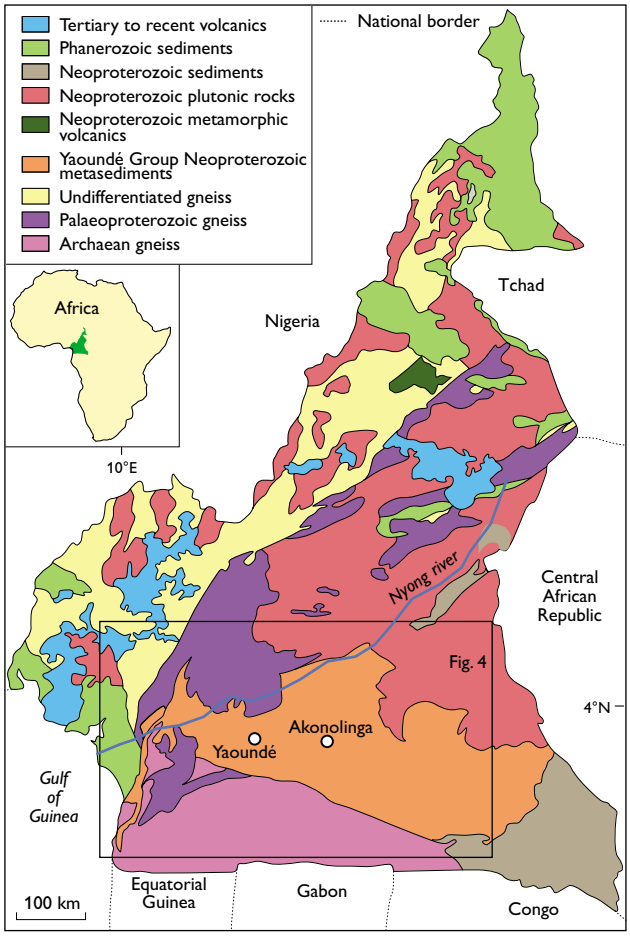

Fig. 1. Simplified geological map of Cameroon.

 Geological Survey of Denmark and Greenland Bulletin 28, 73–76. Open access: www.geus.dk/publications/bull

sediments are believed to have been deposited on the passive margin of the Congo Craton (Nzenti *et al.* 1988), and available isotope data suggest that the sediments that formed the precursor of the Yaoundé Group were deposited during Late Neoproterozoic time. Toteu *et al.* (2004) interpreted some of the sediments as deposited between 626 and 600 Ma.

In order to elucidate the timing of deposition and metamorphism of the Yaoundé Group, zircons from three samples of the Yaoundé Group have been dated by laser ablation inductively coupled plasma mass spectrometry at the Geological Survey of Denmark and Greenland (Kalsbeek *et al.* 2013; for analytical procedures see Frei *et al.* 2006). The results for one of the samples, a garnet-kyanite gneiss (GGU 512411), are shown in Fig. 2. Zircon grains from this sample have wide metamorphic rims which surround cores that are interpreted to represent remnants of originally detrital grains (inset in Fig. 2). The rims yielded a weighted mean age of 635 ± 10 Ma (N = 41, MSWD = 0.48). Most of the cores are of Neoproterozoic age (mainly 650–1100 Ma); a small number of Palaeoproterozoic zircon grains are also present. In contrast to GGU 512411, two other samples from the Yaoundé Group (GGU 512401 and 512415) did not yield zircon ages younger than *c.* 950 Ma. Most zircon grains from these samples are of Palaeoproterozoic age, but some Mesoproterozoic and Archaean grains are also present. The different detrital zircon age distributions indicate different source areas of the Yaoundé Group sediments. One source area may have been dominated by either Palaeoproterozoic or Neoproterozoic zircon grains, and another source area showed diverse age distribution patterns with Archaean to Neoproterozoic zircon grains.

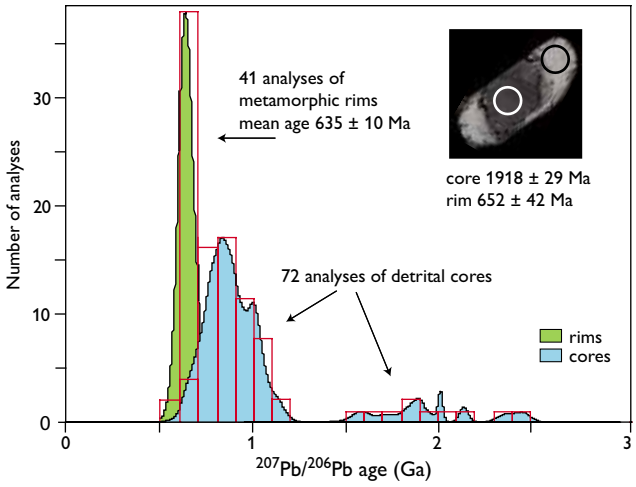

Fig. 2. $^{207}Pb/^{206}Pb$ age distribution (Sircombe 2004) of zircons from sample GGU 512411 from the Yaoundé Group. The inset shows a zircon grain with a distinct metamorphic rim. Ages of cores and rims are shown separately; for simplicity no distinction is made between concordant and discordant analyses.

The rutile-forming event

The metamorphic event that affected the sediments was related to the Pan-African orogeny and the formation of the Gondwana supercontinent. In Cameroon, the Pan-African orogeny was caused by the collision of the Congo Craton to the south with the Nigerian Shield to the north. In the areas where placer rutile deposits are found, the bedrock often consists of kyanite-bearing mica schist, indicating high-pressure, metamorphic conditions during this orogeny. Rutile occurs together with garnet and kyanite and was formed by breakdown of titanium-bearing minerals such as ilmenite, biotite and muscovite. In Cameroon, the rutile is commonly located within kyanite and garnet crystals (Fig. 3)

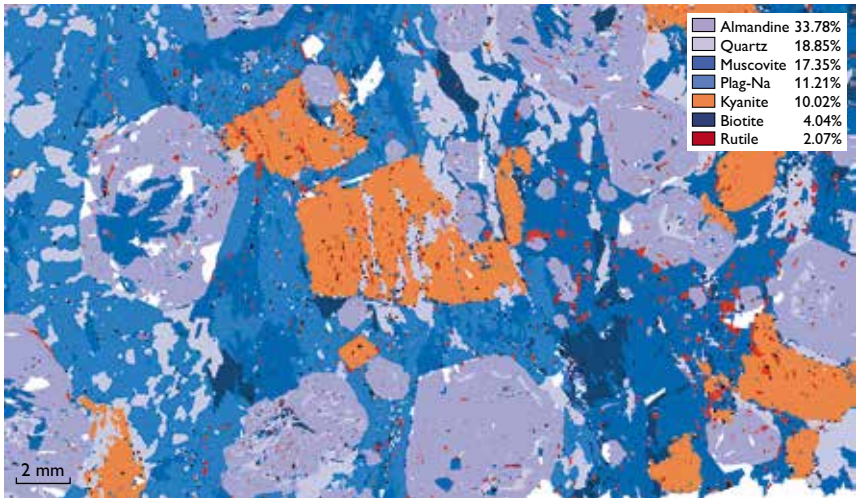

Fig. 3. Mineral Liberation Analysis (MLA) image of a kyanite garnet gneiss sample (GGU 512921) in which the rutile is enclosed in both garnet and kyanite; this indicates that the rutile was formed during prograde metamorphism – i.e. during increasing pressure and temperature. MLA is a scanning electron microscope-based method where a polished, mounted part of the sample is divided into 10 × 10 μm pixels. The beam of electrons generates an X-ray spectrum, which is subsequently compared with a library of spectra representing different minerals. In this way, the instrument can recognise the minerals in the sample and generate an image of the mineralogy. The MLA technique was described by Fandrich *et al.* (2007).

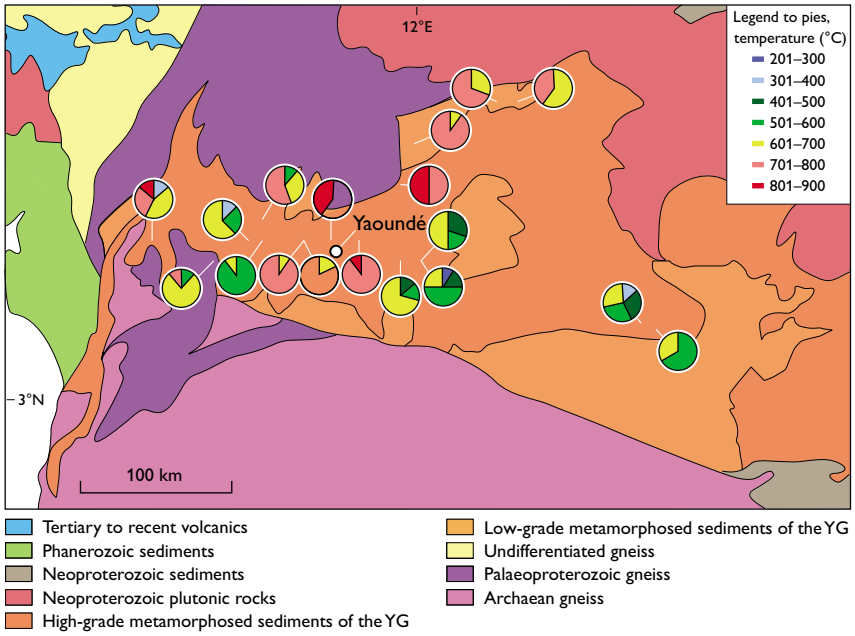

Fig. 4. Pie diagrams showing temperatures during formation based on the Zr content in rutile from 18 rock samples from the Yaoundé Group. The calculation of the temperature T (in °C) = 127.8 × ln (Zr in rutile in ppm) –10 is based on Zack *et al.* (2004). **YG:** Yaoundé Group. For location see Fig. 1.

that formed during high-pressure metamorphism, and thus rutile must have formed during the same episode when pressure and temperature were rising (prograde metamorphism). However, it is possible that some of the rutile grains in the rocks of the Yaoundé Group are inherited from older rocks, as suggested by Stendal *et al.* (2006).

The temperature of rutile formation can be inferred from the rutile geothermometer (Zack *et al.* 2004; Tomkins *et al.* 2007). Eighteen rutile-bearing rock samples from the Yaoundé Group were studied. As shown in Fig. 4, the temperature during formation of the rutile varies significantly. The geographical distribution of the temperatures appears to show a pattern with a core area around Yaoundé characterised by high temperatures in the 700–900°C range with areas to the north-east and south-west characterised by temperatures of 600–700°C. Both east and west of the core area, the estimated temperatures of formation are lower, mainly in the range 500–700°C. It is not known if there was only one episode of rutile formation. Geochronological work on the rutile is planned to test if it is possible to tie the formation of the rutile in the area to the Pan-African orogeny.

Fig. 5. Two sampling methods being tested. Left: a light auger driven by a small engine mounted on a tripod; right: a hand auger. At this location, the hand auger was superior as it penetrated 4.5 m in 30 minutes whereas the engine-driven auger penetrated 2 m during the same time.

Sediment sampling and analysis

A programme combining collection of sediment samples from modern rivers and sampling of older river deposits was initiated in an area in the southern part of Cameroon (Figs 1, 4). The samples from streams were collected as heavy mineral concentrates, and the alluvial deposits were sampled using either a light auger driven by a small engine mounted on a tripod or a hand auger (Fig. 5). The samples were analysed for major and trace elements using X-ray fluorescence and inductively coupled plasma mass spectrometry, respectively. The ratio between TiO_2 and Fe_2O_3 was used to identify areas where the titanium is primarily located in rutile. The results show that areas with a TiO_2/Fe_2O_3 ratio > 2 in stream sediments and alluvial deposits coincide with areas where Yaoundé Group sediments are found below the surficial deposits.

In order to study the texture of the titanium mineral grains in stream sediments and alluvial sand, samples were subjected to 'Mineral Liberation Analysis' (Fig. 6). The analysis shows that the detrital rutile grains often have a rim of ilmenite. This is also seen in rock samples from the area

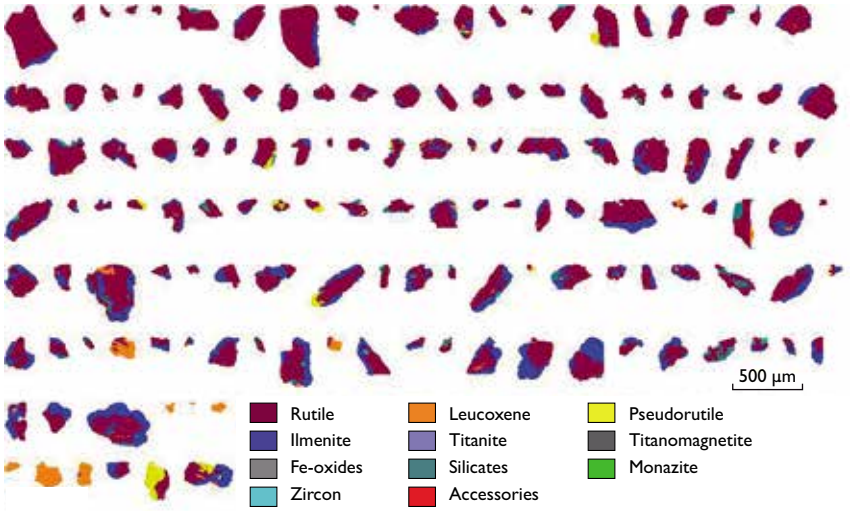

Fig. 6. Mineral Liberation Analysis image of detrital grains from Nyong river in Cameroon (GGU 517615). The purple coloured parts are rutile and the blue is ilmenite. The orange grains are altered ilmenite grains (leucoxene).

where rutile is overgrown by ilmenite. This is caused by recrystallisation of the rock under lower-grade metamorphic conditions, probably retrogression during the late part of the Pan-African orogeny.

Conclusions

The titanium mineral rutile was formed by high-grade metamorphism of sedimentary rocks of the Neoproterozoic Yaoundé Group during the Pan-African orogeny *c.* 635 Ma ago. The temperature of the rutile-forming event has been estimated using the 'rutile geothermometer' based on the Zr content in the rutile, and it is found that the highest temperatures (*c.* 750 ± 100°C) are found in the area from Yaoundé towards the north-east. Both north-west and south-east of this area the rutile geothermometer indicates lower metamorphic temperatures (*c.* 600 ± 100°C).

Acknowledgements

We thank J.V. Hell, Director of Institut de Recherches Géologiques et Minières in Cameroon for enthusiastic support and permission to use vehicles from the institute during the field work. J. Boserup constructed the small tripod drillrig and Alfons Berger assisted with the Electron Microprobe analyses at the Department of Geosciences and Natural Resource Management, University of Copenhagen. We thank J.Z. Johansen, J.M.U.O. Njel and B. Kankeu for help during field work in Cameroon. DuPont Titanium Technologies, Wilmington, Delaware, USA, provided financial support.

References

Fandrich, R., Gu, Y., Burrows, D. & Moeller, K. 2007: Modern SEM-based mineral liberation analysis. International Journal of Mineral Processing **84**, 310–320.

Frei, D., Hollis, J.A., Gerdes, A., Harlov, D., Karlsson, C., Vasques, P., Franz, C., Johansson, L. & Knudsen, C. 2006: Advanced *in situ* geochronological and trace element microanalysis by laser ablation techniques. Geological Survey of Denmark and Greenland Bulletin **10**, 25–28.

Kalsbeek, F., Ekwueme, B.N., Penaye, J., de Souza, Z.S. & Thrane, K. 2013: Recognition of Early and Late Neoproterozoic supracrustal units in West Africa and North-East Brazil from detrital zircon geochronology. Precambrian Research **226**, 105–115.

Nzenti, J.P., Barbey, P., Macaudière, J. & Soba, D. 1988: Origin and evolution of the late Precambrian high-grade Yaoundé gneisses (Cameroon). Precambrian Research **38**, 91–109.

Sircombe, K.N. 2004: AgeDisplay: an Excel workbook to evaluate and display univariate geochronological data using binned frequency histograms and probability density distributions. Computers & Geosciences **30**, 21–31.

Stendal, H., Toteu, S.F., Frei, R., Penaye, J., Njel, U.O., Bassahak, J., Nni, J., Kankeu, B., Ngako, V. & Hell, J.V. 2006: Derivation of detrital rutile in the Yaoundé region from the Neoproterozoic Pan-African belt in southern Cameroon (Central Africa). Journal of African Earth Sciences **44**, 443–458.

Tomkins, H.S., Powell, R. & Ellis, D.J. 2007: The pressure dependence of the zirconium-in-rutile thermometer. Journal of Metamorphic Geology **25**, 703–713.

Toteu, S.F., Penaye, J. & Djomani, Y.P. 2004: Geodynamic evolution of the Pan-African belt in central Africa with special reference to Cameroon. Canadian Journal of Earth Sciences **41**, 73–85.

Zack, T., Moraes, R. & Kronz, A. 2004: Temperature dependence of Zr in rutile: empirical calibration of a rutile thermometer. Contributions to Mineralogy and Petrology **148**, 471–488.

Authors' addresses

C.K., F.K. & M.M., *Geological Survey of Denmark and Greenland, Øster Voldgade 10, DK-1350 Copenhagen K, Denmark.* E-mail: *ckn@geus.dk*

J.P., *Institut de Recherches Géologiques et Minières, Rue Mgr Vogt, P.O. Box 4110 Nlongkak, Yaoundé, Cameroon.*

R.K.McL., *DuPont Titanium Technologies, Experimental Station, E352/217, Route 141 and Henry Clay Road, Wilmington, DE 19808, USA.*

De Nationale Geologiske Undersøgelser for Danmark og Grønland (GEUS)

Geological Survey of Denmark and Greenland
Øster Voldgade 10, DK-1350 Copenhagen K
Denmark

The series *Geological Survey of Denmark and Greenland Bulletin* started in 2003 and replaced the two former bulletin series of the Survey, viz. *Geology of Greenland Survey Bulletin* and *Geology of Denmark Survey Bulletin*. Some of the twenty-one volumes published since 1997 in those two series are listed on the facing page. The present series, together with *Geological Survey of Denmark and Greenland Map Series*, now form the peer-reviewed scientific series of the Survey.

Geological Survey of Denmark and Greenland Bulletin

1	The Jurassic of Denmark and Greenland, 948 pp. (28 articles), 2003. *Edited by* J.R. Ineson & F. Surlyk.	500.00
2	Fish otoliths from the Paleocene of Denmark, 94 pp., 2003. *By* W. Schwarzhans.	100.00
3	Late Quaternary environmental changes recorded in the Danish marine molluscan faunas, 268 pp., 2004. *By* K.S. Petersen.	200.00
4	Review of Survey activities 2003, 100 pp. (24 articles), 2004. *Edited by* M. Sønderholm & A.K. Higgins.	180.00
5	The Jurassic of North-East Greenland, 112 pp. (7 articles), 2004. *Edited by* L. Stemmerik & S. Stouge.	160.00
6	East Greenland Caledonides: stratigraphy, structure and geochronology, 93 pp. (6 articles), 2004. *Edited by* A.K. Higgins & F. Kalsbeek.	160.00
7	Review of Survey activities 2004, 80 pp. (19 articles), 2005. *Edited by* M. Sønderholm & A.K. Higgins.	180.00
8	Structural analysis of the Rubjerg Knude Glaciotectonic Complex, Vendsyssel, northern Denmark, 192 pp., 2005. *By* S.A.S. Pedersen.	300.00
9	Scientific results from the deepened Lopra-1 borehole, Faroe Islands, 156 pp. (11 articles), 2006. *Edited by* J.A. Chalmers & R. Waagstein.	240.00
10	Review of Survey activities 2005, 68 pp. (15 articles), 2006. *Edited by* M. Sønderholm & A.K. Higgins.	180.00
11	Precambrian crustal evolution and Cretaceous–Palaeogene faulting in West Greenland, 204 pp. (12 articles), 2006. *Edited by* A.A. Garde & F. Kalsbeek.	240.00
12	Lithostratigraphy of the Palaeogene – Lower Neogene succession of the Danish North Sea, 77 pp., 2007. *By* P. Schiøler, J. Andsbjerg, O.R. Clausen, G. Dam, K. Dybkjær, L. Hamberg, C. Heilmann-Clausen, E.P. Johannessen, L.E. Kristensen, I. Prince & J.A. Rasmussen.	240.00
13	Review of Survey activities 2006, 76 pp. (17 articles), 2007. *Edited by* M. Sønderholm & A.K. Higgins.	180.00
14	Quaternary glaciation history and glaciology of Jakobshavn Isbræ and the Disko Bugt region, West Greenland: a review, 78 pp., 2007. *By* A. Weidick & O. Bennike.	200.00
15	Review of Survey activities 2007, 96 pp. (22 articles), 2008. *Edited by* O. Bennike & A.K. Higgins.	200.00
16	Evaluation of the quality, thermal maturity and distribution of potential source rocks in the Danish part of the Norwegian–Danish Basin, 66 pp., 2008. *By* H.I. Petersen, L.H. Nielsen, J.A. Bojesen-Koefoed, A. Mathiesen, L. Kristensen & F. Dalhoff.	200.00
17	Review of Survey activities 2008, 84 pp. (19 articles), 2009. *Edited by* O. Bennike, A.A. Garde & W.S. Watt.	200.00
18	Greenland from Archaean to Quaternary. Descriptive text to the 1995 Geological map of Greenland, 1:2 500 000. 2nd edition, 126 pp., 2009. *By* N. Henriksen, A.K. Higgins, F. Kalsbeek & T.C.R. Pulvertaft.	280.00
19	Lithostratigraphy of the Cretaceous–Paleocene Nuussuaq Group, Nuussuaq Basin, West Greenland, 2009. *By* G. Dam, G.K. Pedersen, M. Sønderholm, H.H. Midtgaard, L.M. Larsen, H. Nøhr-Hansen & A.K. Pedersen.	300.00
20	Review of Survey activities 2009, 106 pp. (23 articles), 2010. *Edited by* O. Bennike, A.A. Garde & W.S. Watt.	220.00
21	Exploration history and place names of northern East Greenland, 368 pp., 2010. *By* A.K. Higgins.	200.00
22	Lithostratigraphy of the Upper Oligocene – Miocene succession of Denmark, 92 pp., 2010. *By* E.S. Rasmussen, K. Dybkjær & S. Piasecki.	240.00
23	Review of Survey activities 2010, 84 pp. (19 articles), 2011. *Edited by* O. Bennike, A.A. Garde & W.S. Watt.	200.00
24	The East Greenland rifted volcanic margin, 96 pp., 2011. *By* C.K. Brooks.	200.00
25	Upper Cretaceous chalk facies and depositional history recorded in the Mona-1 core, Mona Ridge, Danish North Sea. 2011. *By* K. Anderskouv & F. Surlyk.	200.00

26	Review of Survey activities 2011, 88 pp. (21 articles), 2012. *Edited by* O. Bennike, A.A. Garde & W.S. Watt.	200.00
27	Neoglacial and historical glacier changes around Kangersuneq fjord in southern West Greenland, 68 pp., 2012. *By* A. Weidick, O. Bennike, M. Citterio & N. Nørgaard-Pedersen.	200.00
28	Review of Survey activities 2012, 76 pp. (17 articles), 2013. *Edited by* O. Bennike, A.A. Garde & W.S. Watt.	200.00

Geological Survey of Denmark and Greenland Map Series

1	Explanatory notes to the Geological map of Greenland, 1:500 000, Humboldt Gletscher, Sheet 6, 48 pp. + map, 2004. *By* P.R. Dawes.	280.00
2	Explanatory notes to the Geological map of Greenland, 1:500 000, Thule, Sheet 5 (1991), 97 pp. + map, 2006. *By* P.R. Dawes.	300.00
3	Explanatory notes to the Geological map of Greenland, 1:100 000, Ussuit 67 V.2 Nord, 40 pp. + map, 2007. *By* J.A.M. van Gool & M. Marker.	280.00
4	Descriptive text to the Geological map of Greenland, 1:500 000, Dove Bugt, Sheet 10, 32 pp. + map, 2009. *By* N. Henriksen & A.K. Higgins.	240.00
5	Descriptive text to the Geological map of Greenland, 1:100 000, Kangaatsiaq 68 V.1 Syd and Ikamiut 68 V.1 Nord, 41 pp. + 2 maps, 2010. *By* A.A. Garde & J.A. Hollis.	280.00

Geology of Greenland Survey Bulletin (173–191; discontinued)

180	Review of Greenland activities 1997, 176 pp. (26 articles), 1998. *Edited by* A.K. Higgins & W.S. Watt.	200.00
181	Precambrian geology of the Disko Bugt region, West Greenland, 179 pp. (15 articles), 1999. *Edited by* F. Kalsbeek.	240.00
182	Vertebrate remains from Upper Silurian – Lower Devonian beds of Hall Land, North Greenland, 80 pp., 1999. *By* H. Blom.	120.00
183	Review of Greenland activities 1998, 81 pp. (10 articles), 1999. *Edited by* A.K. Higgins & W.S. Watt.	200.00
184	Collected research papers: palaeontology, geochronology, geochemistry, 62 pp. (6 articles), 1999.	150.00
185	Greenland from Archaean to Quaternary. Descriptive text to the Geological map of Greenland, 1:2 500 000, 93 pp., 2000. *By* N. Henriksen, A.K. Higgins, F. Kalsbeek & T.C.R. Pulvertaft.	225.00
186	Review of Greenland activities 1999, 105 pp. (13 articles), 2000. *Edited by* P.R. Dawes & A.K. Higgins.	225.00
187	Palynology and deposition in the Wandel Sea Basin, eastern North Greenland, 101 pp. (6 articles), 2000. *Edited by* L. Stemmerik.	160.00
188	The structure of the Cretaceous–Palaeogene sedimentary-volcanic area of Svartenhuk Halvø, central West Greenland, 40 pp., 2000. *By* J. Gutzon Larsen & T.C.R. Pulvertaft.	130.00
189	Review of Greenland activities 2000, 131 pp. (17 articles), 2001. *Edited by* A.K. Higgins & K. Secher.	160.00
190	The Ilímaussaq alkaline complex, South Greenland: status of mineralogical research with new results, 167 pp. (19 articles), 2001. *Edited by* H. Sørensen.	160.00
191	Review of Greenland activities 2001, 161 pp. (20 articles), 2002. *Edited by* A.K. Higgins, K. Secher & M. Sønderholm.	200.00

Geology of Denmark Survey Bulletin (36–37; discontinued)

36	Petroleum potential and depositional environments of Middle Jurassic coals and non-marine deposits, Danish Central Graben, with special reference to the Søgne Basin, 78 pp., 1998. *By* H.I. Petersen, J. Andsbjerg, J.A. Bojesen-Koefoed, H.P. Nytoft & P. Rosenberg.	250.00
37	The Selandian (Paleocene) mollusc fauna from Copenhagen, Denmark: the Poul Harder 1920 collection, 85 pp., 2001. *By* K.I. Schnetler.	150.00

Prices are in Danish kroner exclusive of local taxes, postage and handling

Note that information on the publications of the former Geological Survey of Denmark and the former Geological Survey of Greenland (amalgamated in 1995 to form the present Geological Survey of Denmark and Greenland) can be found on *www.geus.dk*